Motion Control of Hydraulic Winch Using Variable Displacement Motors

Geir-Arne Moslått

UiA University of Agder

Doctoral Dissertations at the University of Agder 305

Geir-Arne Moslått

Motion Control of Hydraulic Winch Using Variable Displacement Motors

Doctoral Dissertation for the Degree *Philosophiae Doctor (PhD)* at
the Faculty of Engineering and Science, Specialisation in Mechatronics

University of Agder
Faculty of Engineering and Science
2020

Doctoral Dissertations at the University of Agder 305
ISSN: 1504-9272
ISBN: 978-82-8427-008-1

Printed by 07 Media
Grimstad

Preface

The research described in this thesis has been carried out at the National Oilwell Varco, Lifting and Handling department, and at the University of Agder, Department of Engineering Sciences. The research was funded by the Norwegian Research Council and National Oilwell Varco Norway, grant number 263525, and lasted from September 2016 to July 2020. Professor Michael Rygaard Hansen from the University of Agder has been the main supervisor, Associate Professor Damiano Padovani from the University of Agder, and Manager at Software and Automation Anders Meisfjordskar at National Oilwell Varco have been the co-supervisors.

From 2012 I have been working with hydraulic design and testing of offshore cranes and heave compensation, and therefore a Ph.D.-project within that field felt like the right way to go. In the field and the office, there are often raised suggestions for equipment improvements. However, the time and resources to follow them are not necessarily available. Thus, the opportunity to investigate one of these ideas felt intriguing.

The idea to be investigated was to control the hydraulic motors and pumps slightly different, to achieve better performance and increased capacity for offshore heave compensated operations. In various ways, this thesis shows what challenges and tasks a company will face, putting a new product or technology into use. Especially in the offshore business were safety is an important factor. The process has included work to obtain a high level of system knowledge, and by this, been able to create high-fidelity models. Therefore, extensive work has been carried out to test and measure the cranes to gather information to build trustworthy models. These models are used to develop and test out the new system controller to ensure the highest level of safety before implementing and testing on the real crane system.

At last, I would like to highlight the fact that this project was executed as an industrial PhD-project. The benefits of access to historical crane data, connections with sub-suppliers, and the unique opportunity to do full-size in-field measurements have been a significant upside to the whole project. However, it also creates extra challenges when it comes to planning and plan execution. For instance, planning for in-field testing is challenging. The fact that you have no control over when exactly you will be given access, and that other priorities or occurrences might squeeze you out of the test-plan, will affect the work plan and progress. The plans were, therefore, adopted and changed during the whole period. However, as Winston Churchill said, "Plans are of little importance, but planning is essential."

Acknowledgments

I especially want to thank my supervisors who have contributed throughout the assignment. They have exercised professionalism and assisted greatly with their excellent knowledge and experience.
I would also like to extend my gratitude to my fellow colleagues. They have made significant contributions with their skills during in-field tests and in the office. Their patience should be applauded. I would also like to thank my employer, National Oilwell Varco, for giving me this opportunity to carry out this project in collaboration with the University of Agder. Last, I want to thank the Norwegian research council which, together with National Oilwell Varco, have funded the project. Without them, the project would never have been conducted.

Geir-Arne Moslått
Grimstad, Norway
June 2020

Abstract

To compete in the open market of the offshore crane industry, it is imperative for the manufacturer to continuously improve crane operability. In this context, the crane operability is expressed by means of a so-called weather window. The weather window is computed from the crane characteristics in combination with that of the vessel and the payload to be handled. It returns a set of boundaries for when it is accepted to perform a planned lift, mainly in terms of current sea-state and wind. The most important crane operability characteristics that enter into the computation of the weather window are maximum wire velocity and load capacity.

This thesis focuses on how to improve the operability of active heave compensated offshore cranes. Two ways of achieving that goal have been investigated, namely, an improved control strategy and the use of model-based lift planning.

The system investigated is the hydraulic active/passive winch system used by National Oilwell Varco. A new control strategy for the system was developed, tested, and implemented. The new strategy utilizes that variable displacement of the hydraulic motors of the active system of the winch drive. The strategy, semi secondary control, gave significant benefits in terms of reduced peak-pressure, increased load capacity, increased wire-speed capacity, and smoother winch performance at low winch speed. The results were validated and verified through simulations and in-field measurements.

The thesis also elaborates on the simulation model development, where the attention was aimed at modeling and identifying friction in hydraulic winch systems. Multiple in-field measurements were performed to identify friction in the winch systems. Two friction models were developed, one that describes the friction losses in the hydraulic motors, and one that describes the friction losses in the remaining power transmission of the winch.

The friction model was used to support the complete winch model. The complete winch model was used for two things. Firstly, it was an important platform to test and develop a new control strategy. Secondly, a trustworthy winch model was shown to be of great value during lift planning. With a model, conservatism in the lift planning phase can be reduced, resulting in a larger weather window. However, when a model is used in planning, the model verification and quality are of high importance. Therefore, a model structure and verification process have also been developed and presented in this work.

Publications

The following listed publications are peer reviewed. The versions presented in this paper will only differ in formatting compared to the published versions.

Paper A G-A. Moslått, M. Hansen, N. Karlsen, (2018) A model for torque losses in variable displacement axial piston motors. Journal of Modeling, Identification and Control. 39 (2):107-114, 2018. doi: 10.4173/mic.2018.2.

Paper B G-A. Moslått, M. Hansen, (2018) Modeling of Friction Losses in Offshore Knuckle Boom Crane Winch System. Global Fluid Power Society PhD Symposium, GFPS 2018. DOI: 10.1109/GFPS.2018.8472316 10.4173/mic.2018.2. ISBN: 9781538647851

Paper C G-A. Moslått, D. Padovani, M. Hansen, (2019) A control algorithm for active/passive hydraulic winches used in active heave compensation. In Proceedings of the ASME/BATH 2019. Symposium on Fluid Powerand Motion Control. DOI: 10.1115/FPMC2019-1710 ISBN: 978-0-7918-5933-9

Paper D G-A. Moslått, M. Hansen, Practise for determining friction in hydraulic winch systems. Modeling, Identification and Control. 2020, Vol 41, No 2, pp. 109-120. DOI: 10.4173/mic.2020.2.6

Paper E Geir-Arne Moslått, Michael Rygaard Hansen, Damiano Padovani, Performance Improvement of a Hydraulic Active/Passive Heave Compensation Winch Using Semi Secondary Motor Control: Experimental and Numerical Verification. Energies 2020, 13, 2671. DOI: 10.3390/EN13102671

Paper F Geir-Arne Moslått, Damiano Padovani, Michael Rygaard Hansen, A digital twin for lift planning with offshore heave compensated cranes. In Journal of Offshore Mechanics and Arctic Engineering. 2020. pp. 1-29.

Contents

List of Figures

List of Tables

Chapter 1

Introduction

When using cranes or other lifting appliances on offshore floating vessels, motion compensation is essential to ensure a high level of safety and to minimize the risk of damaging the crane or the payload. Examples could be lowering a large subsea template to the seabed, supplying an offshore platform with tools, or replacing damaged parts of a wind turbine installation. In any case, the motion compensation is essential in order to obtain a commercially useful weather window for any offshore operation.

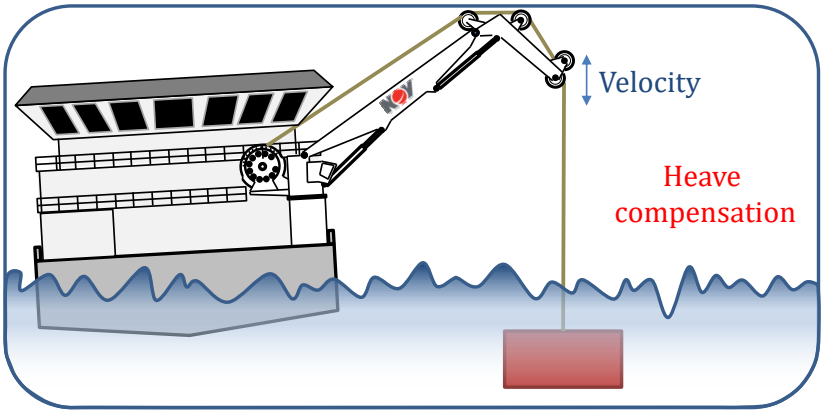

Figure 1.1: Crane placed on a vessel.

The weather window is calculated during the lift-planning phase and describes under what conditions the lifting equipment is allowed to perform the operation. These conditions are mainly associated with wave height and wind speed. Outside the weather window, the risk for overloading the crane or damaging the lifted installation is calculated to be so high that operations are canceled. Increasing the weather window is a huge motivation factor for several research topics like ship-to-ship compensation [9], use of tuggers [10], 3D compensation, and crane anti-sway control [11],[12]. The reason is obvious; if it is possible to reduce the number of days with a vessel offshore, the cost savings are significant.

It is most common that the motion compensation is divided between the vessel and the crane itself. The horizontal positioning is handled by the dynamic positioning (DP) system of the vessel, and the remaining motion compensation is handled via motion

control of the crane. Usually, this is done by controlling the rotation of the main winch and, thereby, the paid-out wire.

This type of motion compensation is normally referred to as heave compensation (HC), and for most operations performed subsea, this is seen as sufficient. However, when lifting from a floater to a fixed platform or to another floater where the lift is performed in air, the motion due to vessel roll, pitch and jaw is not insignificant and may result in an even more limited weather window. Despite this, the main focus on most subsea operations remains the vertical heave compensation directly derived from the control of the main winch. Therefore, the obtainable weather window is directly related to the load capacity, the maximum speed, and the motion control of the main winch.

1.1 Motivation

Active heave compensation (AHC) has been a common feature for offshore subsea cranes since the 1990's. The AHC functionality has played a significant role in the offshore industry since it decouples the vessel movement from the load motion and reduces the influence of load variations on the heave compensation.

This project's primary motivation has been to increase the weather window for NOVs offshore knuckle boom cranes and, simultaneously, the operational efficiency by means of a change in the control strategy. The production of new cranes to the market has been massively reduced the last years since 2014. Thus, a focus on possible improvements and general cost reductions are essential. Therefore, a new control strategy should be able to retrofit the conventional active/passive hydraulic systems. This system was chosen because it is the most common system used, and it is still a cost-effective system compared to electric winch systems.

Figure 1.2: A NOV offshore box boom crane.

AHC cranes are commonly placed and used on construction vessels, as seen in Fig. 1.2.

On these kinds of vessels, the crane is of high importance. Active heave compensated cranes are a critical component on a vessel and crane downtime should be reduced to a minimum. This explains why the offshore crane business is very conservative when it comes to changes and upgrades. A failed implementation of a new feature can easily be extremely costly, both for the supplier's reputation and the vessel owner's economy.

When pursuing new control strategies, it is therefore important to have a high level of confidence in the obtained results. To accommodate this, new control strategies must be modeled, analyzed, simulated in a theoretical environment, and, at the same time, be implemented and tested on full-scale systems.

1.2 State of the art

1.2.1 Digital twin

A digital twin is a virtual model of a real system, process, or service [13]. The benefits of having a digital twin (DT) is that it enables realistic predictions of the physical asset. The DT can be used as a standalone model or in a cluster combined with other DTs. It can typically be used in two ways:

- as an offline unit for system performance predictions or virtual prototype testing.
- as an embedded unit with continuous data exchange with the real system.

An embedded DT is well suited for live decision support, predictive or diagnostic maintenance, decision making (automation), and process optimization. The DT enables advanced analysis of gathered data, which can be used to optimize a process or system, see the current need for maintenance, or predict future needs. The DT is also an excellent tool for development, such as testing new modifications or analyzing potential interaction of the physical twin with other systems or processes.

The concept of a digital twin was first introduced in 2002 by Michael Grieves [13]. Grieves describes three main parts of a DT: (1) the physical twin, (2) the virtual twin, and (3) a connection between the virtual and the physical twin. This concept is commonly accepted in the literature [13], [14]. However, some additional criteria are often added. Bacciega [15] states that a DT is a real-time digital replica of a physical device, and Miskins describes it as a near real-time copy [16]. On the other hand, other authors describe the digital twin as simulations of a system that uses the best available physical models [17], or that the DT is placed in cloud-services [18]. A combination of simulations with the most advanced models and/or cloud-based services will struggle to achieve real-time properties. All the different statements about a DT indicate that there are many variations of the concept Grieves presented. Madni et al. addressed this in 2019 [13] and divided the DT into 4 different levels, seen in Table 1.1:

Table 1.1: Levels of digital twins

Level	**Name**	**Model sophistication**	**Data acquisition from physical twin**
1	Pre-Digital Twin	Virtual system model	NA
2	Digital twin	Virtual system model	Batch updates
3	Adaptive digital twin	Virtual system model with adaptive UI	Real-time updates
4	Intelligent digital twin	Virtual system model with adaptive UI and reinforcement learning	Batch and Real-time updates

Level 1 is a pre-digital twin and is more of a traditional prototype model. The model is typically developed during concept design and engineering before the physical system is built. Hence, the model has no automated data exchange with the physical twin. Level 2 of a digital twin has exactly that, but the model is typically not real-time capable, and therefore data is received in batches. Level 3 is a digital model with the ability to adapt itself towards the physical twin. A model of such level will need advanced adaptive controllers such as supervised machine learning algorithms. Level-4-twins have the same capabilities as level 3, but have, in addition, unsupervised machine learning capability.

Madni's categorization covers a broad range of digital twins and also stresses that the user interface (UI) is essential when assessing which level the DT belongs to. There are other important aspects of digital twins that, in the author's view, are not covered by the above definitions. In a panel discussion [1], DNV GL pointed out that a DT can be seen as a cluster of functional elements or sub-models. These functional elements will be at different maturity levels and levels of sophistication, as shown in Fig. 1.3.

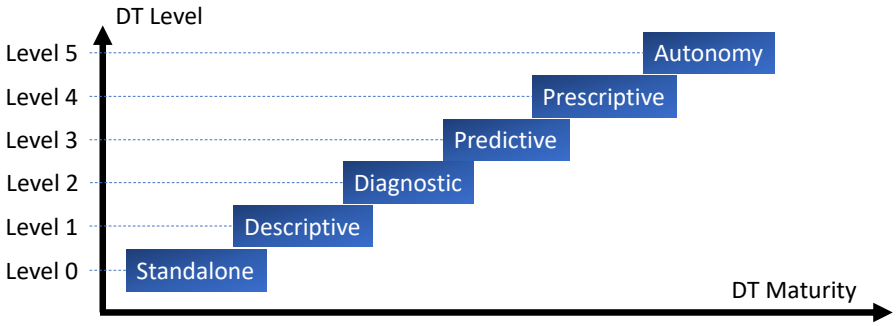

Figure 1.3: Levels of digital twins [1][2]

A pre-digital twin or a digital twin is a typical tool for virtual prototyping where an unproven, or non-validated and non-verified model, is used as a base for further modification or new product development. Hence, the use cases for a digital twin overlap the areas of what is known as virtual prototyping (Fig. 1.4).

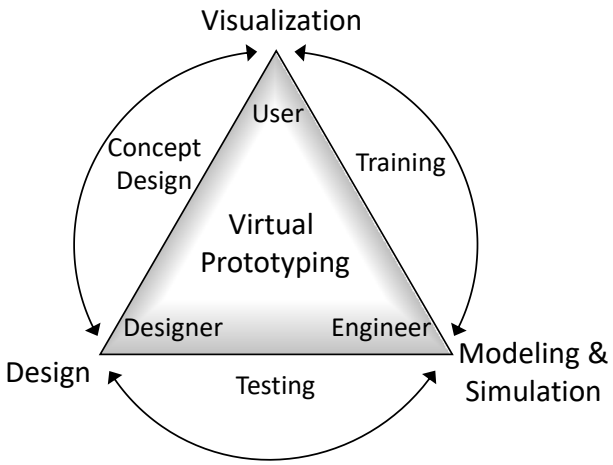

Figure 1.4: Areas of virtual prototyping [3].

For heave compensated offshore cranes, the use of digital twins is highly beneficial. Potentially, it allows for design optimizations, performance prediction, lift planning, and controller development that, depending on the level of the DT, are synchronized with the actual behavior of the physical crane. A significant challenge when developing a DT for a heave compensation system is the model accuracy, the costs associated with acquiring data from the physical system, and the need for validation and verification procedures.

1.2.2 Heave compensation

Heave compensation is used to decouple the vessel motion from the load, making it possible to lift and lower loads on the seabed safely. The vessels roll, pitch, and heave, affect the boom tip heave motion and cause the load to move relative to the fixed seabed (see Fig. 1.5). Heave compensation is a 1-dimensional compensation strategy, obtained by motion dampening or feeding an inverse motion reference to the crane-tip or wire. For larger cranes, wire control is used exclusively, i.e., the crane-tip is held fixed relative to the vessel. This is because the hydraulic cylinders that control the crane-tip must manipulate the mass of the crane-booms together with the payload. Furthermore, the hydraulic motors are symmetrical, and there is a linear relationship between the motor rotation and wire pay-out. Both of these advantages are absent when using the boom cylinders.

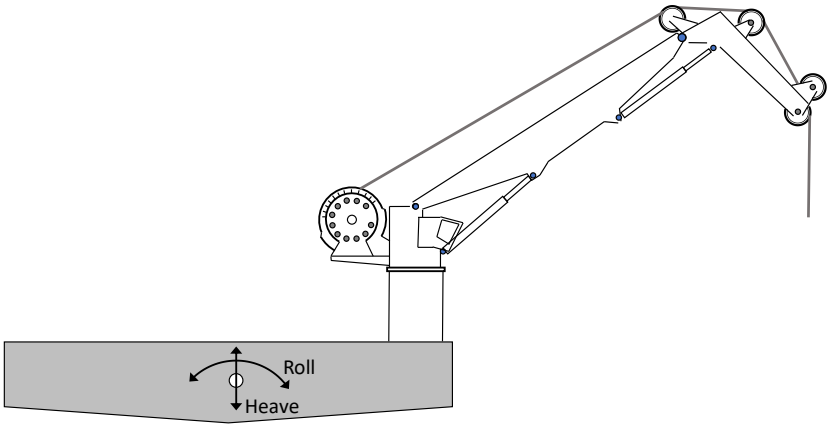

Figure 1.5: Heave and roll illustration

There exists three compensation techniques:

- Passive compensation
- Pure active compensation
- A combination of the two, called active/passive compensation

1.2.2.1 Passive heave compensation

A passive system (PHC) does not need any input energy [19]. Also, it is not subjected to any active control and, basically, corresponds to a large spring placed in series with

the suspended load and the hook. The spring must be pre-tensioned to the weight of the load and with a stiffness that yields an eigenfrequency well below the frequency of the waves. The passive heave compensation system acts as a mechanical low pass filter between the crane tip and the load. The spring is designed as a gas spring, using a hydraulic accumulator in series with a hydraulic cylinder and multiple gas bottles (see Fig. 1.6).

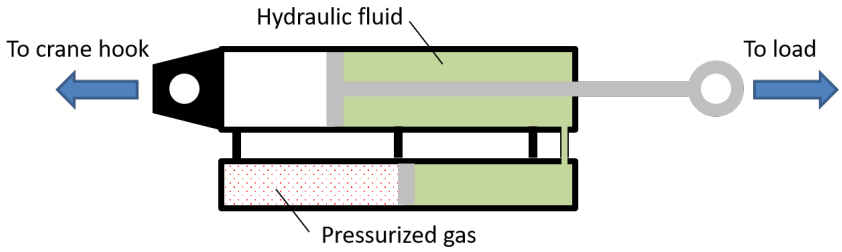

Figure 1.6: Simplified schematics for a PHC system

The method is still widely used by cranes that do not have integrated heave compensation, and several companies have specialized in making passive heave compensators, like Cranemaster® and Hydratech Industries®. PHC systems are proven to have a positive effect on tension variations in the wire while going through the splash zone and when landing payloads on the seabed [20]. The main problem with passive heave compensation is that the friction force acts as a significant disturbance that strongly reduces the low pass filter functionality [21][22],

1.2.2.2 Pure active and active/passive compensation

In contrast to a PHC system, an active HC system needs energy input and an active closed-loop controller. The system is designed to actively decouple the vessel movement from load movement by measuring the vessel motion, computing the vertical crane-tip motion, and extending or retracting the wire with the computed amount. The vessel movement is captured using an inertial measurement unit (IMU). The most widely used sensor in the offshore business is Kongsberg's Motion Reference Unit (MRU). Less advanced and more affordable sensors have been a research topic by many, to be able to make motion prediction or sensor fusion [23], [24]. So far, the crane manufacturers are reluctant to introduce this due to the aforementioned conservatism. The heave compensation is performed by extension and retraction of the wire. This is, in most cases, either done by the winch or a cylinder-compensator.

A cylinder-compensated system, as seen in Fig. 1.7, uses a hydraulically actuated cylinder in a pulley system to extract and retract the wire. The system is known for its low AHC control errors and high-velocity capabilities. Additionally, it enables retrofit of AHC on winches. The drawback is the limited stroke length and increased wire wear.

In general, the most common approach to heave compensation is AHC with direct winch control. The AHC control strategy is either pure active or active/passive. Pure active control means that the winch is controlled directly in one control loop.

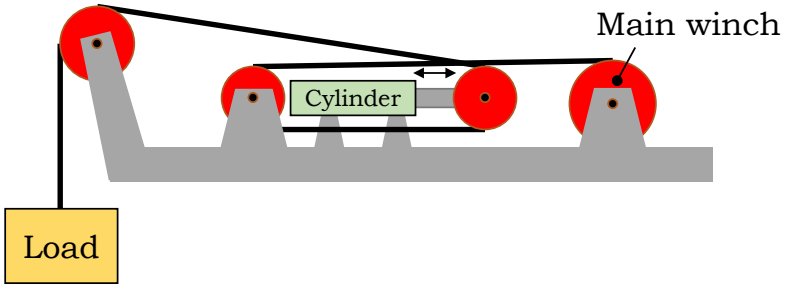

Figure 1.7: Simplified sketch of a cylinder-compensated system.

Hydraulic systems with pure active control are typically designed with an open-loop system with a directional flow valve or secondary motor-control, or a closed-loop hydraulic system with either primary pump-controlled system or a secondary motor-controlled system, see Fig. 1.8 – Fig. 1.12.

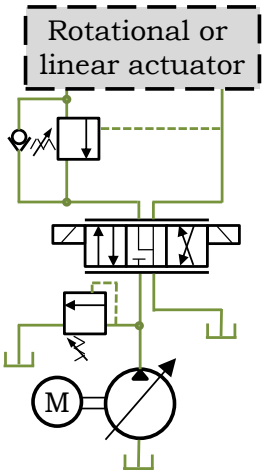

Figure 1.8: Simplified schematics for open-loop circuits with directional valve.

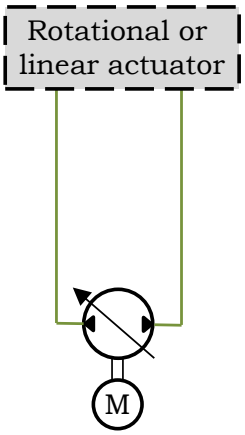

Figure 1.9: Simplified schematics for closed-loop circuits with primary pump control.

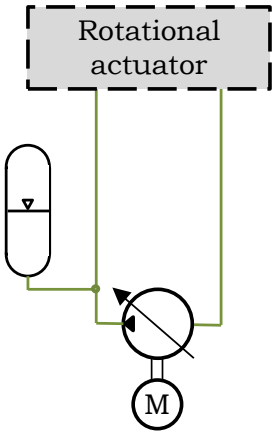

Figure 1.10: Simplified secondary controlled system schematics

For smaller winch systems with lifting capacity up to 50 t, the open-loop systems with a directional control valve are most common, see Fig. 1.8. These systems are common when relatively low amounts of flow are needed, and lifting capacity is low. The main benefits are low installation cost because it can be connected to a common pressure line system, a fast response time, and the availability of a wide variety of components. The main downside is low efficiency due to valve throttling losses, hence for a larger system up to 100 t, the typical system to be used at NOV and its competitors is the pure active closed-loop hydraulic system, see Fig. 1.9. These systems use primary motor-control and are much more efficient. However, the recuperated energy cannot be stored within the system and must be fed back to the vessel. For even larger winch systems, this becomes a challenge for two reasons. Firstly, the demand for installed power of the hydraulic winch system increases. Secondly, the significant recuperated amount of energy that is fed back to the vessel will require expensive equipment installed. Due to this, systems with energy

storage capacity are preferred for larger systems such as the pure secondary controlled systems with hydraulic accumulator banks seen in Fig. 1.12 or the active/passive systems seen in Fig. 1.11.

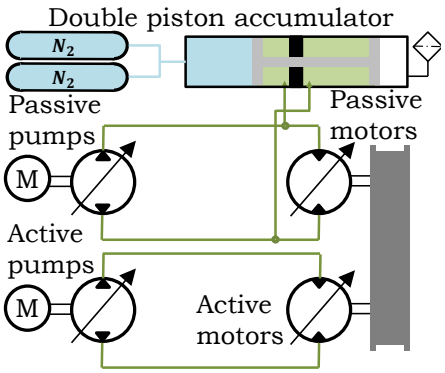

Figure 1.11: Simplified active/passive system schematics

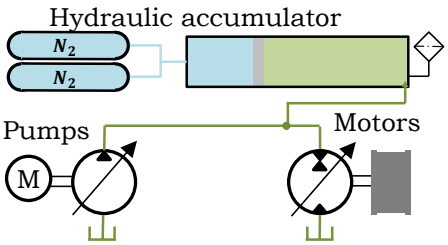

Figure 1.12: Simplified secondary controlled system schematics

An active/passive system is basically a winch with both a secondary controlled system (passive part) and a primary controlled system (active part) connected. The passive part of the system is torque-controlled to hold the passive weight of the load and store all recuperated energy. The active part is doing the positional winch control and uses the pumps as the primary controller, see Fig. 1.11. In NOV, the active/passive system is the preferred choice compared to pure secondary, see Fig. 1.12. This is related to the disadvantages associated with secondary control, such as higher cost and an increase in control complexity and more error-prone systems [25].

1.2.3 Friction losses in hydraulic motors

Modeling of hydraulic motors and particularly their hydromechanical losses have been a research topic for several decades. The original work in this area comes from Wilson [26] and Schlösser [27]. Both had relatively simple models, were Wilson included dry friction proportional to shaft torque, viscous friction proportional to a viscosity(μ), and speed(ω_m), and a constant torque loss (Eqn. 1.1).

$$T_f = C_a \cdot D_{m,max} \cdot \Delta p_m + C_b \cdot \mu \cdot D_{m,max} \cdot |\omega_m| + C_c \cdot D_{m,max} \tag{1.1}$$

Schlösser [27] replaced Wilson's last term with a term for the acceleration of the liquid. He assumed a loss term proportional to the square of the tangential velocity of the revolving barrel of an axial piston machine.

$$T_f = C_a \cdot D_{m,max} \cdot \Delta p_m + C_b \cdot \mu \cdot D_{m,max} \cdot |\omega_m| + C_d \cdot D_{m,max}^{5/3} \cdot \rho \cdot \omega^2 \tag{1.2}$$

Both of these models attempt to replicate physical phenomena in the axial piston pump/motor. Unfortunately, both models fail to achieve decent accuracy for the entire

3-dimensional workspace, including torque, displacement, and rotational speed [28]. Numerous attempt to improve these models have been made (see Table 1.2), and the different types of models can, in general, be divided into three categories:

- models based on physical interactions in the motor (or pump)
- numerical models based on curve fitting to experimental data
- analytical models that are based on both numerical and physical models

Table 1.2: Summary of steady state loss models for hydraulic pumps/motors [8]

Author	**Year**	**Model type**
Wilson [26]	1948	Physical
Sclösser [27]	1961	Physical
Olsson	1973	Physical
Pacey, Turnquist and Clark	1979	Physical
Zarotti and Nevegna	1981	Analytical
Bavendiek	1987	Physical
Dorey [29]	1988	Analytical
Ivantysyn, Ivantysynova	1993	Numerical
Kögl	1995	Physical
Huhtala	1997	Numerical
Baum	2001	Numerical
Ortwig [30]	2002	Numerical
Jeung [31]	2006	Physical

In general, it is seen that the complexity and number of adjustable parameters included in the models have increased. This is due to increased knowledge about how and where the losses occur. The losses mainly occur between sliding surfaces within the motor but also due to friction losses within the liquid. The most significant sliding surfaces in the motor, see Fig. 1.13, are associated with sliding between the pistons and the barrel, between the barrel and port plate, and between the pistons' joint-surface in the shaft flange.

Increased complexity occurs when phenomena like non-uniform gap heights are considered. As an example, the gap height between the rotating barrel and the port plate can be studied. The gap between these two components has a significant effect on leakage and friction. Manring [32], showed a relationship between barrel tipping and rotational speed. Later, in 2017, Achten [33] showed that the operating pressures have an even more significant effect on the barrel tipping. In addition, there will be tribological effects due to the properties of the sliding surfaces and the hydraulic oil. Miller et al. [34] concluded that under low-speed, high-torque conditions, the hydraulic motors operate in a boundary regime and mixed friction. Therefore, hydraulic fluid additives will have a significant impact on friction and wear.

A place of leak and friction is between the swash-plate and slippers, where the tribology and lubrication effects have been a topic of research in addition to alternative component geometry of these components [35], [36].

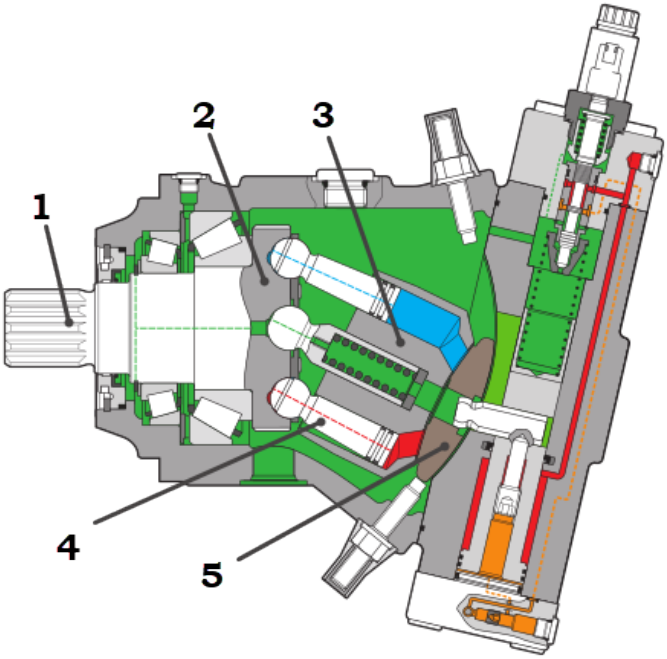

Figure 1.13: Cross section of a bent axis motor with variable displacement. Output shaft (1), shaft flange (2), barrel (3), piston (4), port plate (5)

The complexity of hydraulic motors is a contributing factor to why these models have been a research topic for over 70 years. Huhtala made a comparison of currently existing models in 1997 [28] and presented a numerical model that should increase the accuracy significantly. The model was for fixed displacement motors and introduced a set of 14 parameters. Ortwig [30] and Jeong [31] later established an even more detailed overview of the losses in the axial piston motor. In 2017 Jeong presented a model for torque and flow losses in axial piston motors [37] where he combined similar terms in the model and reduced the number of parameters to six. However, the model was independent of the displacement and, therefore, not directly useful for variable displacement motors.

1.3 Problem statement

As the worldwide demand for a reduced cost in offshore operations increase, the need for cost reduction within crane operations is significant. There are at least three ways to deal with this problem. One, exploit more of the full potential of the cranes. In that way, operators do not need to hire expensive vessels at high rates. However, this is not a trivial thing to do since it requires higher accuracy when predicting the potential crane load dynamics. The desired solution for this challenge is to have high-fidelity models verified to attain the needed accuracy. These models can then be used during lift planning and dynamic load analysis, and a higher crane capacity can be utilized. Another way to achieve the crane capacity increase is to enable the crane itself to utilize a higher proportion of the installed power. Better crane controllers can achieve this. A third option is to develop new technology or new functionality better suited for the specific crane operation. The key challenges when introducing new technology and functionality are to convince the client to buy it and the user to use it. The end-user/operator will rarely be capable or allowed to test out new functionality without having documentation on the actual real-life impact of using the system.

Based on an active heave compensated winch with closed-loop hydraulic circuits, combined with the aforementioned challenges and the state-of-the-art in digital twins, heave compensated systems and loss modeling in hydraulic motors, the two main scientific questions to be answered in this PhD-project are:

- Is it possible to develop a dynamic model of a heave compensated winch system that allows for lift planning?
- It is possible to develop new controllers that increase the utilization rate of heave compensated winches?

1.4 Methodology & contributions

The motivation for the current project has been to increase the weather window for offshore operations dependent on active heave compensated cranes. The main demarcation has been to look for improvement in the utilization of the existing winch systems, i.e., improve the controller rather than redesign the heave compensation system. Due to the challenges associated with prototype testing, the overall approach has been heavily model-based. However, experimental work has been used to develop and validate the simulation models and to verify the developed controller.

This has led to the following main contributions: Firstly, a new friction loss model has been developed for the hydraulic motors used in the heave compensated winches. Secondly, a total friction model has been developed for the remaining friction associated with the total mechanical transmission from the output shaft of the hydraulic motors to the wire hook holding the payload. Furthermore, these models have been implemented in an existing simulation model, a digital twin, of the entire heave compensated crane. Thirdly, a new control method utilizing the variable displacement of both the hydraulic pumps and the hydraulic motors has been developed. With the latter being a feedforward

design to reduce risks of instabilities and, simultaneously, maintain controller robustness, i.e., no new sensors of feedback loops have been added. This new controller has been implemented in the previously mentioned digital twin, yielding a tool that can be used for non-conservative model-based lift planning with expanded weather windows as a result. Finally, a method for experimental validation of a digital twin to be used in lift planning for active heave compensated equipment has been put forward. All the work has been verified and validated by numerous full-scale experimental tests that have been carried out at the quay-side, as well as offshore.

1.5 Summary of papers

1.5.1 Paper A - A model for torque losses invariable displacement axial piston motors

Summary: This paper presents some earlier presented models for modeling torque loss in hydraulic axial piston motors. In addition, some new models based on previous work from Jeong and Kim [31] were introduced. The goal was to make relatively simple torque loss models that also worked for variable displacement motors. Torque loss data was retrieved from Bosch Rexroth, which is a significant supplier of axial piston motors to the offshore crane industry. A set of models was then optimized based on this data and compared. The new model designs showed very good accuracy in a large window of operational range. Down to 50 % motor displacement setting and 15 % of maximum speed, the torque deviation was less than 1 % of nominal torque output.

Contributions: Several torque models were investigated to be used for variable displacement axial piston motors. The new preferred model is relatively simple with few parameters to be adjusted. This contrasts with many of the alternatives that are published, which often include many parameters. The number of parameters will in most cases increase the complexity and decrease the usability of the model. The model proposed in this paper is therefore a good alternative to complex models and shows good performance in a large operational region.

Published as: Geir-Arne Moslått, M. R. Hansen, and N. S. Karlsen. A model for torque losses in variable displacement axial piston motors. *Modeling, Identification and Control*, 39(2):107-114,2018.

1.5.2 Paper B - Modeling of friction losses in offshore knuckle boom crane winch system

Summary: This paper presents a method for measuring and modeling the friction losses in the winch system in an offshore knuckle boom crane. The paper includes some measurements taken on a real offshore crane under several different load conditions. The friction modeling is divided into two parts, motor model, and system model. The motor model is based on the model designed and defined by the method described in paper A. The system friction is the remaining torque loss and is defined by subtracting the estimated motor loss from the total loss. A model was then created to fit the remaining loss.

Contributions: The paper presents friction measurements of a full-scale offshore crane with a lifting capacity of up to 150 tons. The total losses are modeled and the deviation between the modeled and the measured loss was shown to be less than 2 % of nominal load applied. The paper showed a new way of determining winch friction loss in offshore winch systems.

Published as: Geir-Arne Moslått and Michael R. Hansen. Modeling of friction losses in offshore knuckle boom crane winch system. In *2018 Global fluid power society PhD symposium, GFPS 2018*, pages 1-7. IEEE, 2018.

1.5.3 Paper C - A control algorithm for active/passive hydraulic winches used in active heave compensation

Summary: This paper explains how state-of-the art active heave compensated cranes are controlled and proposes a new method that uses more active control of the hydraulic motors in the active part of an active/passive hydraulic system. A prototype of the new controller is tested in a state-of-the art simulation model giving the results high credibility.

Contributions: The new control strategy is shown to have several positive effects on the dynamic properties of the system. Additionally, the new controller is able to improve the overall performance with regard to wire speed capability and control error. The low-speed performance is improved, and the winch speed capacity is increased up to 30 %, while the system peak pressures are reduced.

Published as: Geir-Arne Moslått, Damiano Padovani, and Michael R. Hansen. A control algorithm for active/passive hydraulic winches used in active heave compensation. In *Proceedings of the ASME/BATH 2019*, Sarasota 2019. Symposium on fluid power and motion control.

1.5.4 Paper D - Practice for determining friction in hydraulic winch systems

Summary: This paper explains the current practice to measure and model friction of a winch system.

Contributions: This paper presents a method for estimating friction in hydraulic active heave compensated (AHC) offshore winches. The method is a two-step approach. The first step is to model the friction loss in the hydraulic motors based on data from the sub-supplier. The second step requires an amount of real-life testing where the remaining friction losses in the winch system is identified and modeled. In this context, the practice is characterized by obtaining a friction loss estimation with the highest possible accuracy over the widest possible range of operating conditions with a limited amount of experimental work. The method benefits from the use of parametric models together with sub-supplier data, and real-life measurements on a 150 t AHC crane from National Oilwell Varco Norway (NOVN). The work forms an important part of the development of a simulation model that can be used actively in virtual testing and verification of crane operations at NOVN. A friction loss model developed from the proposed method was implemented in a NOVN simulation model, and computed and measured hydraulic pressures showed deviations of less than 10 % from measured results for a 150 t crane operating in AHC.

Published as: Geir-Arne Moslått, Michael Rygaard Hansen, Practice for determining friction in hydraulic winch systems. Modeling, Identification and Control. 2020, Vol 41, No 2, pp. 109-120. DOI: 10.4173/mic.2020.2.6

1.5.5 Paper E - Performance Improvement of a Hydraulic Active/Passive Heave Compensation Winch Using Semi Secondary Motor Control: Experimental and Numerical Verification

Summary: This paper shows numerical and experimental tests of the semi secondary control approach in an active/passive, hydraulic, heave compensated system.

Contributions: Experimental testing of the semi secondary control approach has never before been done. The experimental testing was performed on a full-scale 250 t offshore crane, which is unique for this field of research. The results confirm the significant impact of the motor displacement in closed-loop hydraulic circuits and explicitly show the positive benefits of controlling both motors and pumps with a semi secondary control approach.

Published as: Geir-Arne Moslått, Michael Rygaard Hansen, Damiano Padovani, Performance Improvement of a Hydraulic Active/Passive Heave Compensation Winch Using Semi Secondary Motor Control: Experimental and Numerical Verification. Energies 2020, 13, 2671. DOI: 10.3390/EN13102671

1.5.6 Paper F - A digital twin for lift planning with offshore heave compensated cranes

Summary: The paper presents a digital twin of an active heave compensated winch system and acceptance criteria for models to be used in lift planning.

Contributions: Simulation models are becoming a commonly used tool for planning offshore lifting operations. However, a common verification method to ensure that a model is a sufficiently accurate representation of the real system does not exist. So far, the classification societies do not have any performance criteria for models to be used in lift planning. However, they do have some guidelines for conservatively estimating compensation efficiency, but the conservative approach often results in great limitations of the planned lift. This paper presents a digital twin for an active heave compensated winch and a set of acceptance criteria by which to ensure acceptable performance. The

model presented shows an acceptable accuracy, with an AHC position control error that deviates on average by less than 5 cm from that of the real system.

Published as: Geir-Arne Moslått, Damiano Padovani, Michael Rygaard Hansen, A digital twin for lift planning with offshore heave compensated cranes. In Journal of Offshore Mechanics and Arctic Engineering. 2020. pp. 1-29.

Chapter 2

Contributions

2.1 Loss modeling in heave compensation

The most common hydraulic heave compensation system delivered by NOV is the active/-passive hydraulic winch system, seen in Fig. 2.1. The active/passive system is a mature technology in the offshore crane industry, and with its combined active and passive functionality, it enables winch system design with large load capacity compared to pure active systems.

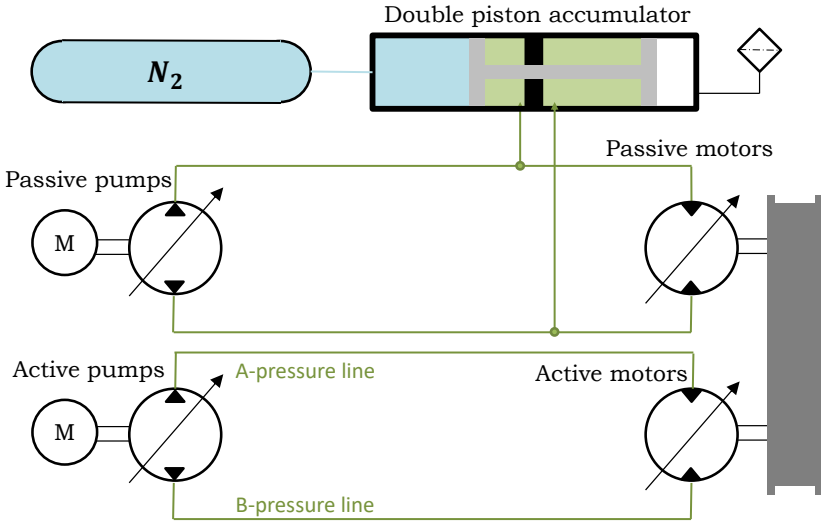

Figure 2.1: Simplified overview of an active/passive hydraulic winch system [4].

The system is divided into two parts, an active and a passive, where both systems are connected to the winch through a gear rim connection. The passive system is a load-holding system with a defined high-pressure and low-pressure side. The high-pressure side is connected to a high-pressure accumulator to maintain constant pressure, and the motor torque is adjusted with the use of variable displacement motors. The passive pump is compensating for piston leakage in the accumulator and leakage in the passive pumps and motors. In the other part, the active system must absorb all friction losses and inertia accelerations of the winch components. The displacement of the active pump is

continuously adjusted to meet the motion reference required to achieve the desired winch performance.

NOV also delivers purely active systems without any passive part. To ensure that the developed control methods can be utilized by both purely active and passive-active systems, this project has focused on control development within the active system.

The classic way to control an active system is to fix the motor displacements and use the active pumps as primary controllers. The primary control strategy poses two significant challenges. Firstly, it causes a limitation on the maximum wire speed and, secondly, it is observed that the most significant contributor to control error during heave compensation is when the winch motion is changing the direction of rotation. The error is caused by stick-slip behavior in the entire power transmission from the hydraulic motor to the payload. In-field experience shows that the combination of stick-slip and small motor displacement in the active system has a significant impact on the oscillations, both hydraulically and structural, of the winch system.

The active system must react to disturbances caused by friction, acceleration, and interaction between the payload and the sea. Also, the effective speed transmission ratio is affected by leakage in the hydraulic components. The leakage models used in this project for pumps and motors are presented in section 2.5.2.4. They are relatively simple and benefit from the oil temperature control systems that are used in the considered offshore cranes. Because of that, the oil temperature is neglected in the models.

The most elusive disturbance parameter is the friction loss. A winch system involves several friction loss components. Between the hanging load and the hydraulic pumps, there are the torque-losses in the hydraulic motors, the gearboxes, the gear rim transmission, the drum bearings, the wire sheaves, and within the wire itself. The main components are seen in Fig. 2.2.

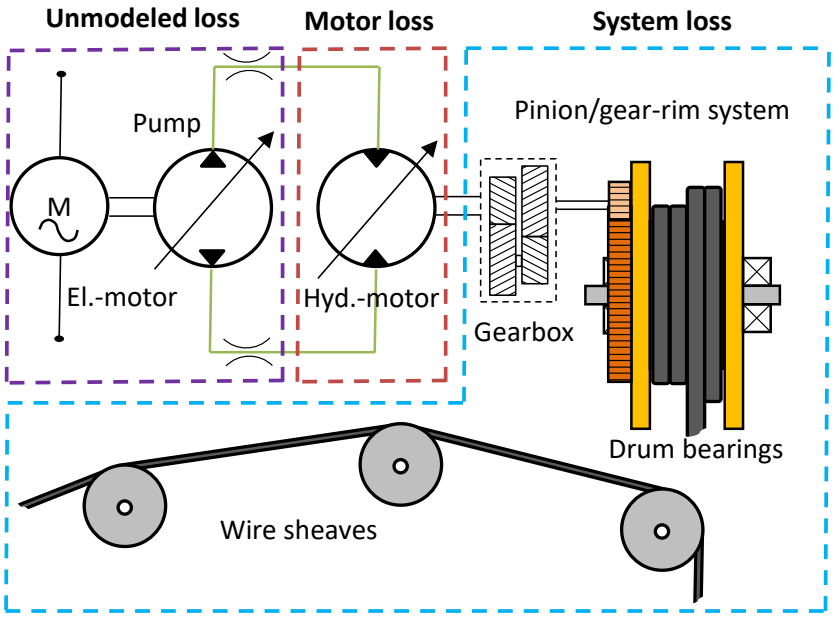

Figure 2.2: Simplified overview of a winch system [5].

Due to the importance of friction, this PhD-project started out by doing in-field tests

of the cranes as elaborated in section 2.2. The main conclusion from the in-field testing-results and measurements was a clear indication that it would not be feasible to create a friction model for the whole winch system without breaking it into submodels. At the same time, it was not possible to measure friction losses component by component. The only feasible way to measure the friction within the time- and budget limitations of the project was to estimate it based on pressure sensors in the hydraulic system, hence the friction measured includes everything from motors and out to the payload. A method was developed that divides the friction into two parts; motor friction and system friction. The background for this is the complexity of the friction losses in the motors, as well as the fact that, normally, a sub-supplier will have measurements available that map the efficiency of the motor in the normal operational range. The system friction is the lumped friction of all the measured friction, except the motor friction. The motor friction is estimated from sub-supplier data, and the system friction is estimated based on the motor friction model and measurements. The process of estimating the friction is explained in section 2.3. Thus, the new approach required sub-supplier data and a friction loss model for the winch motors. No existing models were found in the literature that described the loss satisfactory, so a new model was developed, see Paper A and D. Having the motor model in place enabled a continuation of in-field testing and the development of a model to estimate the remaining as well as the total friction in the winch system (2.3).

The developed friction model of the system was implemented in a full digital twin model of the entire winch system. Further, the digital twin has been used to implement a prototype of the new controller and to test it. After successful simulation results, the controller was tested on a real crane, and the results were analyzed (Fig. 2.3).

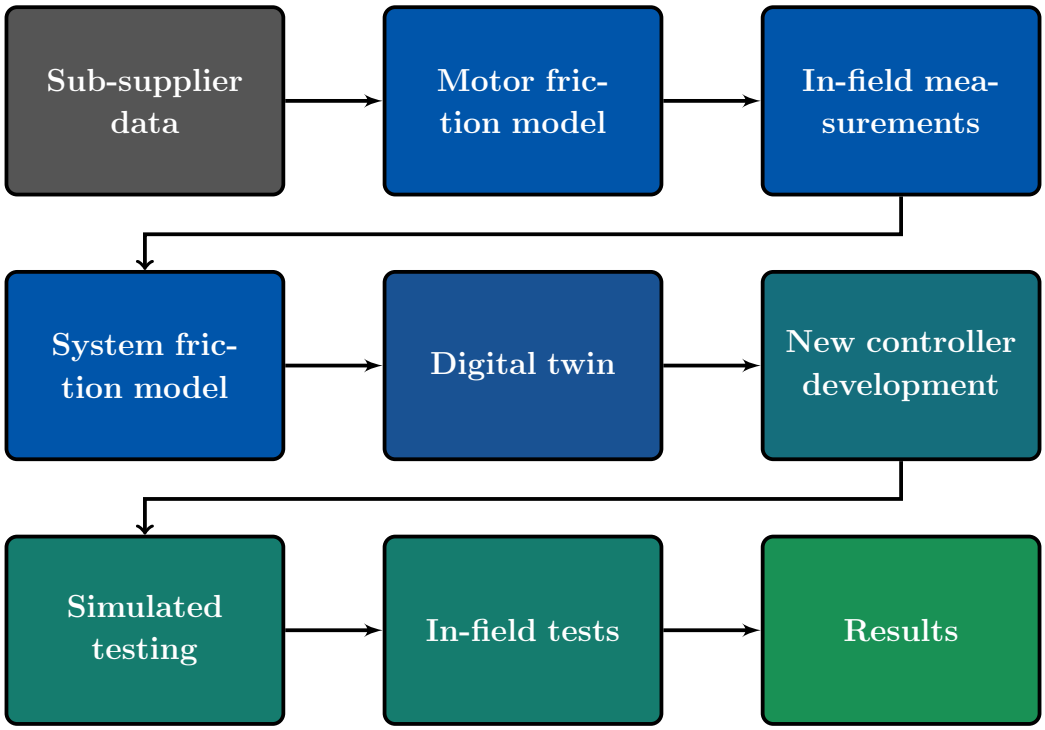

Figure 2.3: Project methodology.

Section 2.5.2 presents the model structure of the digital twin model, while the digital

twin concept is discussed in section 2.6. In section 2.4 the new controller is presented and in section 2.7 it is tested and verified.

2.2 In-field measurements

Figure 2.4: Crane L4571, tested in Kristiansand Norway [6].

When working with friction modeling, it is quickly revealed that the sub-suppliers of components other than the motors, did not have the necessary information about friction losses in their components. Most of them operate with fixed efficiency factors, i.e., losses that are linearly dependent on the load but not the speed. Because of this, they will only be valid for a small range of the operational window and in most cases the information on where the given efficiency factor is valid is not given either. Thus, the only proper way to get a realistic picture of the friction is to do some real-life measurements. It was decided to do testing on fully assembled cranes, and to analyze the data to get an understanding of the actual losses. In Table 2.1, the set of cranes that has been tested is shown.

Table 2.1: Tested cranes

No.	Description	Date	Location	Size	Type
1	V6842 Metro II	Q4 2011	Korea	165 t	Active/passive AHC
2	F7937 Noble	Q2 2013	Korea	165 t	Active/passive AHC
3	G1721	Q3 2014	Denmark	50 t	Pure active AHC
4	G1771	Q3 2014	Denmark	50 t	Pure active AHC
5	G1780	Q4 2014	Denmark	50 t	Pure active AHC
6	F9627 Rowan	Q4 2014	Korea	165 t	Active/passive AHC
7	G1257 West Jupiter	Q4 2014	Korea	165 t	Active/passive AHC
8	L2714	Q4 2014	Norway	250 t	Active/passive AHC
9	F6271 ENSCO 5006	Q1 2015	Australia	165 t	Active/passive AHC
10	L2756 Edda Freya	Q2 2016	Norway	70 t	Pure active AHC
11	G8439 Harvey Interv.	Q4 2016	USA	165 t	Active/passive AHC
12	L4501 Deep Explorer	Q4 2016	Norway	58 t	Pure active AHC
13	L4593 Scandi Vinland	Q2 2017	Norway	100 t	Pure active AHC
14	L5029	Q3 2017	Korea	150 t	Active/passive AHC
15	L4571	Q2 2018	Norway	150 t	Active/passive AHC
16	F1799 Polar Onyx	Q2 2019	Ghana	250 t	Active/passive AHC
17	L4526 Island Victory	Q3 2019 Q4 2019	Norway	250 t	Active/passive AHC

In general, all of this experimental work was used extensively in the modeling development of the winch system. More specifically, no. 1 and no. 11 were referenced directly in paper C, whereas no. 14 and no. 15 were referenced in paper B, no. 14 and no. 15 was also referenced in paper D, no. 17 was referenced directly in paper E, and no. 16 was referenced directly in paper F.

Gathering and post-processing these data was not trivial, and there were mainly three

challenges. Firstly, it is not easy to get the necessary time needed to perform the tests. The cranes are either sent to a customer, waiting for shipment, or subjected to internal testing. All these stages are planned in a rigid time-schedule with substantial economic consequences if deadlines are not met. These obstacles have been solved by proper planning, working night-shift, exploiting delays, and combining scientific experiments with regular internal testing. Secondly, access to the desired measurement points may not be possible. A full, in-depth measurement, of the losses in each winch component, is unlikely to happen. The result has been to rely on a minimum of sensors. In this case, the high priority sensors were pressures on each side of the motor, a tachometer measure the speed of the winch, and a load cell placed inside one of the wire sheaves measuring the crane-tip-load. With these sensors, a combined friction loss from hanging load to hydraulic motors was measured. Thirdly, performing post-processing on a large amount of data that is not standardized is time-consuming. Since the crane had to be operated with real clump-weights, and the winch would be hoisting and lowering with high speeds during the testing, a standardized, automated sequence would not be possible without a substantial amount of programming hours. The fact that the crane had to be run manually rather than subjecting it to standardized tests also added to the workload because new data handling programs had to be coded for each measurement that ensured the correct timestamp for the data.

The main goal was to measure the pressure close to the hydraulic motors at steady-state pump command, displacement, and speed. Steady-state values were then gathered for different pump settings, different motor displacement, and different winch loads. The steady-state values were gathered by running the winch system with fixed motor displacements and fixed pump command until the winch ran with a steady speed. One sequence of testing consisted of an alternating pattern between hoisting and lowering while increasing the pump command for each time, as illustrated in Fig. 2.5. During a sequence like this, the hook load and motor displacement were kept constant.

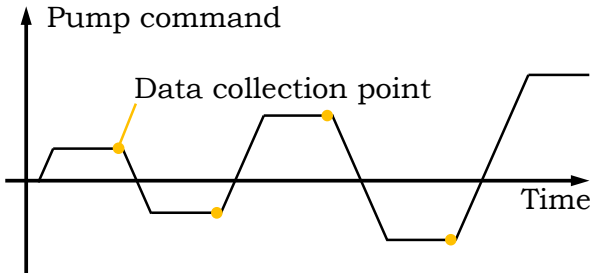

Figure 2.5: Shape of pump command during friction test sequence.

This pattern was executed for the whole pump command range, and the data was extracted from the last part of the steady-state situation to ensure stabilized pressures and velocities. At these measuring points, the pressures and winch velocity were registered. By assuming that all losses work opposite to velocity, it is possible to calculate the actual loss by comparing the pressure drop over the motors while hoisting and lowering with the same velocity. Since the steady-state measured velocities for hoisting and lowering are not the same (mainly due to leakage), the pressure values are interpolated such that the

two sequences are comparable with regards to the winch velocity. From this point, the pressure difference can be calculated.

$$\Delta p_m = p_{mA} - p_{mB} \tag{2.1}$$

$$\Delta p_m^{(wu)} = \Delta p_L + \Delta p_F \qquad \text{(winch up)} \tag{2.2}$$

$$\Delta p_m^{(wd)} = \Delta p_L - \Delta p_F \qquad \text{(winch down)} \tag{2.3}$$

Where $\Delta p_m^{(wu)}$ is the pressure drop across the motor when hoisting and $\Delta p_m^{(wd)}$ when lowering, respectively. Δp_F is the total friction losses and Δp_L is the pressure difference due to the winch load. When the pressure differences are known, the friction loss as a pressure drop is derived from the equations (2.2) and (2.3):

$$\Delta p_F = \frac{\Delta p_m^{(wu)} - \Delta p_m^{(wd)}}{2} \tag{2.4}$$

An example of the friction pressure-loss, Δp_F, from crane F6271 is seen in Fig. 2.6. The friction torque at the given speed is derived by multiplying with the motor displacement.

$$T_f = \Delta p_F \cdot D_m \tag{2.5}$$

,where D_m is the motor displacement on each motor and T_f is the friction loss as torque on each motor shaft. Total loss, T_{ft}, will be the friction pressure multiplied with the total displacement, D_{mt}. An example of the resulting friction torque, T_f, applied to each motor shaft is seen in Fig. 2.7.

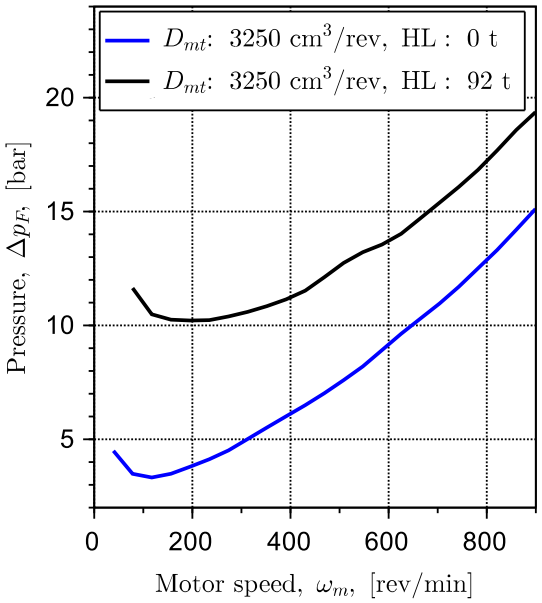

Figure 2.6: Friction pressure, Δp_F from two tests on crane F6271.

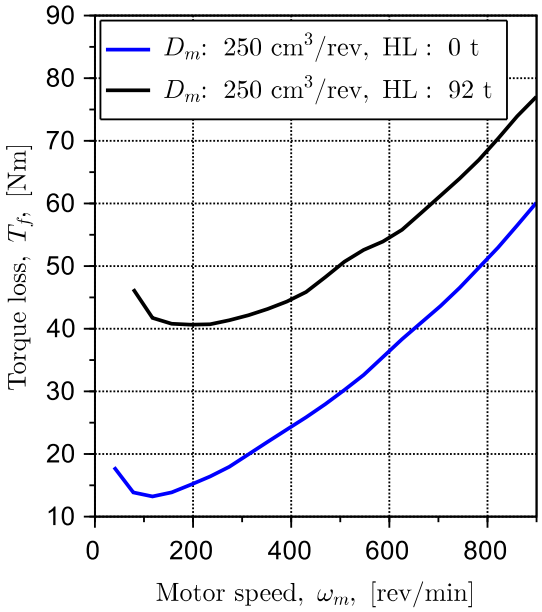

Figure 2.7: Friction torque, T_f from two tests on crane F6271.

2.3 Friction modelling example

When the friction model of a crane is needed, the best practice workflow, established from paper D and shown in Fig. 2.8, is used.

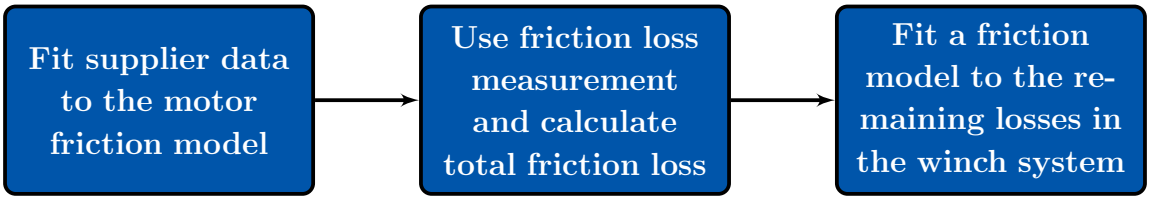

Figure 2.8: Workflow flowchart.

In the following sections an example of this method is being used on crane L4593, seen in Fig. 2.9. L4593 is an active heave compensated crane with a lifting capacity of up to 100 t.

Figure 2.9: Photo of the L4593 crane.

The motors used on L4593 are six Bosch Rexroth A6VM NG215. They are connected to the winch through a gearbox and a pinion and ring gear system as seen in Fig. 2.10.

Figure 2.10: Motor and pinion system on L4593

2.3.1 Motor friction model

The friction model for this motor can be found in the paper A [38] and is shown in Eqn. 2.6. The friction loss for each motor shaft, T_{fm}, is calculated based on the rotational speed of the motor shaft, ω_m, motor displacement, D_m, and the pressure drop across the motor, Δp_m. The optimal parameter set is found by the use of sub-supplier data and optimization routines. This work is already conducted and shown in paper B [39], with the results seen in table 2.2.

$$T_{fm} = X_1 \cdot \omega_m + X_2 \cdot \omega_m^2 \cdot D_m^3 + X_3 \cdot \Delta p_m \cdot D_m + X_4 + X_5 \cdot {\Delta p_m}^2 \tag{2.6}$$

The motor friction model is supposed to have similar losses as derived from the hydromechanical efficiency data provided by the supplier. The model includes Coulomb and viscous friction, turbulent flow losses across notches and valves, and some high-pressure losses.

Table 2.2: Friction model parameters for Bosch Rexroth A6VM hydraulic motor

$\mathbf{D_{m,max}}[\mathrm{cm^3/rev}]$	215	$\mathbf{X_3}[-]$	0.0050
$\mathbf{X_1}[\mathrm{Nm \cdot s}]$	$4.05 \cdot 10^{-3}$	$\mathbf{X_4}[\mathrm{Nm}]$	14.0
$\mathbf{X_2}[\frac{\mathrm{N \cdot s^2}}{\mathrm{m^8}}]$	$3.69 \cdot 10^{10}$	$\mathbf{X_5}[\frac{\mathrm{m^5}}{\mathrm{N}}]$	$1.16 \cdot 10^{-14}$

In Fig. 2.11, the comparison between the table data from the sub-supplier and the model is shown. Since sub-supplier data is extracted from a table, values are interpolated to achieve a continuous curve.

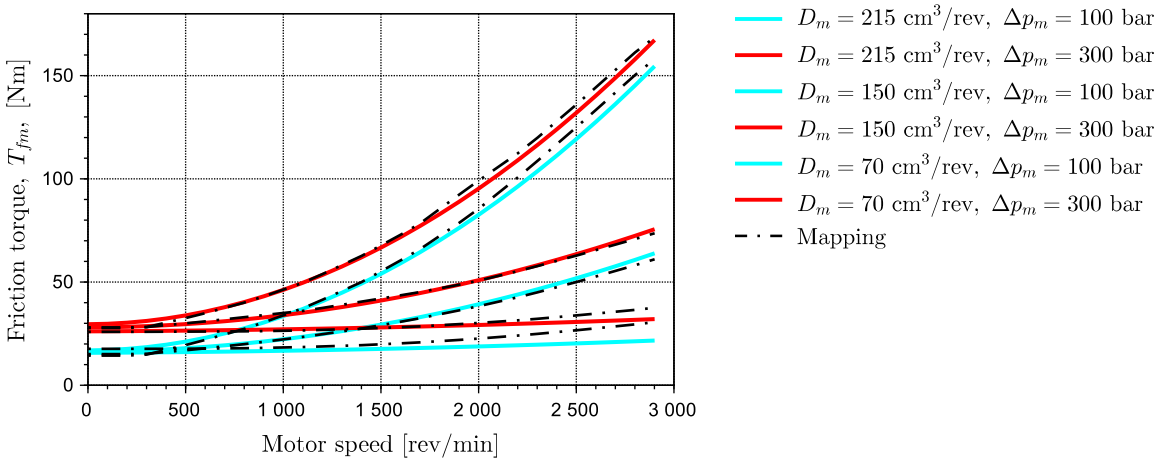

Figure 2.11: A comparison between the friction data given from supplier (mapping) and the model.

2.3.2 Friction measurements

The next step is to use friction measurements performed on the crane, seen in Fig. 2.12, to identify parameters for the remaining friction, which in this context is referred to as the system friction. This crane was tested in April 2017, and friction estimates were extracted. The data consists of a wide range from 0-100 % SWL and a displacement range from 120 cm^3/rev to a full 215 cm^3/rev per motor. The gathered set of tests are shown in Table 2.3.

Table 2.3: Friction tests performed on L4593

No.	D_{mt}	Hook load
#1	720 cm^3/rev	0 t
#2	960 cm^3/rev	0 t
#3	1120 cm^3/rev	0 t
#4	1290 cm^3/rev	0 t
#5	720 cm^3/rev	55 t
#6	960 cm^3/rev	55 t
#7	1120 cm^3/rev	55 t
#8	1290 cm^3/rev	55 t
#9	1120 cm^3/rev	100 t
#10	1290 cm^3/rev	100 t

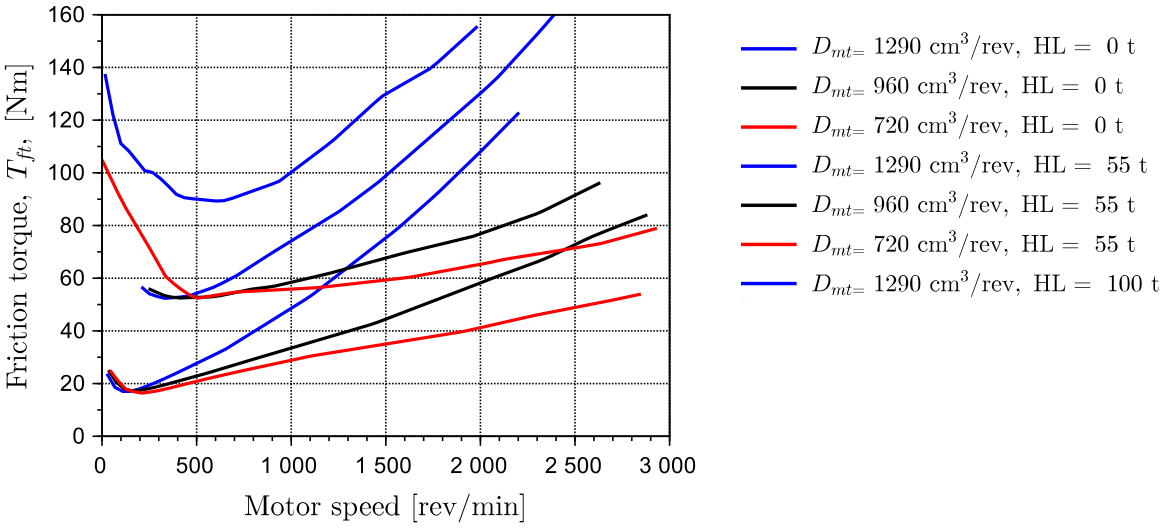

Figure 2.12: Total friction torque, measured at the hydraulic side of the motor. HL is the attached hook-load during the test sequence.

2.3.3 System friction model

Now for the last step of the workflow shown in Fig. 2.8, where the model for the remaining system is defined. The remaining system is simply the whole winch system except the

hydraulic system and the hydraulic motors. The model to represent the system friction is presented in papers B [39] and D, and shown in Eqn. 2.7.

$$T_{fs3} = (Y_1 \cdot T_d + Y_3) \cdot e^{\frac{-|\omega_m| \cdot 60}{Y_4 \cdot 2\pi}} + Y_2 + Y_5 \cdot \omega_m + Y_6 \cdot T_d \tag{2.7}$$

The parameters, Y_{1-6} were found by use of the so called complex optimization method [40][41] mentioned in paper B. The optimization routine is an iterative process working on a design population. In each iteration the procedure aims to improve the worst design set in the population by mirroring it in the design centroid (point in design space) of the remaining design. In this case, the size of the population was set to 36 and the initial population was generated as random designs within a defined boundary for each parameter. The test-data includes a displacement range from 120 cm^3/rev to 215 cm^3/rev for the hydraulic motors, and the test-loads included were in the range of 0 t to 100 t. The chosen data for optimization were datasets 4, 5, 6, 7, 8, 9, and 10 (see Table 2.3). The model parameters were identified by minimizing the squared error between the measured friction and the modeled, seen in Fig 2.13. The error was calculated over the whole range of measured velocities (from i_{min} to i_{max}) with an iteration step of 25 rev/min. The squared error for each step was summarized to the total cost, E (Eqn. 2.8).

$$E = \sum_{test=4}^{10} \sum_{i=i_{min}}^{i_{max}} (T_{ft} - (T_{fs} + T_{fm}))^2 \tag{2.8}$$

Table 2.4:
Optimized system friction parameters

$\mathbf{Y_1}[-]$	$\mathbf{Y_2}[Nm]$	$\mathbf{Y_3}[Nm]$	$\mathbf{Y_4}[\frac{rev}{min}]$	$\mathbf{Y_5}[Nm \cdot s]$	$\mathbf{Y_6}[-]$
$474 \cdot 10^{-7}$	3.9	0.000084	178	0.0038	$328 \cdot 10^{-7}$

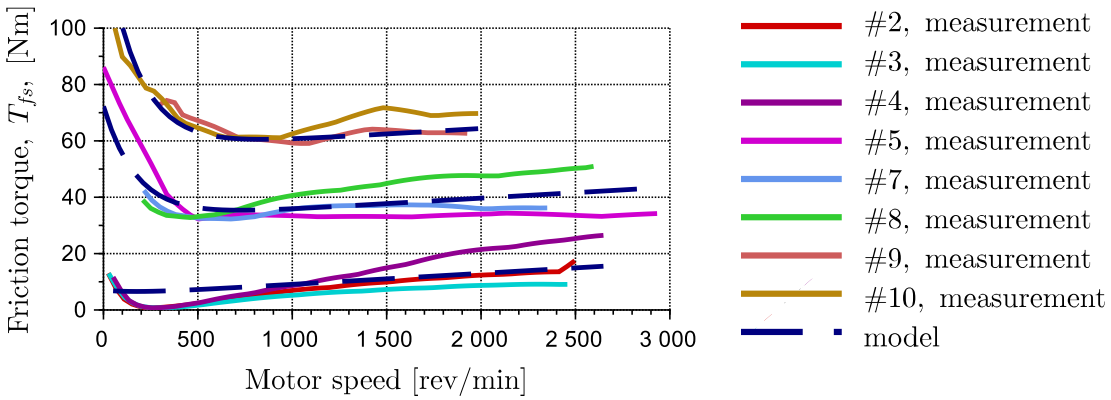

Figure 2.13: System friction torque, where measurements and model are compared.

2.3.4 Summery

The parametric models for system friction and motor friction show a good correlation. Using the complete map of test data as a model could also have been done with a similar outcome, but parametric models were preferred mainly due to three aspects. Firstly, the capability to better estimate losses outside the measured operating scenarios. This will reduce the needed amount of test data needed to determine the parametric model, compared to a mapped model. Secondly, making adjustments in only a couple of parameters is more accessible than changing values in a large map of data. Finally, the parametric models give the opportunity to easily collect and compare model parameters for different cranes and motors. In this way, it is possible to build a library of parameters representing different cranes and motors.

2.4 Controller design

The classic active/passive HC system uses a secondary controlled system for the passive portion of the system (upper circuit in Fig. 2.14). The active portion (lower circuit in Fig. 2.14) historically have three levels of advancement. Level 1 would be to use fixed displacement motors. This allows for the simplest level of control, but the downside is that the variable transmission ratio due to changes in wire-layer as the wire pay-out increase will reduce the speed capacity of the wire. Level 2 uses variable displacement motors and thereby overcomes this weakness. The motor displacement is controlled to have a fixed wire-force capacity. Hence the displacement will be adjusted according to the wire-layer diameter. However, a wire-layer typically has more than 100 m of wire, and therefore the motors' displacement control will be fixed during an operation in AHC. A level 3 advancement was developed before this Ph.D.-project due to a need for even higher wire-speed capacities. Level 3 has the exact same working principles as level 2, but, additionally, it has a dual speed mode option. The dual-speed mode option allows the operator to choose a different speed mode where the fixed wire-force capacity is reduced, and the wire-speed capacity is increased. The mode is often referred to as the high-speed mode.

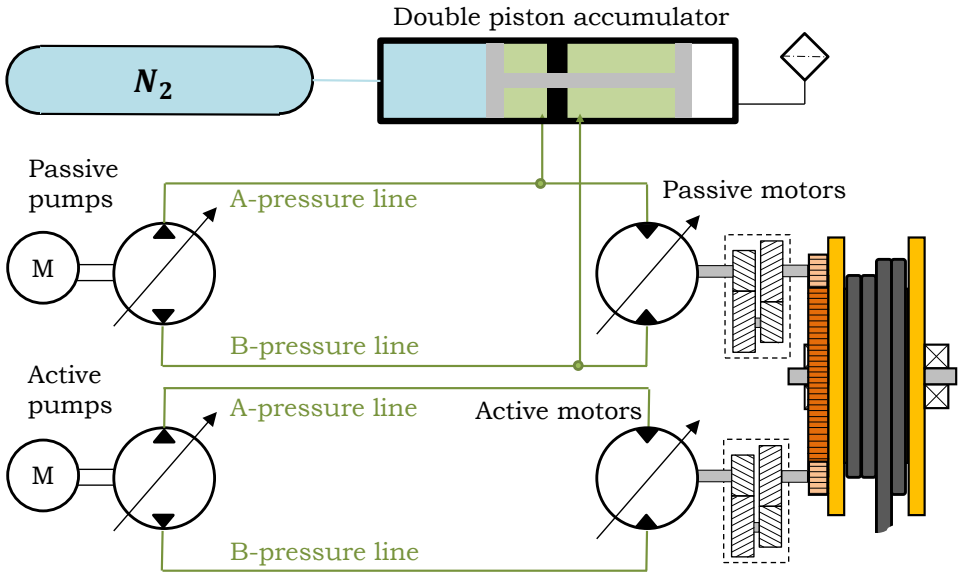

Figure 2.14: Simplified schematic for a hydraulic active/passive winch system [5].

The classic AHC controller of the active circuit is today typically using level 3. This means that every system is equipped with variable displacement pumps and motors. However, the classic AHC controller works as a basic variable pumps and fixed motors (VPFM) system, where the displacement of the motors only changes when the drum layer or the maximum allowable winch-load capacity is changed. The motor displacements are set based on a lookup table, ensuring that the winch torque capacity can cope with the maximum friction and acceleration forces with the maximum allowable winch-load. Since the system's maximum flow capacity is fixed, the given motor displacements will be a direct limiter of the maximum rotational velocity of the winch.

The two-mode speed selector, level 3, is an improvement because it enables the operator to choose a mode that allows higher wire-speeds with reduced load or normal-speeds with full load capacity. However, the selection has to be done before starting the operation, and choosing between only two modes is often causing the load-capacity to be too much reduced when the high-speed mode is desired. However, it is not given that the winch operates at its maximum load capacity, i.e., the motors may have excessive displacement. Excessive displacement will result in an unnecessary reduction in maximum wire velocity. Additionally, the friction and acceleration forces are typically highest at low speeds. It is seen as highly conservative to dimension motor displacement for zero-speed load cases. Therefore, unnecessary limiting the maximum speed capacity.

For these reasons, a new controller was proposed to continuously adjust the displacement of the motors due to the actual applied winch-load and not based on maximum winch capacity. Additionally, it has been seen from field-tests over time that reduced displacement at low-speed has a negative impact on the winch performance. A new controller was developed with the means of solving the aforementioned issues, but at the same time have minimal impact on the existing control strategy in terms of stability and level of sophistication. Additionally, adding physical components to the crane system had to be avoided with respect to potential retrofit upgrades and, therefore, represented a boundary condition on the controller development.

In paper C, the benefits of using a more dynamic motor displacement strategy are highlighted. When it is possible to maximize the motor displacement at low speed, the system performs better with lower control error. Additionally, a dynamic variation of the displacement will enable higher wire-velocities for larger winch-loads. The research suggests an active control of the motors' displacement. The controller is mainly of the feedforward type, considering the parameters and states; wire-on-drum diameter, crane-tip velocity, crane-tip acceleration, and motor displacements. The control structure is shown in Fig. 2.15, where the part marked in red includes the changes from the classical VPFM controller.

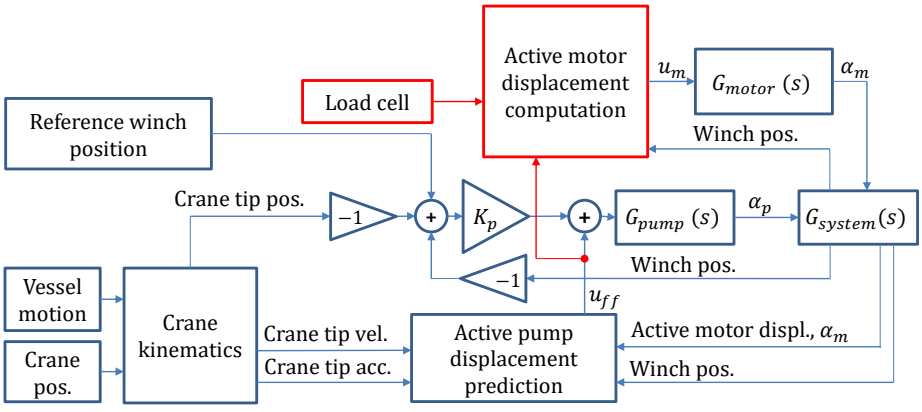

Figure 2.15: Control structure [7].

The new controller improves the performance compared to the classical. One of the main reasons for this is that the motor displacements are set to maximum whenever the winch passes zero velocity. Considering that the feedforward signal is the most significant

part of the pump command, it is clear from Fig. 2.16 that the displacement of the motors will be at a maximum when the pump is passing zero.

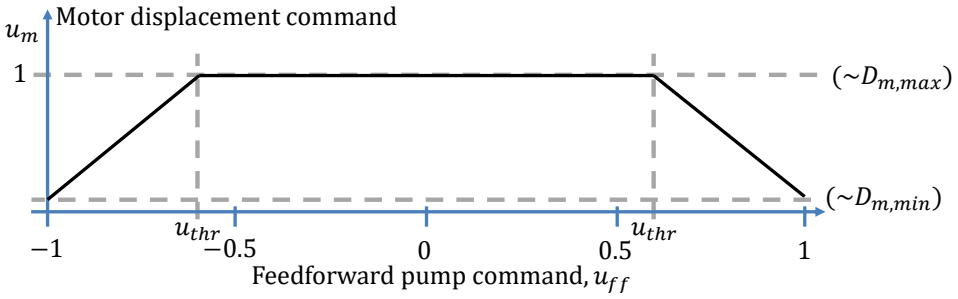

Figure 2.16: Motor displacement control due to u_{ff} [7].

The relative reduction of the motor displacement between the maximum and a dynamically set minimum (load dependent) is here (Eqn. 2.10) referred to as, k_{vgred}. If $k_{vgred} = 1$ it implies that the motor displacement is reduced to its minimum allowable displacement, $D_{m,min}$. The k_{vgred}, factor is controlled by the feedforward command, u_{ff}, which is based on vessel movement, actual displacement, and the exit diameter of the wire (on the drum). The threshold-value, u_{thr}, is defining at what point the motor displacement should start to be reduced. These two equations, Eqn. 2.9 and Eqn. 2.10, constitute the new control algorithm of the variable displacement motors:

$$u_m = 1 - k_{vgred} \cdot \frac{D_{m,max} - D_{m,min}}{D_{m,max}}, \tag{2.9}$$

$$k_{vgred} = \begin{cases} \frac{1}{1-u_{thr}} \cdot |u_{ff}| - \frac{u_{thr}}{1-u_{thr}}, & |u_{ff}| \geq u_{thr} \\ 0, & |u_{ff}| < u_{thr} \end{cases}. \tag{2.10}$$

The second major benefit of using the variable motor displacement control is the maximum velocity. The classic system has a conservative fixed motor displacement to be able to cope with winch the stiction and the winch acceleration. This momentum peaks when the winch is switching direction (low speed and high acceleration). At higher speed demand, the torque needed for acceleration is less, and the motor displacement can be reduced with low risk for exceeded pressure levels. The reduction of displacement has a higher velocity capacity as a direct outcome. To make sure the displacement is not reduced too much, the new controller uses the loadcell sensor to calculate a minimum displacement level, $D_{m,calcMin}$. Additionally, an absolute minimum ($D_{m,absMin}$) is set to make sure none of the winch components risks exceeding their speed limitations. The maximum of the two is used for $D_{m,min}$ (Eqn. 2.11).

$$D_{m,min} = max(D_{m,absMin}, D_{m,calcMin}) \tag{2.11}$$

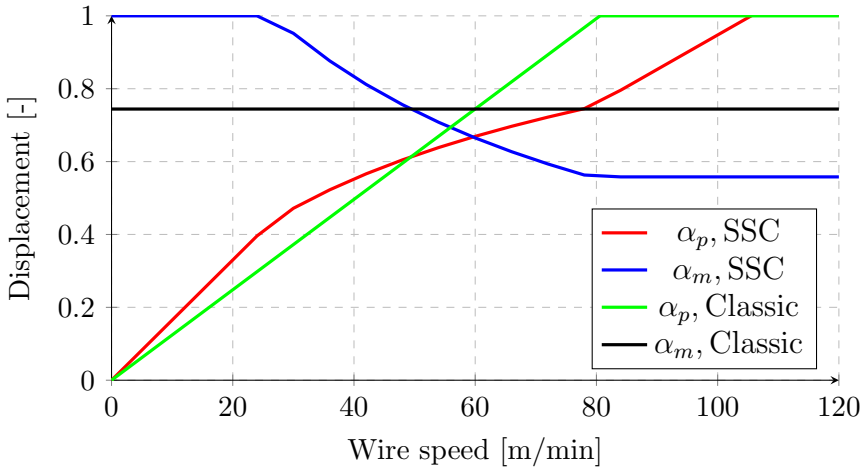

Figure 2.17: Steady-state motors' and pumps' displacement setting (α_m and α_p).

Due to the dynamic motor displacement setting, the new controller will be able to reach higher wire speed. An example, shown in Fig. 2.17, clearly illustrates how the new controller will be able to reach higher velocities without saturating the pumps. How much extra speed will mainly depend on the winch load, and the minimum allowed motor displacement.

2.5 Controller Verification

2.5.1 Motivation

To evaluate the controller described in the previous section, it is necessary with prototype-testing in a virtual environment. This is important to reduce costs and risks before final implementation. Additionally, a virtual representation of the new system could also be used to present new technology to potential customers or investors.

A solution to both the need for further testing and the need to show off the performance of new technology to potential customers, is to make a high-fidelity simulation model, a digital twin.

2.5.2 Model development

To review the potential benefits of any winch modification, there is a need for a high-fidelity non-linear model that can simulate the heave compensated crane in the time domain. The developed simulation model is built in SimulationX™, a computer-aided multi-domain engineering program for physical simulations. In this section, some of the main model elements used to simulate the winch hydraulics and mechanics are explained. The system being modeled is an active/passive winch system used for active heave compensation, and the model components are displayed in Fig. 2.18.

Figure 2.18 display how the model is visualized in the simulation software. The elements identified are 1: the pump in the active circuit, 2: the passive circuit, 3: the pumps and motors controller, 4: the motor in the active circuit, 5: block elements with functions that calculate friction and volumetric losses, and 6: the block containing all functions needed to calculate wire-wraps on drum and corresponding inertia.

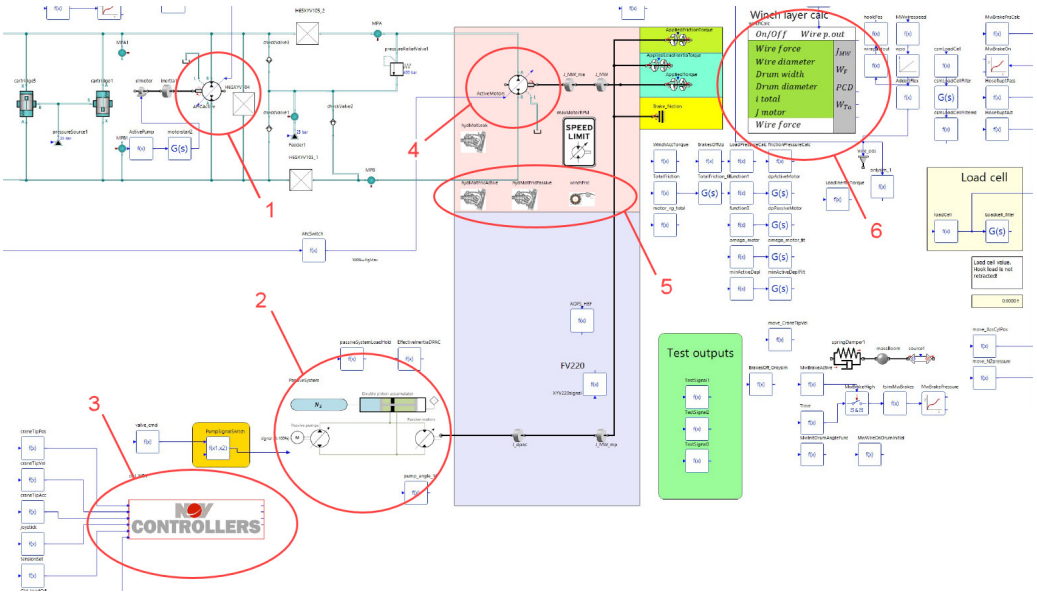

Figure 2.18: Simplified overview of a winch system.

2.5.2.1 Friction

Friction is included as parametric models. Three models are included, one for the active motors, one for the passive motors, and one for the remaining system friction. Several models for representing the motor losses were introduced in paper A, and models for the remaining friction were shown in paper B. In paper D, the combination of the two most preferred models is used to show a best practice solution to measure and estimate the friction in a crane system. The preferred motor loss model used in the simulation model is shown in Eqn. 2.12.

$$T_{fm} = X_1 \cdot \omega_m + X_2 \cdot \omega_m^2 \cdot D_m^3 + X_3 \cdot \Delta p_m \cdot D_m + X_4 + X_5 \cdot {\Delta p_m}^2 \tag{2.12}$$

Where X_{1-5} are adjustable parameters, Δp_m is pressure drop across the motor, D_m is motor displacement, and ω_m is the rotational speed of the motor shaft.

In Eqn. 2.13, the following formula to estimate the remaining friction is used,

$$T_{fs} = (Y_1 \cdot T_d + Y_3) \cdot e^{\frac{-|\omega_m| \cdot 60}{Y_4 \cdot 2\pi}} + Y_5 \cdot \omega_m + Y_6 \cdot T_d \tag{2.13}$$

where Y_{1-5} are the adjustable parameters and T_d is the drum torque. The model is similar to a so-called Stribeck model.

The friction models are based on a typical grey-box approach where some terms are based on physical properties. Although the models are satisfactory, they contain two main simplifications. Firstly, the model does not take into account temperature changes. The models are based on tests performed under normal operating conditions with fluid temperatures around 40^oC. The effect of fluid temperature change is neglected because active cooling and temperature control of the hydraulic liquid is installed on all cranes. Secondly, it is not feasible to perform friction tests on all cranes. Hence the applied friction model is, in many cases, not based on the exact crane that is being subjected to a virtual investigation. The overall effect, because of this, is assumed to be minimal.

2.5.2.2 Hydraulic capacitance

The specific hydraulic modeling of the physical twin includes piping, valve blocks, and hoses between the hydraulic pumps and the hydraulic motors. To include all these elements in a simulation environment is possible. However, many of these elements need to be defined in a detailed manner. As an example, for piping, it is possible to define wall capacity, fluid volume, and dynamics due to bends and pipe layout. The result of modeling the hydraulics with a high level of detail is that the model itself becomes significantly harder to adapt to real-life results, just because of the amount of adjustable and unknown parameters.

To avoid too many adjustable and unknown parameters, the hydraulic lines were simplified to a single hydraulic volume in each hydraulic line with a set of restrictions corresponding to the overall steady-state losses of the transmission line. The method of using an effective capacitance of the hydraulic lines has been in use before this project, and the capacitance is simply derived from measured pressure gradients combined with the bulk modulus of the hydraulic liquid using

$$C_h = \frac{\partial V}{\partial p} \tag{2.14}$$

Where C_h is the ratio of volume change over the change in pressure over a closed volume at a constant temperature. In practice, this capacitance represents the inverse effective bulk modulus of the series connection of the liquid, the undissolved gas in the liquid, and the structural components (pipes, hoses, bends, fittings, valve blocks, etc.) that surround the liquid.

2.5.2.3 Mechanics

On the mechanical side, an important parameter of the total system is the inertia. A winch system has several sources of inertia, where the most significant ones are; motors, gear-transmissions, drum, and wire. Figure 2.19 depicts the contributions from the different sources in the 250 t AHC winch used for the testing of the new controller in section 2.7.

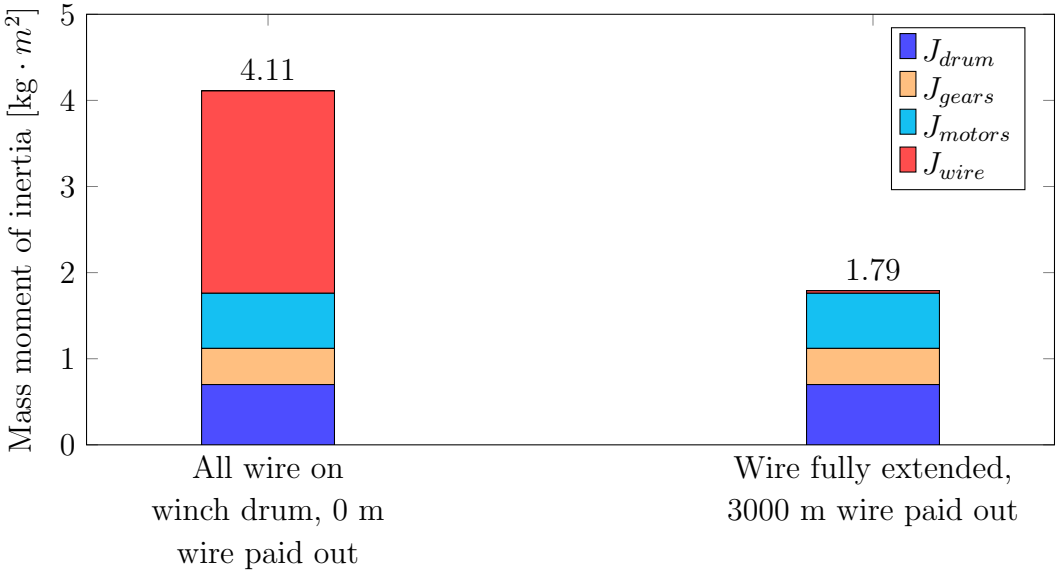

Figure 2.19: Effective mass moment of inertia in AHC at motor shaft when all wire is wrapped on the drum and when wire is fully extended (empty drum).

The total inertia in the simulation model is lumped into one effective inertia. The effect of this is that the whole mechanical system except the wire is evaluated as one stiff mechanical component. This is seen as a proper solution because the wire's stiffness will be the dominant spring stiffness of the system. The acceleration torque of inertia is modeled as follows,

$$T_a = \alpha \cdot J - \dot{J} \cdot \omega \tag{2.15}$$

where α is the angular acceleration of the inertia J, which corresponds to the time derivative of the angular velocity ω.

The wire stiffness was calculated as a linear spring,

$$k_w = \frac{E \cdot A}{L} \cdot f \tag{2.16}$$

where k_w is the effective wire stiffness, E is the elasticity module for the steel, A is the cross-sectional area of the wire based on the given diameter, L is the wire length paid out, and f is the filling factor to compensate for gaps between the cord in the wire.

2.5.2.4 Volumetric efficiency

The volumetric efficiency plays a significant role in hydraulics and is directly affecting the winch speed. The pumps and the motors have basically three leakage paths each. The most significant one is the leakage from the high-pressure side to the low-pressure side, also referred to as internal leakage. Additionally, there are two other leakage paths, from the high-pressure and low-pressure sides to the drain/housing.

In general, the total leakage flow is assumed to be laminar and is computed as:

$$Q_{leak} = C_{leak} \cdot \Delta p \tag{2.17}$$

For the pumps, there was limited efficiency-data to be found, and a simplified model was chosen. The pumps in the hydraulic winch systems in this research are typically in the size range from 180 cm^3/rev to 500 cm^3/rev. However, only leak tests performed on A4VSG355 were found. The tests were performed in a lab with hydraulic oil temperature regulated to 40 °C, and the oil type was HLP46. Both properties are similar to the ones to be found in the hydraulic winch system. The test data retrieved from the manufacturer, namely Bosch-Rexroth [42], showed a leak conductance with small variations when the pump is operated at a constant speed. Hence, the leakage conductance was modeled to be independent of pressure. The extracted leak conductances for pump speed at 1500 rev/min and at 2000 rev/min are shown in Table 2.5 and 2.6. The conductances are calculated based on the total flow leakage at 100 bar and 350 bar.

Table 2.5: A4VSG leak at 1500 rev/min

Displacement	C_{Pleak}
355 cm^3/rev	0.034 $\frac{l/min}{bar}$
384 cm^3/rev	0.024 $\frac{l/min}{bar}$
213 cm^3/rev	0.027 $\frac{l/min}{bar}$
142 cm^3/rev	0.030 $\frac{l/min}{bar}$
71 cm^3/rev	0.030 $\frac{l/min}{bar}$

Table 2.6: A4VSG leak at 2000 rev/min

Displacement	C_{Pleak}
355 cm^3/rev	0.057 $\frac{l/min}{bar}$
384 cm^3/rev	0.039 $\frac{l/min}{bar}$
213 cm^3/rev	0.040 $\frac{l/min}{bar}$
142 cm^3/rev	0.037 $\frac{l/min}{bar}$
71 cm^3/rev	0.035 $\frac{l/min}{bar}$

The total volumetric loss in the pumps is modeled as variable hydraulic conductances based on Table 2.6 and scaled linearly dependent on the actual installed pump size. Hence, the pump leak conductance is assumed independent of pressure variations but dependent on pump displacement. The efficiency variations between the different pump sizes are neglected.

The test data is only sorted based on outlet pressure and with no differentiation between internal and external leakage flow. To estimate a more realistic distribution between internal and external leakage, the external leakage path is set to twice as restrictive as that of the internal leakage path, assuming a dominant internal flow loss.

For the motors, the same pressure independence is assumed, and a simplified conductance model dependent on the motor's shaft speed is used (Eqn. 2.18).

$$C_{leak} = C_1 + C_2 \cdot n_m \tag{2.18}$$

Where C_{leak} is the total leak conductance. The parameters, C_1 and C_2, are adjusted to make the model represent the data provided by the sub-supplier [43]. A comparison between the adjusted model for an A6VM series 63 size 250 and the supplier data is depicted in Fig. 2.20.

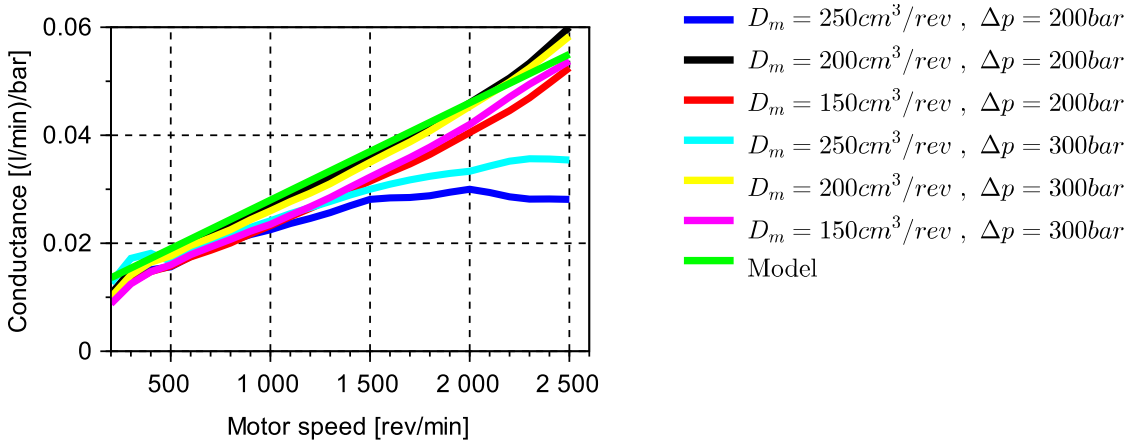

Figure 2.20: Comparison of sub-supplier measurements and the leak conductance model for a A6VM s63 size 250. [5]

2.5.2.5 Controllers

The controllers are modeled based on reverse engineering of the controller codes in the physical twin, the crane's programmable logic controller (PLC). The controller-model is verified from real-time measurements. The cycle-time of calculations in the real system is 10 ms. This is neglected in the model, which runs at 1 ms or lower. However, the verification results show a high level of accuracy, and compared to the tolerances in the remaining part of the model, the small deviation between the physical and virtual control system can be neglected.

2.5.3 Controller evaluation tool

Associated with introducing new control strategies, the crane manufacturer has one major challenge. Namely, to explain and prove the performance of the new controller. The classical controller-performance is trusted through years of experience, but any new controller is not. Additionally, there is a challenge related to both the new and the classic controller. That challenge is how to predict the system performance in order to perform lift planning of offshore lifts. Today, a part of the lift planning is computer-based, where the vessel together with load and wire dynamics are modeled, and the lifting operation

is simulated. When the lifting operation includes the use of heave compensation, that operation must be included in the simulation. When a certified model is not available, the common practice is to use simplified models with a high level of conservatism. As a result, the crane has a higher capacity than sometimes necessary, and the operational window shrink. All this contributes to an increased total cost of the lifting operation due to the hiring of a larger crane and more vessel standby time.

A solution to both the need for a lift-planning tool and the need to show off the performance of new technology to potential customers is to make a high-fidelity executable model, a digital twin. The digital twin should be a verified model, able to sufficiently replicate the performance of the active heave compensated winch system. A digital twin exists in many companies, and simulation models of winch systems do already exist. However, a common standard to qualify such a system is missing. This became the topic of paper F, where a qualification standard for a digital twin of active heave compensated winches was proposed and experimentally validated.

2.6 Digital twin concept for lift planning

Today, a digital twin is defined as a digital model representing a physical asset. Some define a DT as a real-time device [15], but one can argue that a DT not necessarily need to run real-time. For instance, the digital twin could receive batches of data to analyze and report back to the physical model every hour. The information could still be of great value even though it has a delay. For instance, maintenance feedback will typically not be needed with high frequency for most systems. The accepted delay will be case sensitive and depend on the physical twin. Although there are many different descriptions of a DT, it can be argued that a DT is a collective term for many different variants and levels of a digital model. The digital twin, as a concept with several levels, was described by Madni et al. [13]. However, the description of the different levels of DT is a bit narrow, and categorizes the different levels based on the digital twins' user interface (UI). Namely, non-adaptive UI, adaptive UI, and adaptive UI using reinforced learning algorithms. A broader definition was introduced by [2], and is the same structure DNV GL is using, shown in Fig. 1.3. In Table 2.7, a different categorization of the different versions of a DT is suggested. Here the adaptive functionality of the model is the defining factor for the DT level, and the UI is not evaluated.

1. Digital twin, Level 1
   This model is without any physical system verification. This is typical for virtual prototyping and visualization of new products.

2. Digital twin, Level 2
   The level 2 model is a verified model. The verification is done by using data from the physical twin. However, the model is not adaptive, and any model updates are performed manually. A level 2 model, with high accuracy, is well suited for offline simulations. The offline simulations could be in a virtual environment, to test how the model interacts with other environments, or it could use batches of

data from the physical twin to analyze model performance. The offline simulation model is also well suited to further develop the physical system by implementing various upgrades to the digital twin. Another option is to use the level 2 model embedded in the physical system as an edge application [44]. In that case, the DT should be simplified enough to run real-time. The model will then run in parallel with the physical twin. The purpose of having it running in parallel could be to feed information to the real system that is not easily reached in the physical twin or to give advanced decision support on the operation or maintenance schedule.

3. Digital twin, Level 3
   The level 3 model is a DT that is updating the digital model automatically. The updates are performed with fixed implemented algorithms. This will give the model a high accuracy throughout the entire lifetime of the physical twin. Due to the continuous update, the model will need a suitable connection to the physical twin. This could be through a cloud service or a direct implementation of the physical twin.

4. Digital twin, Level 4
   The level 4 model, is a DT with the same capabilities as the level 3 model but is additionally using intelligent machine learning algorithms.

Table 2.7: Digital twin versions

Variant	**Level**	**Embedded**	**Real-time**	**Data transfer**	**Adaptive model**	**Adaption**
1	1	No	Yes/No	NA	NA	NA
2	2	No	No	NA	No	Only during model design
3	2	No	No	Batch	No	Only during model design
4	2	Yes	Yes	Real-time	No	Only during model design
5	3	No	Yes/No	Batch	Yes	Automatic
6	3	Yes	Yes	Real-time	Yes	Automatic
7	4	No	Yes/No	Batch	Yes	Intelligent
8	4	Yes	Yes	Real-time	Yes	Intelligent

For offshore lifting operations, conditions like waves, currents, and wind, affect both the vessel and the hanging load during a lift. These dynamics need to be simulated in programs made explicitly for calculating vessel dynamics, and hydrodynamical forces. Two well-known software programs for this type of analysis is Simo™and OrcaFlex™. A challenge that is faced during these analyses is when the crane functions are used in different kinds of motion compensation. For instance, compensation modes for entering or exiting the splash zone, or landing a load in AHC on the seabed. During these operations,

the resulting forces are crucial and will directly result in approval or disapproval of the planned lift. According to DNVGL rules and regulation for offshore lifting, a DAF (dynamic amplification factor) analysis should be made in heave compensated modes [45]. Hence a simulation of the operation is needed. Without a verified model of the heave compensating equipment, DNVGL approves simplified models. However, these models have to be proven conservative, and cannot exceed compensation efficiency above 80 % [46]. In other words, the simplified model results in higher DAF ratings than the real system actually needs. Increased DAF rating will reduce the allowed operational weather window for the crane, and thus possibly increase the cost of operation. Hence, accurate models without the need for high conservatism is desired.

High-fidelity digital twins are also a desired tool when it comes to prototyping. An example is TechnipFMC, who had bought a splash zone mode for their cranes from NOV. The mode is designed to reduce the impact of dynamic forces subjected to the lifted object when passing through the splash zone. The challenge was that the mode was new, and qualitative and well-documented data was not available. Additionally, the lifted object itself would have a high impact on the results. The solution became that NOV made a digital twin for the winch system, including the new mode functionality. TechnipFMC further used this model together with their vessel and load models, as shown in Fig. 2.21. The simulations resulted in a reduced waiting time of 11 days [47].

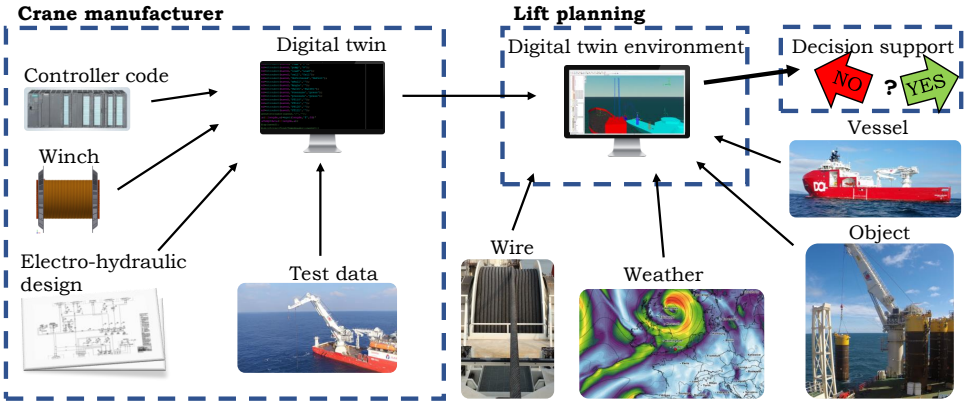

Figure 2.21: Digital twin example.

Another significant advantage of having the digital twin of the winch system is related to collaboration. Grieves stated in 2014 [48]: "The most powerful things that humans do is collaborate with each other in order to bring more intelligence, more variability of perspectives, and better problem solving and innovation to situations". Without the digital twin, each manufacturer and designer are optimizing their products in a separate environment. Including and sharing the DT, introduce new ways to collaborate, and more ideas to enhance the product will occur.

2.7 Controller testing

The methodology used when developing and implementing the controller is shown in Fig. 2.22. The first step is to go from controller-design to simulation tests. In the simulation model, extreme scenarios were tested with variations of load and crane-tip velocities. This verified the functionality of the controller and provided information on how to modify the controller before conducting tests on the full-scale equipment. The expected benefits associated with the new controller has been described in detail in section 2.4, paper C, and paper E. In general, the new controller will have significant benefits in terms of reduced peak-pressure, increased load capacity, increased wire-speed capacity, and smoother winch performance at low winch-speed.

Since the simulation tests verified the expected benefits, the controller code was implemented on a similar programmable logic controller (PLC) to the one installed on the real crane. That PLC was used to perform some in-house-testing in a simple simulation environment. Also known as hardware-in-the-loop (HIL) testing. In this environment, it was possible to manipulate the controller input and verify that the controller is working as it should and that the code was implemented without errors. After that validation, the testing was taken to the final stages, with full-scale real-life tests. The first full-scale test was performed along quay-side, with no winch load, and simulated waves. Finally, the controller was tested offshore, with winch loads up to 200 t.

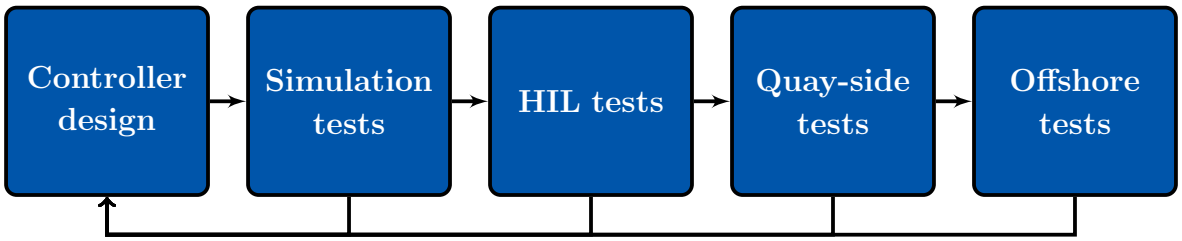

Figure 2.22: Workflow chart.

2.7.1 Quay side tests

At the quay-side tests, the main focus was to test if the physical system could work correctly with the new controller and do some measurements that could directly compare the classic control strategy with the new. The main tests are listed in Table 2.8

Table 2.8: Quay-side tests

Test	Description
1	Physical motor controller verification
2	Standard AHC, with simulated crane-tip motions (new controller)
3	Standard AHC, with simulated crane-tip motions (classic controller)
4	Variation in controller parameters (K_1 and K_2)

First, it had to be verified that the motor displacement controller could handle the rapid changes required. Since the motor will be fixed to maximum displacement around zero winch speed, the time available to adjust the displacement depends on the threshold value, u_{thr}, and the period of the moving crane-tip. A criterion for the crane investigated is that it should be able to handle motion periods down to 6 seconds. Experiments with threshold values from 0.4 to 0.6 were performed, where 0.6 ended up as the preferred choice. That yields a motor displacement that is at maximum displacement more often than if the threshold value was 0.4. Even larger values of u_{thr} was not examined since the maximum displacement would only be of importance at the low speeds. A high threshold value would also increase the demands to the motor displacement reaction time and could mean that the overall performance would suffer. Moreover, as the analysis from paper C shows, working at maximum displacement improves the overall performance. The largest u_{thr} requires shorter response time from the motors. However, the results from test 1 (Table 2.8) shown in Fig.2.23, shows that the motor displacement controller works sufficiently.

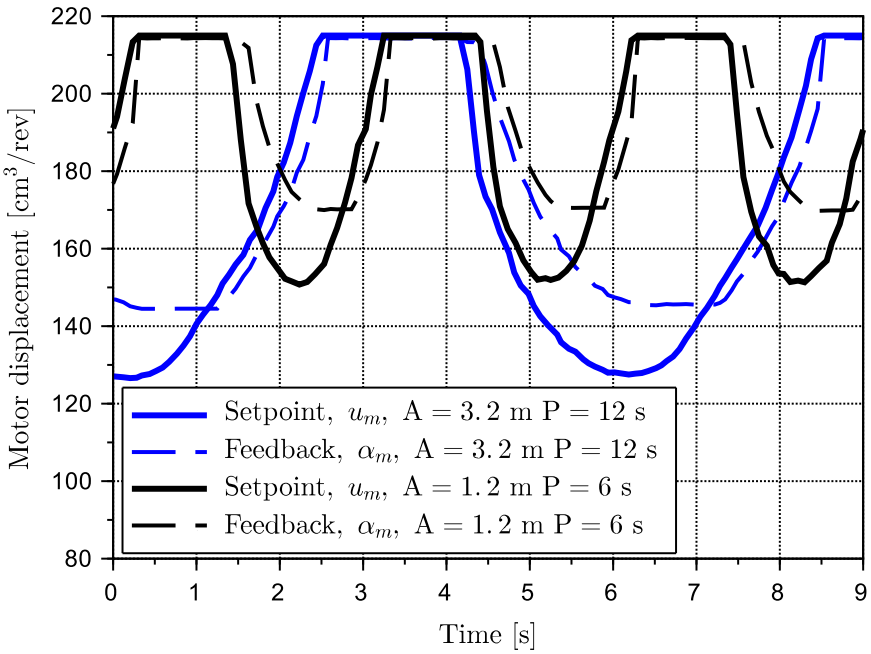

Figure 2.23: Simulated sinusoidal motion with 12 s period and 6 s period. The motor displacement controller runs in open-loop.

A noticeable issue, from test 1, was the offset between feedback and setpoint. The offset will cause a reduction in the maximum winch velocity potential. However, the speed requirements were fulfilled, and the offset had no other practical impact on system performance.

With that conclusion, the winch testing was continued. The rest of the tests focused on the active heave compensation performance with an empty hook and emulated crane-tip heave. The emulated heave was a pure sinusoidal reference. For each of the different crane-

tip motions emulated, the crane was tested in three different AHC modes: normal-speed (NS) mode, high-speed (HS) mode, and, using the new controller, the semi-secondary control (SSC) mode. The test results confirmed the simulation-tests' predictions that the peak-pressure in the hydraulic circuit would decrease and that the winch would run more smoothly. This was especially pronounced when comparing the use of the HS and the SSC mode at low speeds (Fig. 2.24-2.27). There are typically four areas of interest when analyzing the results. Firstly, the wire velocity which describes the wire velocity where it leaves the winch drum. Secondly, the pressure in the active circuit presented as the A-side pressure. Thirdly, the control error, which is a position error, computed as the difference between the wire position reference and the measured wire position, and, finally, the pump and motor displacements.

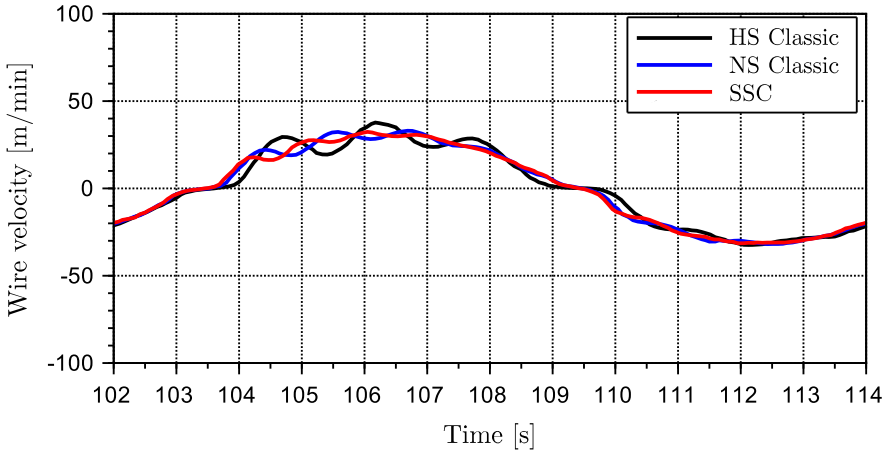

Figure 2.24: Wire velocities for the low-speed scenario [7].

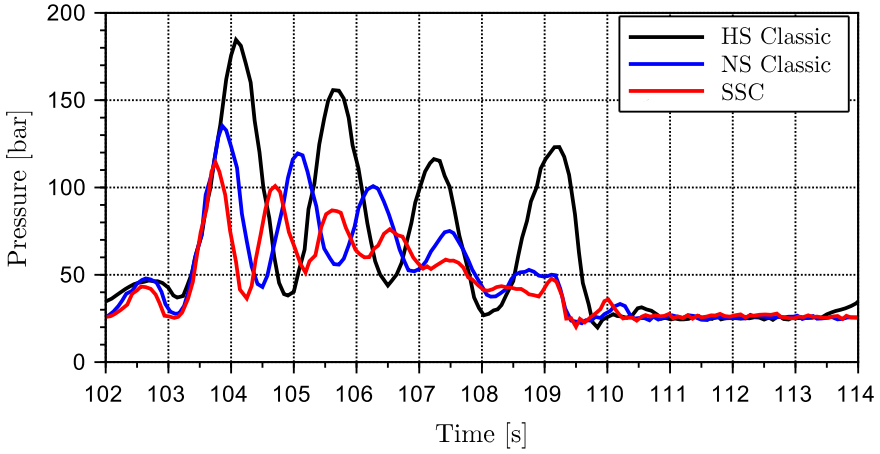

Figure 2.25: Pressure levels on the A-side of the active system for the low-speed scenario [7].

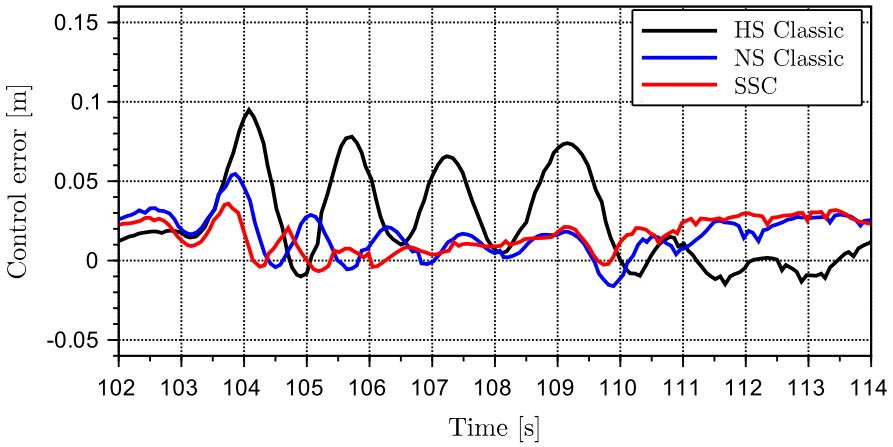

Figure 2.26: Control error for the low-speed scenario [7].

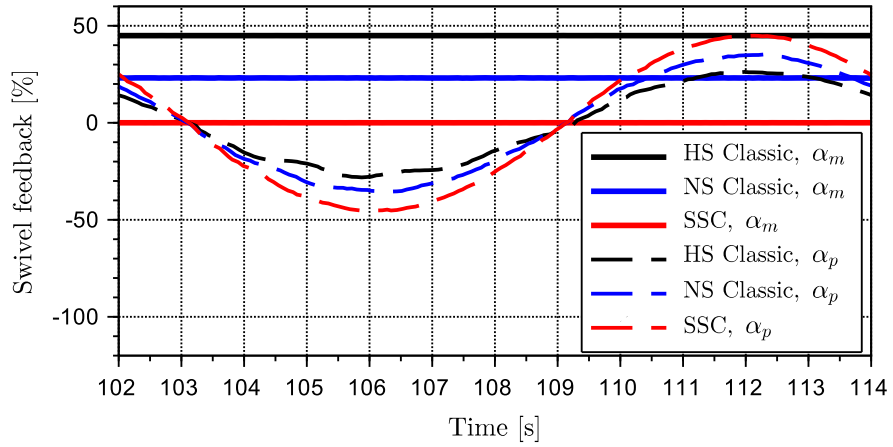

Figure 2.27: Pump and motor displacement settings for the low-speed scenario (0 % for the motor means maximum displacement) [7].

In the other end of the velocity scale, when the wire speed is close to the winch's maximum speed capacity, the benefits are still significant. The result is lower peak pressure and smoother winch movements with the additional benefit of giving a reduced control error (Fig. 2.28-2.31).

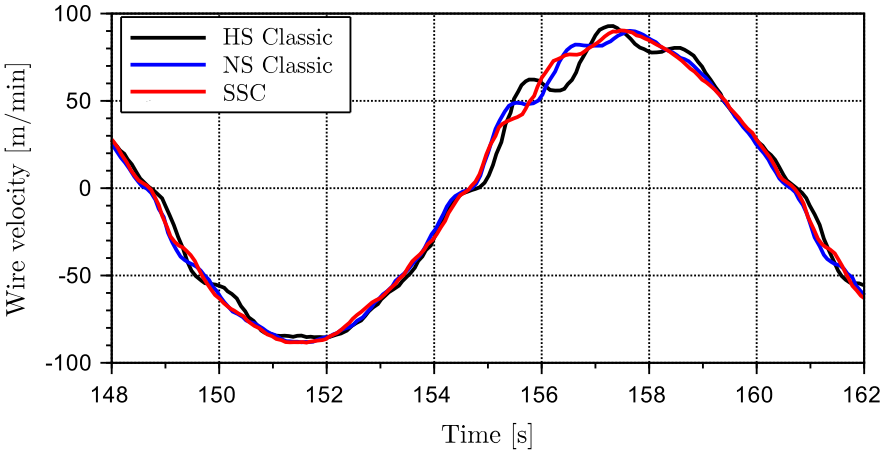

Figure 2.28: Wire velocities for the high-speed scenario [7].

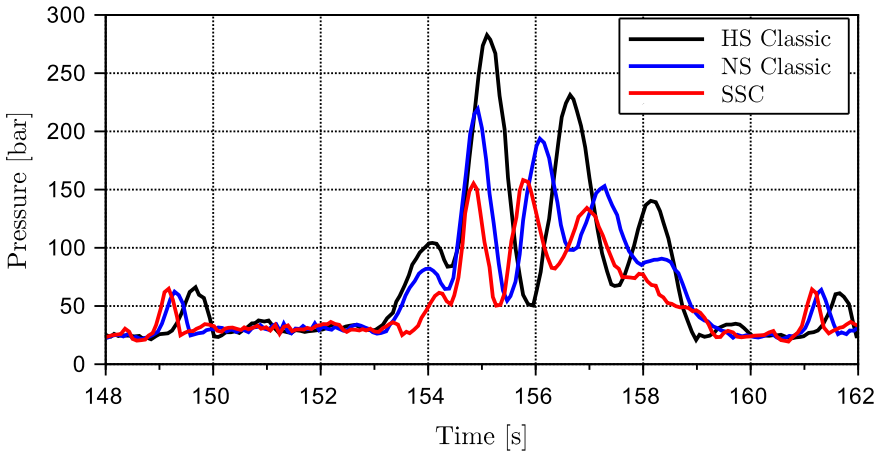

Figure 2.29: Pressure levels on the A-side of the active system for the high-speed scenario [7].

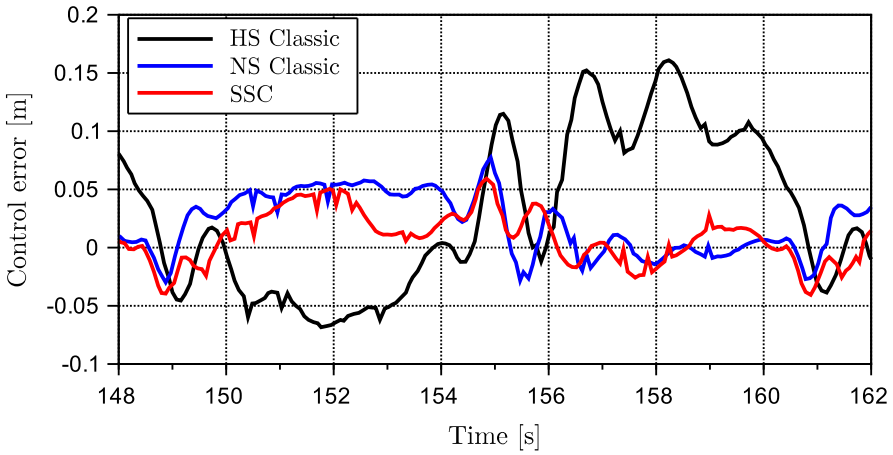

Figure 2.30: Control error for the high-speed scenario [7].

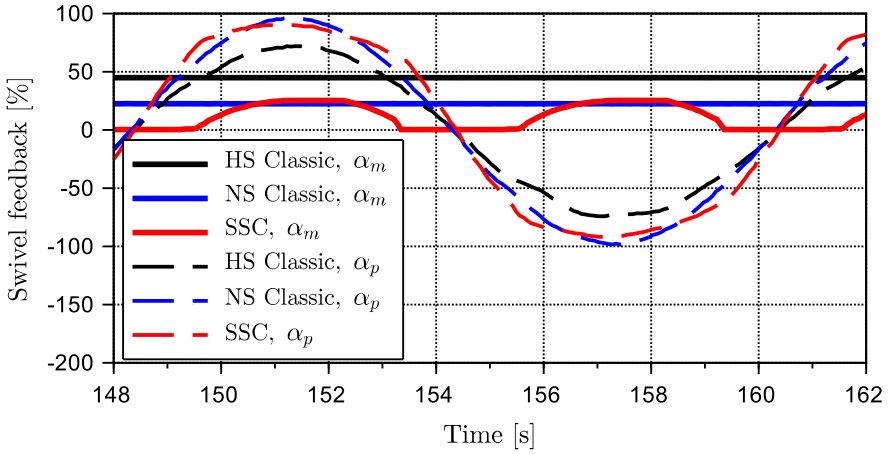

Figure 2.31: Pump and motor displacement settings for the high-speed scenario (0 % for the motor means maximum displacement) [7].

2.7.2 Offshore tests

When preparing the vessel and the crane for the offshore trial, the new controller was implemented in such a way that it was easy and safe to swap between the classic controller and the SSC. The testing of the new controller was performed with steel weights up to 200 t. Unfortunately, the weather was rather calm, which meant that the new controller, the SSC, could not be fully tested. In the tests with 100 t weight (Fig. 2.32-2.34), it was only possible to trigger motor displacement variations caused in the SSC by reducing the controller threshold value, u_{thr}.

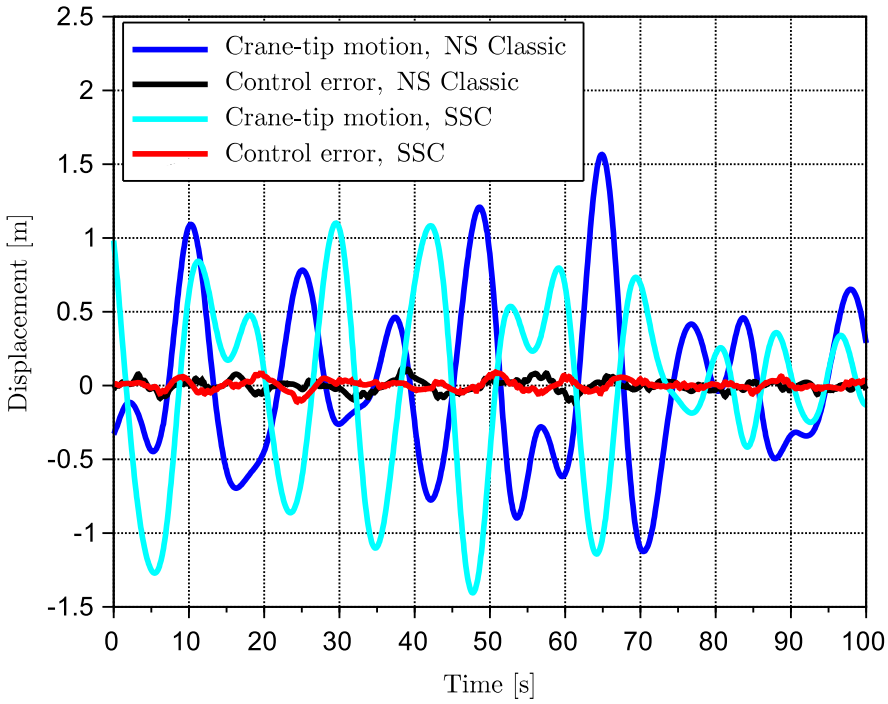

Figure 2.32: Crane-tip motion and control error for the offshore tests with 100 t.

The threshold value was reduced to 0.3 instead of the original 0.6. With that it was possible to reach a total peak reduction of the motor displacement of approximately 100 cm^3/rev as shown in Fig. 2.33.

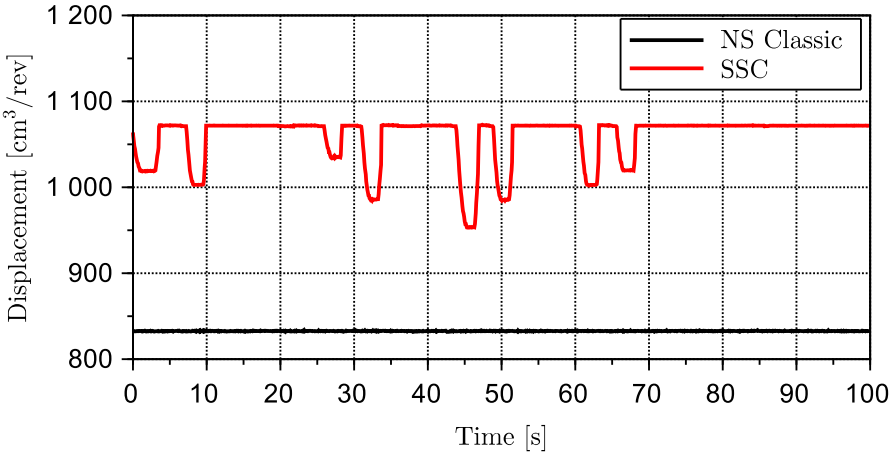

Figure 2.33: The total motor displacement settings for the offshore tests with 100 t.

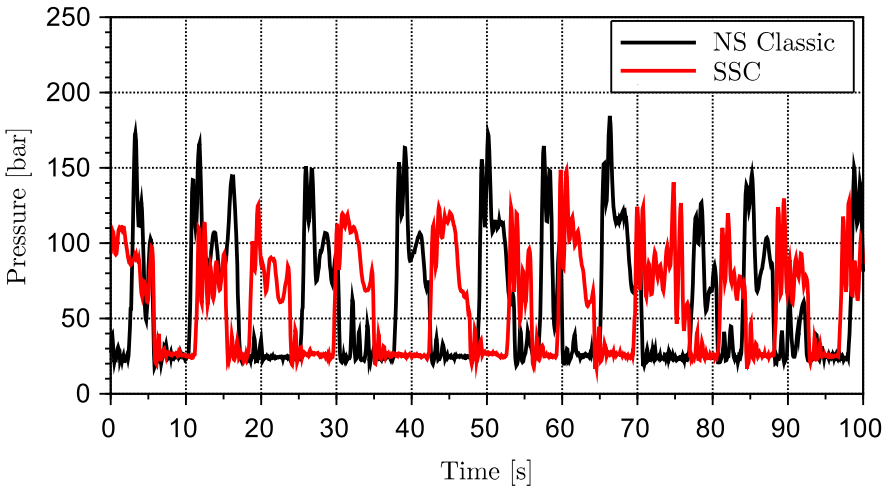

Figure 2.34: Pressure levels on the A-side of the active system for the offshore tests with 100 t.

When deploying the 200 t weight, the weather was even calmer, and the peak-to-peak crane tip was now just about 1 m (Fig. 2.35). As seen in Fig. 2.36, that was not enough to trigger any change in motor displacement. With the SSC, the motor displacement was continuously kept at a maximum. However, it should be recognized that the classic controller has a fixed displacement at a lower setpoint than for the SSC. This is a result of using fixed displacement and, at the same time, being obliged to consider the maximum speed capacity. As a visible result seen in Fig. 2.37, the SSC has a slightly lower pressure level in the active circuit.

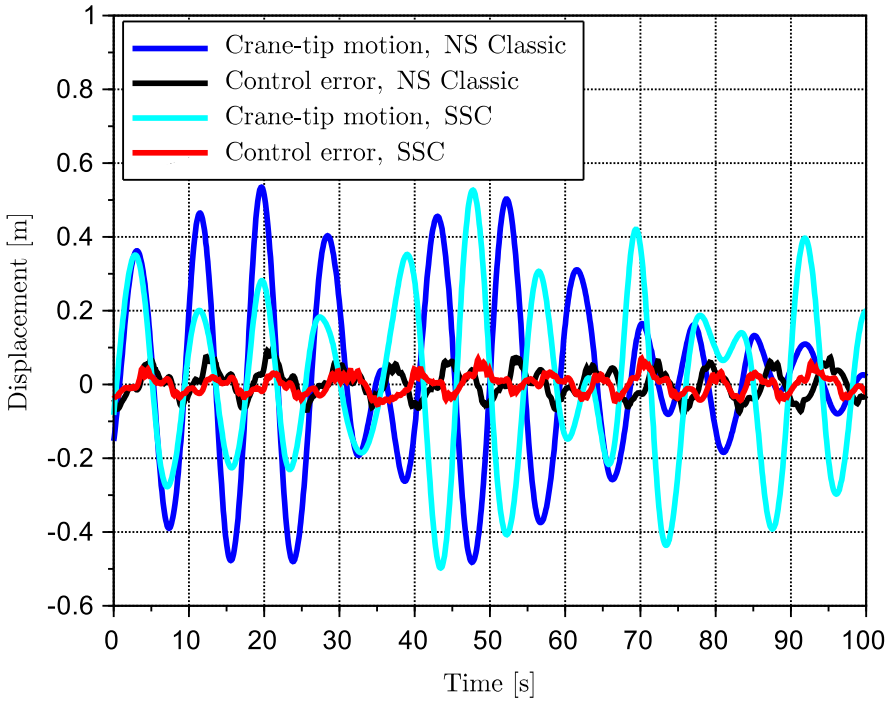

Figure 2.35: Crane-tip motion and control error for the offshore test with 200 t.

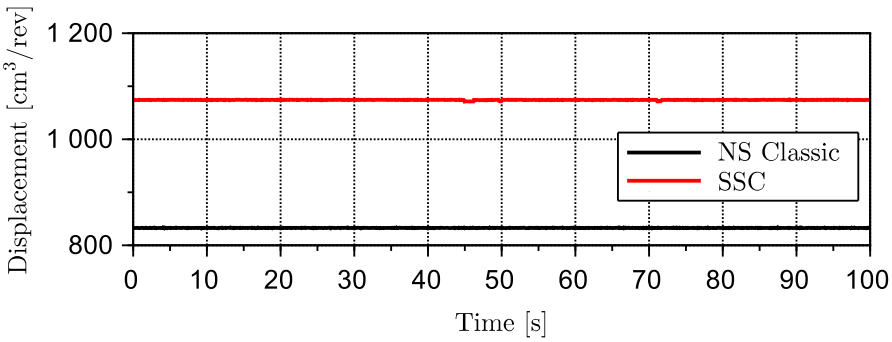

Figure 2.36: The total motor displacement settings for the offshore tests with 200 t.

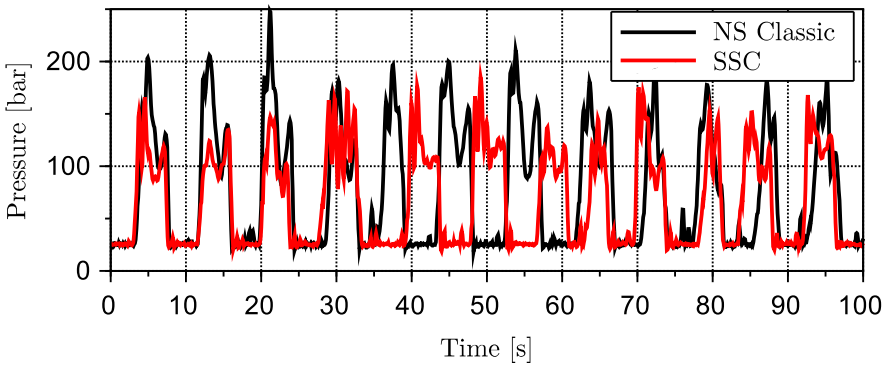

Figure 2.37: Pressure levels on the A-side of the active system for the offshore tests with 200 t.

Chapter 3

Conclusions

The Ph.D. project described in this thesis has focused on increasing the weather window for offshore operations that use active heave compensated cranes. Two significant factors contributing to the operational weather window were identified. Firstly, the utilization of the installed capacity of the crane winch system. Secondly, the engineered lift planning process, which calculates the actual weather window for the operation.

This yielded the following research questions:

- Is it possible to develop a dynamic model of a heave compensated winch system that allows for lift planning?
- Is it possible to develop new controllers that increase the utilization rate of heave compensated winches?

In response to the second question, an improved controller for the active heave compensation system of the winch was developed. However, a total redesign of the system was not considered due to the large fleet of existing cranes already in the market and a strong desire to offer retrofit solutions. Additionally, an upgrade using existing systems would open up possibilities for real-life tests. The system investigated was the active/passive heave compensated winch systems used in the offshore cranes from National Oilwell Varco. Due to the challenges with prototype testing, the approach was heavily model-based. Thus, the main focus was directed at winch system knowledge and how to model such a system with the desired accuracy, thereby answering the first research question. The initial focus with regards to modeling was to get an informative and quantitative knowledge about the friction losses in a crane winch system. It was concluded that the total winch friction had to be divided into two parts for proper investigation. Therefore, in Paper A, a review of different friction models of the hydraulic motors was investigated together with efficiency data from the motor-supplier. The work yielded a model for friction losses that was suitable to be used for variable displacement motors. However, the model has to be adapted to measurement data. Thus, a parameter optimization with the sub-supplier's efficiency-data will always be needed. The second part, the remaining winch system friction, was determined by examining real-life data measurements. A suitable model was defined in Paper B as a Stribeck shaped friction model. In Paper D, the full process of identifying the friction in the hydraulic winch system was presented. Even

though more effort could be used to identify model uncertainties, the focus was redirected towards setting up a simulation model for a crane fit for purpose and investigating the benefits of adopting an improved controller.

Due to the desire for a possible retrofit, model development led to a feedforward solution added to the existing speed controller. By doing this, any new sensors and feedback loops, as well as any questions regarding stability, were avoided. The new controller was proposed in Paper C. The proposed controller utilized a dynamic controller of the variable displacement motors in the active circuit of the active/passive hydraulic system. Dependent on the measured load and the feedforward signal in the existing controller, a new control approach was presented. The approach was shown to have significant benefits in terms of reduced peak-pressure, increased load capacity, increased wire-speed capacity, and smoother winch performance at low winch-speed. In Paper C, this was all documented with the use of the winch simulation model. However, in Paper E, the control approach was implemented on a real crane, and tests were performed onshore and offshore. The in-field tests were successfully conducted and confirm the findings from earlier simulations.

The results from the simulation model/digital twin were useful to test the new controller strategy. Such a model can also be beneficial for performance prediction. As a final part of the research, a focus on how a digital twin can be used during the lift planning phase and how it should be validated was investigated. In Paper F, the author suggests a method for modeling and validating hydraulically actuated winch systems with active heave compensation. Different companies have already started using digital twins of equipment, vessels, or weather forecasts during a planning phase. However, the quality required of the different models being used is vague or non-existing. Paper F explicitly describes a set of criteria to be fulfilled. The criteria should be thought of as a guideline, based on the current level of needs from the lift planners and the current level of simulation models.

Bibliography

[1] Kjell Eriksson, Erlend Fjøsna, Roy Ruså, and Per Myrseth. Digital twins - Are they valuable? Can you trust them? `https://www.dnvgl.com/oilgas/webinars/digital-twins-are-they-valuable-receipt.html?utm_content=webinar-attendees&utm_campaign=OG_GLOB_20Q2_WBNR_PostDigitalTwinPanelDiscussion-Attendees&utm_medium=email&utm_source=Eloqua`, 2020. Webinar by DNV GL.

[2] Edmary Altamiranda and Eliezer Colina. A System of Systems Digital Twin to Support Life Time Management and Life Extension of Subsea Production Systems. In *OCEANS 2019 - Marseille*, pages 1–9. IEEE, jun 2019.

[3] Yingguang Chu. *Virtual Prototyping for Marine Crane Design and Operations*. Doctoral thesis, Norwegian University of Science and Technology, 2018.

[4] Geir-Arne Moslått, Damiano Padovani, and Michael Rygaard Hansen. A Control Algorithm for Active/Passive Hydraulic Winches Used in Active Heave Compensation. In *ASME/BATH 2019 Symposium on Fluid Power and Motion Control*, page 11, Sarasota, Florida, USA, nov 2019. American Society of Mechanical Engineers.

[5] Geir-Arne Moslått, Damiano Padovani, and Michael Hansen. A digital twin for lift planning with offshore heave compensated cranes. *Journal of Offshore Mechanics and Arctic Engineering*, pages 1–29, oct 2020, doi:10.1115/1.4048881.

[6] Geir-Arne Moslått and Michael Rygaard Hansen. Practice for determining friction in hydraulic winch systems. *Modeling, Identification and Control: A Norwegian Research Bulletin*, 41(2):109–120, 2020, doi:10.4173/mic.2020.2.6.

[7] Geir-Arne Moslått, Michael Rygaard Hansen, and Damiano Padovani. Performance Improvement of a Hydraulic Active/Passive Heave Compensation Winch Using Semi Secondary Motor Control: Experimental and Numerical Verification. *Energies 2020, Vol. 13, Page 2671*, 13(10):2671, may 2020, doi:10.3390/EN13102671.

[8] Samuel Jason Hall. *Statistical analysis of multiple hydrostatic pump flow loss models*. Master thesis, Iowa State University, 2014.

[9] Sondre Sanden Tørdal. *Real-Time Motion Compensation in Ship-to-Ship Load Handling*. Doctoral dissertation, University of Agder, 2019.

[10] Sten Martin and Grønlund Andersen. *Motion Control During Offshore Lift Operations*. Master thesis, NTNU Norwegian University of Science and Technology, 2017.

[11] Jan Thomas G Olsen. *Simulation and control of an anti-swing system for a suspended load attached to a moving base robot*. Master thesis, University of Agder, 2018.

[12] Yao Cheng. *SimulationX-based simulation of offshore hydraulic crane systems with active heave compensation and anti-sway control*. Master´s degree thesis, Høgskolen i Ålesund, 2014.

[13] Azad Madni, Carla Madni, and Scott Lucero. Leveraging Digital Twin Technology in Model-Based Systems Engineering. *Systems*, 7(1):7, 2019, doi:10.3390/systems7010007.

[14] David Jones, Chris Snider, Aydin Nassehi, Jason Yon, and Ben Hicks. Characterising the Digital Twin: A systematic literature review. *CIRP Journal of Manufacturing Science and Technology*, 1(2019), 2020, doi:10.1016/j.cirpj.2020.02.002.

[15] Gianluca Bacchiega. Developing an Embedded Digital Twin for HVAC Device Diagnostics. `https://www.slideshare.net/gbacchiega/embedded-digital-twin-76567196?from_action=save`, 2017.

[16] Carlos Miskinis. Explaining the definition of digital twin and how it works. `https://www.challenge.org/insights/what-is-digital-twin/`, 2018.

[17] E. H. Glaessgen and D. S. Stargel. The digital twin paradigm for future NASA and U.S. Air force vehicles. In *53rd AIAA/ASME/ASCE/AHS/ASC Structures, Structural Dynamics and Materials Conference*, pages 1–14, Honolulu, Hawaii, USA, 2012. AIAA/ASME/ASCE/AHS/ASC.

[18] Bernard Marr. What Is Digital Twin Technology - And Why Is It So Important? *Forbes*, pages 4–7, 2017.

[19] J K Woodacre, R J Bauer, and R A Irani. A review of vertical motion heave compensation systems. *Ocean Engineering*, 104:140–154, 2015, doi:10.1016/j.oceaneng.2015.05.004.

[20] Arvind Keprate. Impact of Passive Heave Compensator on Offshore Lifting. *Journal of Shipping and Ocean Engineering*, 5(4), 2015, doi:10.17265/2159-5879/2015.04.003.

[21] Morten Ottestad, Kjell Olav Haland, and Michael Rygaard Hansen. A model based approach to design of passive and active heave compensation of crown mounted drilling equipment. *Proceedings of the IASTED International Conference on Modelling, Identification and Control*, 1(Cmc):128–135, 2010.

[22] Jørgen Haaø, Steffen Vangen, Martin Choux, Geir Hovland, and Michael R. Hansen. The Effect of Friction in Passive and Active Heave Compensators of Crown Block Mounted Compensators. *IFAC Proceedings Volumes*, 45(8):316–320, 2012, doi:10.3182/20120531-2-NO-4020.00040.

[23] J.G. Kusters, K.L. Cockrell, B.S.H. Connell, J.P. Rudzinsky, and V.J. Vinciullo. FutureWaves™: A real-time Ship Motion Forecasting system employing advanced wave-sensing radar. In *OCEANS 2016 MTS/IEEE Monterey*, pages 1–9, Monterey, CA, USA, sep 2016. IEEE.

[24] M. Richter, S. Schaut, D. Walser, K. Schneider, and O. Sawodny. Experimental validation of an active heave compensation system: Estimation, prediction and control. *Control Engineering Practice*, 66(December 2016):1–12, 2017, doi:10.1016/j.conengprac.2017.06.005.

[25] Karl Pettersson. *Secondary Controlled Swing Drive*. Master thesis, Linköping University, 2009.

[26] W Wilson. Performance criteria for positive displacement pumps and fluid motors. In *ASME Semi-annual Meeting*, number paper No. 48-SA-14, 1948.

[27] W Schlösser. Mathematical model for displacement pump and motors part 2. In *Hydraulic power transmission*, pages 324–328. London, 1961.

[28] K Huhtala and M Villenius. *Comparison of Steady-State Models of Hydraulic Pump*. Linköping University, Department of Mechanical Engineering, Division of Fluid and Mechanical Engineering Systems, Linkoping, Sweden, 1997.

[29] R Dorey. Modelling of losses in pumps and motors. *First Bath International Fluid Workshop*, 1988.

[30] Harald Ortwig. New Method of Numerical Calculation of Losses and Efficiencies in Hydrostatic Power Transmissions. *SAE International Off-Highway Congress*, 1418(724), 2002, doi:0148-7191.

[31] Heon S. Jeong and Hyoung E. Kim. A novel performance model given by the physical dimensions of hydraulic axial piston motors: Experimental analysis. *Journal of Mechanical Science and Technology*, 21(4):630–641, apr 2007, doi:10.1007/BF03026968.

[32] Noah D. Manring, Viral S. Mehta, Bryan E. Nelson, Kevin J. Graf, and Jeff L. Kuehn. Scaling the Speed Limitations for Axial-Piston Swash-Plate Type Hydrostatic Machines. *Journal of Dynamic Systems, Measurement, and Control*, 136(3), may 2014, doi:10.1115/1.4026129.

[33] Peter Achten and Sjoerd Eggenkamp. Barrel tipping in axial piston pumps and motors. In *Proceedings of 15:th Scandinavian International Conference on Fluid Power, 15th Scandinavian International Conference on Fluid Power, Fluid Power in the Digital Age, SICFP'17, June 7-9 2017 - Linköping, Sweden*, volume 144, pages 381–391, 2017.

[34] Meghan K Miller, Hassan Khalid, Paul W Michael, Jeffrey M Guevremont, Kenneth J Garelick, Grant W Pollard, Aaron J Whitworth, and Mark T Devlin. An Investigation of Hydraulic Motor Efficiency and Tribological Surface Properties. *Tribology Transactions*, 57(4):622–630, 2014, doi:10.1080/10402004.2014.887167.

[35] Monika Ivantysynova and Jonathan Baker. Power loss in the lubricating gap between cylinder block and. *International Journal of Fluid Power*, 10(2):29–43, 2009.

[36] Andrew Schenk and Monika Ivantysynova. A Transient Thermoelastohydrodynamic Lubrication Model for the Slipper/Swashplate in Axial Piston Machines. *Journal of Tribology*, 137(3):031701, jul 2015, doi:10.1115/1.4029674.

[37] Heon-Sul. Jeong. A novel performance model given by the physical dimensions of hydraulic axial piston motors: model derivation. *Journal of Mechanical Science and Technology*, 21(1):83–97, 2007.

[38] Geir-Arne Moslått, M R Hansen, and N S Karlsen. A model for torque losses in variable displacement axial piston motors. *Modeling, Identification and Control*, 39(2):107–114, 2018, doi:10.4173/mic.2018.2.5.

[39] Geir-Arne Moslatt and Michael R. Hansen. Modeling of Friction Losses in Offshore Knuckle Boom Crane Winch System. In *2018 Global Fluid Power Society PhD Symposium (GFPS)*, pages 1–7, Samara, Russia, jul 2018. IEEE.

[40] M. J. Box. A New Method of Constrained Optimization and a Comparison With Other Methods. *The Computer Journal*, 8(1):42–52, 1965, doi:10.1093/comjnl/8.1.42.

[41] Petter Krus, Arne Jansson, and Jan-Ove Palmberg. Optimization for Component Selection Hydraulic Systems. In *Fourth Bath International Fluid Power Workshop*, 1991.

[42] Brueninghaus Hydromatik and Bosch Rexroth AG. Testreport 1229 A4VSG355DS, 2000.

[43] Total Efficiency, Volumetrischer Wirkungsgrad, and Mechanisch-hydraulischer Wirkungsgrad. Sales Information Variable Displacement Motor A6VM Series 63, 2003.

[44] Siemens. Industrial Edge, the SIEMENS Edge Computing Platform, 2020.

[45] Technical Standards Committee, Technical Policy Board, and Technical Policy Board. DNVGL-ST-N001 Marine operations and marine warranty, 2015.

[46] DNV GL. Recommended practice DNVGL-RP-N201, 2019.

[47] Hulpa Marlin, Anders Meisfjordskar, and Jan Petter Svennevig. Subsea lifting: better performance through combined knowledge. *DYP, Magasinet fra forening for fjernstyrt undervannsteknologi*, 2(2):14–15, 2018.

[48] Michael Grieves. Digital Twin : Manufacturing Excellence through Virtual Factory Replication. `https://www.researchgate.net/publication/275211047_Digital_Twin_Manufacturing_Excellence_through_Virtual_Factory_Replication`, 2015.

Appended Papers

A A model for torque losses invariable displacement axial piston motors

Modeling, Identification and Control, Vol. 39, No. 2, 2018, pp. 107–114, ISSN 1890–1328

A model for torque losses in variable displacement axial piston motors

G-A. Moslått [1] M.R. Hansen [2] N.S. Karlsen [3]

[1] *University of Agder and National Oilwell Varco, 4898 Grimstad, Norway.*
E-mail: geir.a.moslatt@uia.no

[2] *Department of Engineering, University of Agder, 4879 Grimstad, Norway.*
E-mail: michael.r.hansen@uia.no

[3] *Bosch Rexroth AS, 1405 Langhus, Norway.*
E-mail: Nicolai.Karlsen@boschrexroth.no

Abstract

This paper includes a comparison of earlier presented models for torque losses in hydraulic motors and several proposed models that all rely on data typically available for a system engineer. The new models and the old ones are compared. The new models are all based on a model developed by Jeong Jeong (2007);Jeong and Kim (2007) with an expansion that include variable displacement. All of the new models yield very good accuracy down to approximately 50% of maximum displacement and down to approximately 15% of maximum speed. In these operational ranges the deviation in torque is less than 1%. The main purpose of the new models is to facilitate simulations of hydraulically actuated winches with a balance between accuracy and model complexity. This purpose is considered fulfilled with several of the proposed models.

Keywords: Hydraulics, torque loss, axial piston motor, winch drive, offshore knuckle boom cranes, Bosch Rexroth.

1 Introduction

The use of mathematical models for hydraulic motors are useful in the industry to estimate losses in a design phase and to be included in simulation models. The main challenge with the use of previously generated research and models in this field is the complexity of the models, especially models that take into account variable displacement. The complexity makes the models harder to use and may increase the cost of computations heavily. This is a huge disadvantage in a design phase when several system configurations, load cases and control algorithms must be evaluated.
In the offshore business today there is a high demand for hydraulic drives in crane and drilling applications. This is especially relevant for large knuckle boom cranes with safe working loads ranging from 80 to 900 metric tons. At the same time the manufacturers have the need to stay competitive both in performance and cost. To maintain a good position in the market the manufacturer mainly has three challenges.
1: Minimization of equipment costs. A system with optimal choice and sizing of components is needed to keep the costs down, however, each delivery is typically tailor-made and there are no prototypes available for testing. This automatically puts more emphasis on modeling and simulation in the design phase.
2: Behavior prediction. It is important for the manufacturers, but also a need from customers (platform operators) to have simulation models that can predict the performance of the equipment under different weather

doi:10.4173/mic.2018.2.5

conditions that are not easily reproduced in tests. Such models can be used in the design phase, virtual testing, and lift preparations. An example is the increasing use of models to engineer subsea lifts for large offshore cranes. These models need a certain accuracy to get approval from third party certification authorities.
3: Minimize test costs. It is a challenge to keep the test time at a minimum especially because there is a trend that crane features are constantly increasing in number and complexity. The manufacturer needs the test time to be as short and effective as possible. Test time is one of the factors that has an important impact on the final cost of a project. Testing is mainly divided into two categories; inhouse testing and real life testing. The first one is done at an office facility and is orders of magnitude less costly than the second one. Due to this, the inhouse testing is preferred when possible. A common factor in all these challenges is that they can all be handled much better with increased component and system knowledge that is implemented in time domain simulation models.
When predicting behavior of a crane it is important to understand what kind of losses and loss properties the different hydraulic actuators have. The focus of this paper is the hydraulic motors of the main winch system found in all offshore knuckle boom cranes. A typical knuckle boom crane design is seen in fig. 1.

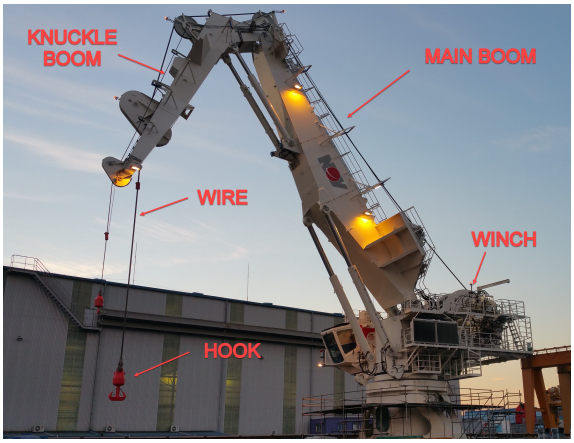

Figure 1: Typical knuckle boom crane design.

There is an increasing demand for accurate modeling of these winch systems to predict the performance during heave compensation, during tension control and when moving payloads through the splash zone. To build these types of models it is important to be able to predict the nonlinear behavior associated with friction and leakage, also referred to as hydromechanical and volumetric losses in hydraulics. The focus of this article is the friction losses in the variable displacement axial piston hydraulic motors of the winch systems, see fig 2.

The overall friction losses are complex combinations of turbulent friction, viscous friction, mixed lubrication friction and dry friction. Despite the importance of accurate modeling there is no unique model of the overall friction loss of hydraulic piston motors with variable displacement. This paper presents a modeling technique that is useful from a crane manufacturers point of view. This means that the following criteria are considered:

- Reasonable trade-off between accuracy and number of parameters
- Computational efficient without introducing complex sub-models concerned with tribology, thermodynamics and structural deformations.
- Developed in cooperation with sub-supplier (motor manufacturer).
- Motor specific.

The paper will investigate the models presented in literature and new models presented in this paper with a view to identify a model that meets the above criteria in the best possible way.

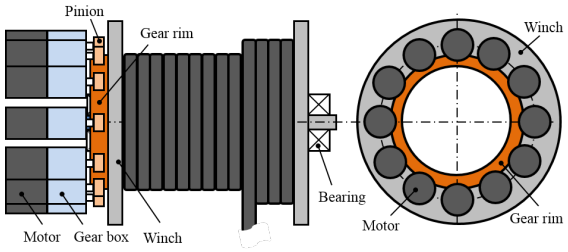

Figure 2: Simple sketch of a winch system.

2 State of the art

The total friction in winch systems has not attracted any research effort, however, the hydraulic motors is a topic subjected to numerous studies. Among the first researchers in this field were Wilson Wilson (1948) and Schlösser Schlösser (1961). Both made some basic and simple models and, normally, both models fail to yield a decent accuracy for the complete 3-dimensional work space of a motor comprising speed, torque and displacement ranges. Due to the lack of accuracy, several methods for model generation have been studied. They can be divided into three categories;

- models based on physical interactions in pump/motor

- numerical models based on curve fitting to experimental data
- analytic models that are based on both numerical and physical models

Huhtala made a comparison in 1997 Huhtala and Villenius (1997) of his own numerical (the two line model) approach with Wilsons physical and Doreys Dorey (1988) analytical approach. He showed that the existing fixed parameter models from Wilson and Dorey did not yield a satisfactory accuracy. Results were especially poor across the displacement range. Huhtala on the other hand, used a numerical approach based on measurements that gave a significantly better accuracy but also introduced 14 parameters for fixed displacement. Ortwig Ortwig (2002) and JeongJeong and Kim (2007) did some work establishing an overview over the different losses in the motor. Based on this knowledge, they made expressions based on assumptions on geometry and tolerances in the motor. Of these advanced expressions Ortwig chose to simplify with a numerical representation of the total loss, while Jeong kept the physical terms and combined them.

3 Model Development

In this section the most common friction loss models are briefly discussed and a number of new models are introduced. The models are presented in the following sections 3.1 to 3.13. The friction torque, T_f, is the absolute friction torque working in opposite direction of ω_m. Hence it can be assumed that all terms in the equations presented can be multiplied with $sign(\omega_m)$.

3.1 Wilson

In 1948 Wilson Wilson (1948) presented a relatively simple model for friction losses in constant displacement motors. The model is grouped into three parts; dry friction proportional with shaft torque, viscous friction proportional with viscosity and speed, and a constant torque loss.

$$T_f = C_a \cdot D_{m,max} \cdot \Delta p_m + C_b \cdot \mu \cdot D_{m,max} \cdot |\omega_m| + C_c \cdot D_{m,max} \quad (1)$$

3.2 Schlösser

Schlösser Schlösser (1961) replaced Wilsons last term with a term for acceleration of the liquid. He assumed a loss term proportional with the square of the tangential velocity of the revolving barrel.

$$T_f = C_a \cdot D_{m,max} \cdot \Delta p_m + C_b \cdot \mu \cdot D_{m,max} \cdot |\omega_m| + C_d \cdot D_{m,max}^{5/3} \cdot \rho \cdot \omega^2 \quad (2)$$

3.3 Thoma

In 1969 Jean Thoma Thoma (1969) made a modification of the Schlösser model by including a displacement variable, α_m, for the liquid acceleration losses. Although the displacement dependency is included for the liquid acceleration losses, the displacement setting is still neglected with regards to the viscous losses in the second term.

$$T_f = C_a \cdot D_{m,max} \cdot \Delta p_m + C_b \cdot \mu \cdot D_{m,max} \cdot |\omega_m| + C_e \cdot \alpha_m^3 \cdot D_{m,max}^{5/3} \cdot \rho \cdot \omega^2 \quad (3)$$

3.4 Pacey

In 1979 Pacey Pacey et al. (1979) presented a modification of the Wilson model to include different displacement settings. He basically took the Wilson model and added $\frac{1-tan\alpha_{m,max}}{1-tan\alpha_m}$, in the dry and viscous friction terms.

$$T_f = C_a \cdot D_{m,max} \cdot \Delta p_m \cdot \frac{1 - tan(\alpha_{m,max})}{1 - tan(\alpha_m)} + C_b \cdot \mu \cdot |\omega_m| \cdot D_m \cdot \frac{1 - \tan(\alpha_{m,max})}{1 - tan(\alpha_m)} + C_e \quad (4)$$

3.5 Huhtala

In 1997 Huhtala Huhtala and Villenius (1997) did a review of the torque loss models of Wilson, Schlösser, Thoma, Zarotti, Dorey, and Rydberg. Huhtala saw the need for better accuracy and a model that would represent the whole working range with regards of pressure, speed and displacement. The model he introduced was based on multiple polynomial fitting and measurements. He reported a better accuracy than Dorey and Thoma, but increased the amount of parameters significantly. For fixed motor displacement you need 14 parameters distributed over four different curve fitted polynomials. The concept is according to Huhtala prepared to represent variable displacement motors, but details are not given and how to adapt is unclear to authors of this paper. Regardless of how to implement, the complexity will increase and several additional curve fitted polynomials will be needed.

3.6 Ortwig

Ortwig Ortwig (2002) did a study in where he investigated 13 different loss terms for describing the total loss in a hydraulic motor. The terms should cover laminar and turbulent flow losses, pulse losses, churning, losses, friction losses at valve plate, piston, roller bearings, seals, mixed bearing friction and solid friction.

Based on these formulas he formed a torque interpolation equation (eq. 5) in exchange for the set of formulas that described each loss term separately. He proved that his new equation gave similar accuracy.

$$T_f = C_e + C_f \cdot \Delta p_m + C_g \cdot |\omega_m| + C_h \cdot |\omega_m| \cdot \Delta p_m + C_i \cdot \omega_m^2 + C_j \cdot \alpha_m + C_k \cdot \alpha_m \cdot \Delta p_m + C_l \cdot \alpha \cdot |\omega_m| \tag{5}$$

3.7 Jeong

A physical model for torque loss was introduced in 2007 by Jeong Jeong and Kim (2007)Jeong (2007). The model considers terms for friction due to forces in moving gaps (piston vs piston block, swash-plate vs slipper, piston block vs port-plate), turbulent port plate inlet loss, port plate notch losses (also assumed turbulent), churning losses and bearing losses. There are similarities between the terms in Jeong and Ortwigs model derivation, but Ortwig ended up simplifying to a numerical model. Jeong simplified his expression, but kept the physical meaning by combining terms with similar parameter dependencies. Unlike Ortwig, Jeong only considered a fixed displacement motor.

$$T_f = C_e + C_f \cdot \Delta p_m + C_g \cdot \mu \cdot |\omega_m| + C_i \cdot \rho \cdot \omega_m^2 + C_k \cdot \frac{\Delta p_m}{|\omega_m|} \cdot \sqrt{\frac{\Delta p_m}{\rho}} + C_m \cdot {\Delta p_m}^2 \tag{6}$$

In this case the C_e term represents Coulomb friction in motor and motor bearings. The C_f term includes pressure dependent bearing losses and piston friction. The C_g term represents viscous losses in bearings, churning losses for the cylinder block, viscous slipper friction and viscous friction between barrel and port plate. Port plate inlet loss and churning losses from pistons and slippers are presented in term C_i. C_k represent the losses due to valve notches in the port plate and C_m is to account for mixed lubrication friction at high pressures.

3.8 Modified Jeong 1 (MJ1)

When forming new alternatives it was chosen to use Jeongs model as a base. Jeongs model was first just modified slightly to account for variable displacement. The effect of these changes are that the term C_i no longer represents both port plate inlet loss and churning losses in a realistic sense, since churning loss is independent of displacement setting.

$$T_f = C_e + C_f \cdot \Delta p_m + C_g \cdot \mu \cdot |\omega_m| + C_m \cdot {\Delta p_m}^2 + C_i \cdot \rho \cdot \omega_m^2 \cdot D_m^3 + C_k \cdot \frac{\Delta p_m}{|\omega_m|} \cdot \sqrt{\frac{\Delta p_m}{\rho}} \tag{7}$$

3.9 MJ2

Next alternative is made to evaluate the impact of removing the losses caused by the turbulent flow through the port notches (C_k).

$$T_f = C_e + C_f \cdot \Delta p_m + C_g \cdot \mu \cdot |\omega_m| + C_i \cdot \rho \cdot \omega_m^2 \cdot D_m^3 + C_m \cdot {\Delta p_m}^2 \tag{8}$$

3.10 MJ3

For MJ3 we removed the term for high pressure boundary and mixed friction (C_m).

$$T_f = C_e + C_f \cdot \Delta p_m + C_g \cdot \mu \cdot |\omega_m| + C_i \cdot \rho \cdot \omega_m^2 \cdot D_m^3 \tag{9}$$

3.11 MJ4

At this point the C_f term is changed such that it varies with displacement. In terms of the physical nature of the C_f-term, it does no longer directly represent the pressure dependent losses in pistons and bearings.

$$T_f = C_e + C_f \cdot \Delta p_m \cdot D_m + C_g \cdot \mu \cdot |\omega_m| + C_i \cdot \rho \cdot \omega_m^2 \cdot D_m^3 + C_m \cdot {\Delta p_m}^2 \tag{10}$$

3.12 MJ5

With alternative 3 (eq.9) as a base, alternative 5 has the exponential in term C_i as a variable parameter. The term is representing the turbulent inlet flow into the chamber. With a perfect turbulent inlet flow the C_o factor will be equal 2. The opposite would be an exponential set to 1 which is used for laminar flow.

$$T_f = C_e + C_f \cdot \Delta p_m \cdot D_m + C_g \cdot \mu \cdot |\omega_m| + C_i \cdot \rho \cdot |\omega_m|^{C_n} \cdot D_m^{C_n+1} + C_m \cdot {\Delta p_m}^2 \tag{11}$$

3.13 MJ6

As an alternative 6 the notch flow loss is set back on but now also dependent on displacement.

$$T_f = C_e + C_f \cdot \Delta p_m \cdot D_m + C_g \cdot \mu \cdot |\omega_m| + C_m \cdot {\Delta p_m}^2 + C_i \cdot \rho \cdot \omega_m^2 \cdot D_m^3 + C_k \cdot \frac{D_m \cdot \Delta p_m}{D_{m,max} \cdot |\omega_m|} \cdot \sqrt{\frac{\Delta p_m}{\rho}} \tag{12}$$

3.14 Comparison

To compare a selection of different models, the model parameters were all determined based on efficiency data from Bosch Rexroth Bosch Rexroth AG (2010) using numerical minimization of the deviation between modeling results and experimental data. A model comparison with the a A6VMs71 280 motor was done first with a fixed displacement setting at $280cm^3/rev$, and then for a whole range of displacement settings. Oil density and viscosity can be considered constants.

Table 1: Basic info, friction models

Author	Year	Model Type	Motor type	Par.
Wilson	1948	Physical	Fixed	3
Sclosser	1961	Physical	Fixed	3
Thoma	1969	Physical	Variable	3
Pacey	1979	Physical	Variable	3
Huhtala	1997	Numerical	Variable	28
Ortwig	2002	Numerical	Variable	8
Jeong	2007	Physical	Fixed	6
MJ1	2017	Physical	Variable	6
MJ2	2017	Physical	Variable	5
MJ3	2017	Physical	Variable	4
MJ4	2017	Phys- and numerical	Variable	5
MJ5	2017	Phys- and numerical	Variable	6
MJ6	2017	Phys- and numerical	Variable	5

For the first comparison (fig 3), parameter identification is performed for a fixed displacement setting of A6VM280 at $280cm^3/rev$. The model error is computed as a normalized summation of squared deviations of modeled and measured friction torques.

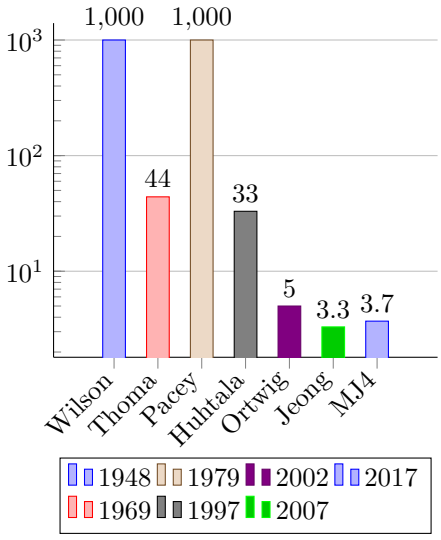

Figure 3: Model error, when optimizing model parameters for fixed displacement. Displacement setting was held constant at maximum value $280cm^3/rev$.

For the fixed motor model identification a complete 2D operation area are considered with rotational speed range of $400rev/min$ to $2500rev/min$ and pressures from $50bar$ to $350bar$. The results show that a significant improvement is obtained with Ortwigs and Jeongs model.

Next, the models are investigated for variable displacements. However, not all of the models listed in table 1 are adaptable to variable displacement motors. For example, Wilson and Jeong do not include any variables related to displacement setting. Pacey's model is an extension of Wilson's model so that variable displacement can be handled and, similarly, the modified Jeong models (MJ1...6) presented earlier are extensions of Jeong's model. The displayed error in figure 4 and 5 is an accumulated normalized error for the complete 3D operational range (displacement, pressure drop, angular speed).

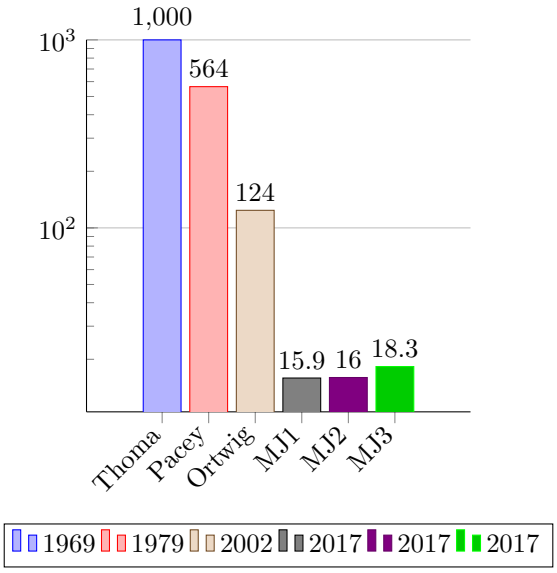

Figure 4: Model error, when optimizing model parameters for variable displacement. Motor type is A6VM 71series size 280.

As can be seen in fig.4 the new models give a significant better results for this variable axial piston motor. Comparing the different new models (see figure 5), it can be seen that models MJ4, MJ5 and MJ6 are the ones with the best accuracy.

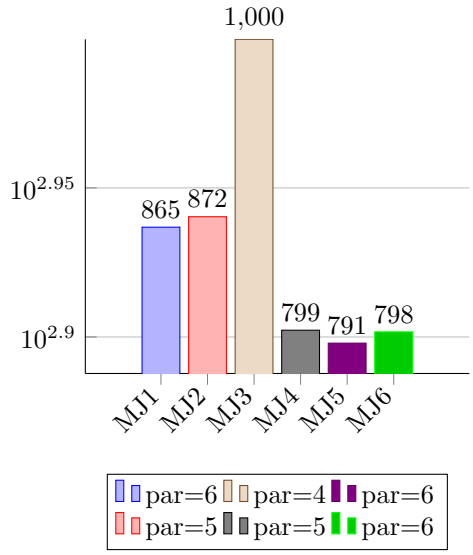

Figure 5: Model error, when optimizing model parameters for variable displacement.

MJ5 has slightly better accuracy but does also have the most parameters (6). MJ4 is seen as the model with the simplest and preferred model structure. This model is used for further investigation of actual model error.

The contributions from the terms (T_{f1-6}) in MJ4, MJ5, and MJ6 are shown in figure 6.

$$T_{f1} = C_g \cdot \mu \cdot |\omega_m| \tag{13}$$

$$T_{f2} = C_i \cdot \rho \cdot |\omega_m|^{C_n} \cdot D^{C_n+2} \tag{14}$$

$$T_{f3} = C_f \cdot \Delta p_m \cdot D_m \tag{15}$$

$$T_{f4} = C_e \tag{16}$$

$$T_{f5} = C_m \cdot \Delta p_m^2 \tag{17}$$

$$T_{f6} = C_k \cdot \frac{D_m \cdot \Delta p_m}{D_{m,max} \cdot |\omega_m|} \cdot \sqrt{\frac{\Delta p_m}{\rho}} \tag{18}$$

$$T_f = T_{f1} + T_{f2} + T_{f3} + T_{f4} + T_{f5} + T_{f6} \tag{19}$$

The contributions are summarized over a range in angular velocity from $n_1 = 300 rev/min$ to $n_2 = 2500 rev/min$ with steps of $10 rev/min$, and then divided by sum of total friction (see eq.20). The two most significant contributors (see fig. 6) in all these models (MJ4, MJ5, MJ6) are the turbulent pressure loss (T_{f2}) and the Coulomb friction loss (T_{f4}).

$$T_{fi\%} = \frac{\sum_{n_1}^{n_2} T_{fi}}{\sum_{i=1}^{i=6} \sum_{n_1}^{n_2} T_{fi}} \tag{20}$$

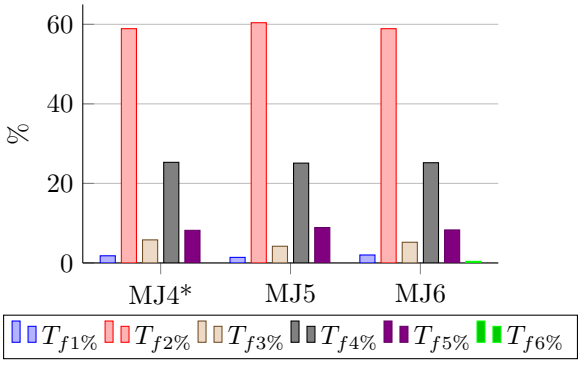

Figure 6: Each term from the friction models in percentage of the accumulated friction force at 200bar, $250 cm^3/rev$ and angular velocity from 300 to 2500rev/min.
*For MJ4, C_n in T_{f2} equal 2.

The contribution of these losses are in figure 7 shown in more detail for model MJ4.

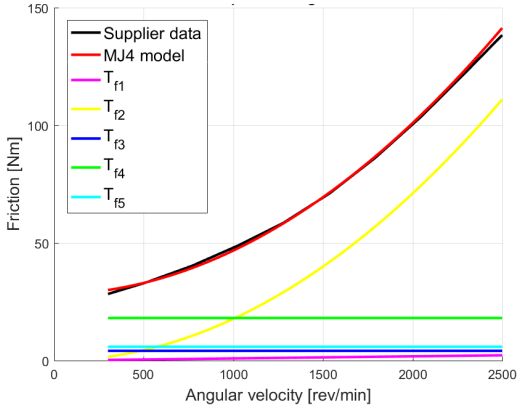

Figure 7: Contributions of the different terms within the motor friction formula MJ4. Motor displacement is set to $250 cm^3/rev$ and pressure drop across motor is held constant at 200bar. C_n in T_{f2} equal 2

4 Results

The results from figure 8 and 9 show a trend that the friction model error is within 1% for displacement settings above $150 cm^3/rev$ and speeds up to 2500rev/min. For lower speeds up to 1500rev/min the error is typically less than 0.5%. The error is calculated as a percentage of the nominal torque, T_N.

$$T_N = D_m \cdot \Delta p_m \tag{21}$$

The lower displacement settings in figure 9, show that the model becomes less accurate as the displace-

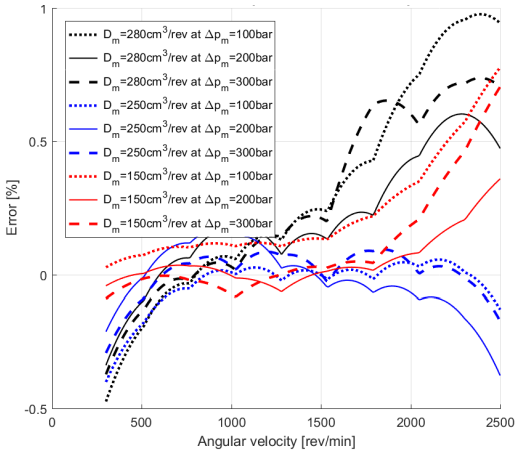

Figure 8: Error between model, MJ4, and the performance data from supplier. Error is measured as a percentage of the nominal motor torque. The comparison is performed at $\Delta p_m = 100bar$ $\Delta p_m = 200bar$ and $\Delta p_m = 300bar$.

ment is reduced below $150cm^3/rev$ and also at speeds above 2000 rev/min.

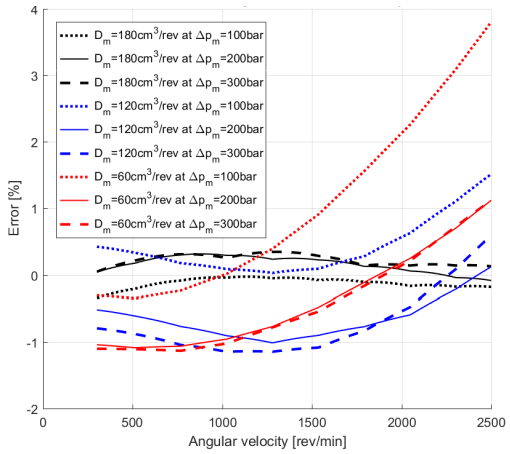

Figure 9: Error between model for low displacement settings, MJ4, and the performance data from supplier. Error is measured as a percentage of the nominal motor torque. The comparison is performed at $\Delta p_m = 100bar$ $\Delta p_m = 200bar$ and $\Delta p_m = 300bar$.

5 Conclusions

For simulation purposes the MJ4 model is showed to have a decent accuracy (within 1% of applied torque) in the range from 400 to $2500rev/min$ and 100 to 300bar. What the model shows is drastically reduced accuracy at motor displacements lower than approx $120cm^3/rev$.
The model tends to have higher accuracy at low speeds near $400rev/min$. For speeds lower than $400rev/min$ the suppliers data-table does not give any information. Stiction forces and friction with mixed lubrication is not represented, but there is reason to believe that it should be detectable at low speeds.
Any temperature dependency is not taken into account and oil density and viscosity is kept constant. The viscosity could be implemented in the formulas, but due to the limited amount of data from supplier it would not be possible to verify their influence.

The model investigation also shows a need for customized models. The MJ4 is good for the Bosch Rexroth 71 series, but fitting the same model to a 63 series $(28-200cm^3/rev)$ does not achieve the same accuracy. An example is shown in figure 10, where the MJ4, MJ5, and MJ6 and tried fitted to a A6VM S63 $200cm^3/rev$, and a A6VM S71 $215cm^3/rev$.

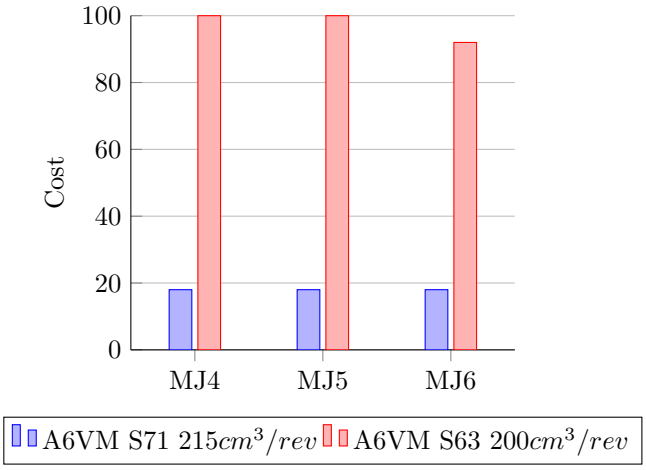

Figure 10: Comparison of two different motors with the same friction model structure. "Cost" is data from the optimization algorithm and is representing the summarized squared error between the supplier data and the model. The data is then normalized from 0 to 100.

As seen in figure 10 the accuracy differs a lot when comparing it to data from a similar but different hydraulic motor. The difference highlights the complexity of the motors and implies that a general friction model cannot fit all range of hydraulic motors without including more model terms.

6 Further work

The low speed friction has a high influence on driving performance and should be investigated further. Figure 11 shows the cyclic behavior for a winch in heave compensation mode, and as can be seen the winch is passing through the low speed area two times for every wave cycle.

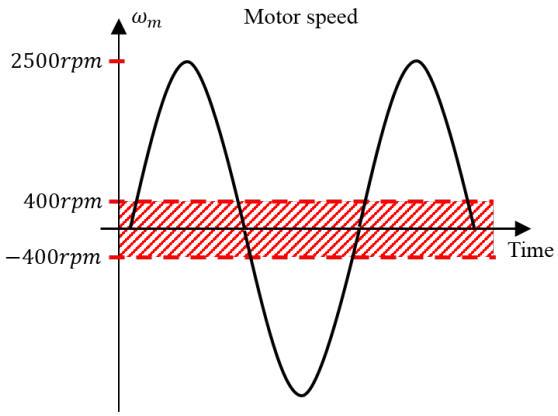

Figure 11: Typical winch speed situation for a winch doing heave compensation.

Since the purpose of this model is closed loop hydraulic crane systems, the current work must be continued with measurement performed on actual cranes with the proposed MJ4 as initial model but with extra terms handling both the remaining friction of the crane power transmission as well as increased motor friction at low-to-zero speed.

References

Bosch Rexroth AG. Sales Information, Axial Piston Units. 2010.

Dorey, R. Modelling of losses in pumps and motors. *First Bath International Fluid Workshop*, 1988. URL www.scopus.com.

Huhtala, K. and Villenius, M. Comparison of Steady-State Models of Hydraulic Pump. 1997.

Jeong, H.-S. A novel performance model given by the physical dimensions of hydraulic axial piston motors: model derivation. *Journal of Mechanical Science and Technology*, 2007. 21(1):83–97. doi:10.1007/BF03161714.

Jeong, H. S. and Kim, H. E. A novel performance model given by the physical dimensions of hydraulic axial piston motors: Experimental analysis. *Journal of Mechanical Science and Technology*, 2007. 21(4):630–641. doi:10.1007/BF03026968.

Ortwig, H. New Method of Numerical Calculation of Losses and Efficiencies in Hydrostatic. *SAE International Off-Highway Congress*, 2002. (724).

Pacey, D. A., Turnquist, R. O., and Clark, S. J. The development of a coefficient model for hydrostatic transmissions. In *In: Proc.35th Nat.conf.on Fluid Power*, volume 33. 35th National Conference in Fluid Power, Chicago, pages 173–178, 1979. URL www.scopus.com.

Schlösser, W. Mathematical model for displacement pump and motors part 2. In *Hydraulic power transmission*, pages 324–328. London, 1961.

Thoma, J. Mathematical models and effective performance of hydrostatic machines and transmission. *Hydraulic and Pneumatic Power*, 1969. pages 642–651. URL www.scopus.com.

Wilson, W. Performance criteria for positive displacement pumps and fluid motors. In *ASME Semi-annual Meeting*, paper No. 48-SA-14. 1948.

B Modeling of Friction Losses in Offshore Knuckle Boom Crane Winch System

C A control algorithm for active/passive hydraulic winches used in active heave compensation

Proceedings of the ASME/BATH 2019
Symposium on Fluid Power and Motion Control
FPMC2019
October 7-October 9, 2019, Sarasota, FL, USA

FPMC2019-1710

A CONTROL ALGORITHM FOR ACTIVE/PASSIVE HYDRAULIC WINCHES USED IN ACTIVE HEAVE COMPENSATION

Geir-Arne Moslått*
Department of Engineering
University of Agder
Grimstad, Norway
Email: geir.a.moslatt@uia.no

Damiano Padovani
Department of Engineering
University of Agder
Grimstad, Norway
Email: damiano.padovani@uia.no

Michael R. Hansen
Department of Engineering
University of Agder
Grimstad, Norway
Email: michael.r.hansen@uia.no

ABSTRACT

The most common active heave compensated offshore cranes have hydraulic winch systems. This paper investigates an active/passive hydraulic winch system with variable-displacement motors and variable-displacement pumps. The paper addresses the challenges when the active motors are set with a low displacement. The active motor displacement is shown to have significant impact on the dynamics of the closed loop hydraulic system. The classical control strategy for this type of system do not address these challenges and will in certain situations have significantly reduced performance. Therefor, a new control method is presented that utilize the variable displacement of the pumps and motors for speed control and to improve dynamics characteristics. The new winch controller is tested in a high-fidelity simulation model and is shown to improve low speed performance, reduce winch speed limitations by up to 30%, reduce system peak pressure by approximately 20%, and reduce control error by approximately 30%.

NOMENCLATURE

α_M	Swash plate angle on motor unit in percentage of maximum angle.
α_P	Swash plate angle on pump unit in percentage of maximum angle.
ω_M	Rotational speed on motor unit.
ω_P	Rotational speed on pump unit.
a_{tip}	Measured vertical acceleration at crane tip.
B_v	Viscous system damping relative to motor shaft speed.
$D_{M,max}$	Maximum allowable motor displacement in AHC.
$D_{M,min}$	Minimum allowable motor displacement in AHC.
$D_{P,max}$	Maximum displacement on pump unit.
J_{eq}	Equivalent mass moment of inertia referred to the hydraulic motor shaft.
K_{red}	Gain for motor reduction.
p_1	Pressure in the high-pressure line between pump and motor unit.
p_2	Pressure in the low-pressure line between pump and motor unit.
u_M	Swash plate control signal on motor unit.
u_P	Swash plate control signal on pump unit.
u_{ff}	Feedforward pump control signal.
v_{tip}	Measured vertical velocity at crane tip.

INTRODUCTION

Offshore knuckle boom cranes are heavy lifting cranes, typically with a lifting capacity from 20 ton and up to 800 ton. These cranes are used for subsea lifts which involve subsea installations being landed to and lifted off the seabed (a representative example is depicted in Fig. 1). These cranes are typically placed on floating vessels which makes them a target for large dynamic

*Address all correspondence to this author.

forces. Due to the high risk of overloading the crane when lifting off and landing installations on the seabed the cranes are equipped with heave compensation.

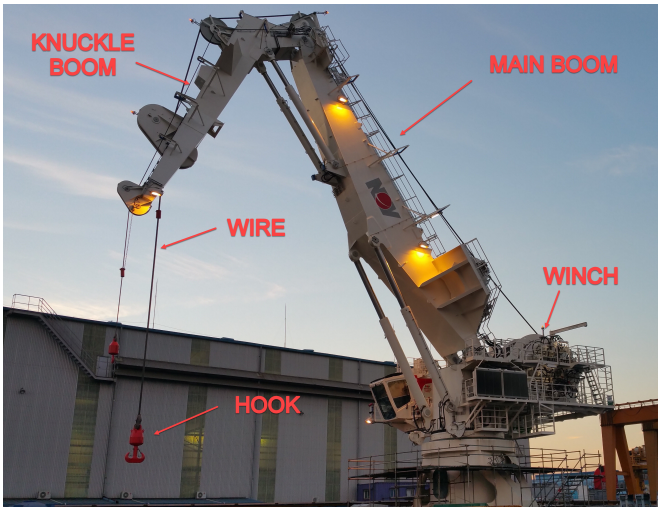

Figure 1: Typical offshore knuckle boom crane with active heave compensation and a maximum lifting capacity of 150 ton. [1].

There are two main types of heave compensation (HC), passive and active, and this paper considers the widespread practical systems that combines both. Passive heave compensation (PHC) is obtained by introducing a gas spring in series with the mechanical load. The main disadvantage of the passive heave compensation is the system friction that directly influences the performance as well as the large gas banks required to create the desired gas spring stiffness. Active heave compensation (AHC) uses position feedback from the winch and motion feedback from the vessel to actively cancel out vessel induced movement on the crane hook. When AHC is combined with PHC its main task is to maintain position control of the load while counteract the forces from acceleration, friction and inertia. Hydralift (now National Oilwell Varco) delivered their first active/passive HC system in 1992. Since then, promising winch drive systems have been developed, such as secondary-controlled (constant pressure) hydraulic drives (digital or analog), and electric drives. These systems are well suited for recuperation of energy when subjected to negative loads [2] [3]. The secondary control units benefit higher speed capabilities, and improved system response compared to the classic primary pump-controlled systems. Secondary control was introduced already back in 1977 [4] for hydraulic systems. Unfortunately there are some common drawbacks with these aforementioned methods. They require expensive components such as electric motors, over-center hydraulic motors or digital displacement hydraulic motors. In addition they require a large amount of coding to adapt old programming for safety features and winch operation. Due to this the industry has been relatively reluctant to change towards these new systems. Several of the existing crane suppliers do offer some of these winch systems [5–8], but often in addition to offer the classical type with active/passive HC. The result is that the classic system is still popular among the clients because the price is lower. The classic active/passive systems have been improved since they first came in the early 90s. At that point the passive torque was controlled by adjusting the pressure in large banks of pressurized air. This was done with huge compressors, but was a slow system which required slow load changes and a long preparation time. From year 2001, the passive system torque has been controlled with variable displacement motors and nitrogen pressure banks with no need for pressure adjustment. Otherwise the active/passive system is more or less the same disregarding some new and some updated sensors for improved safety and control. The current system has however huge unexplored possibilities for improved performance due to how the system controls the variable pumps and motors. This will be investigated further in this paper.

Figure 2 show a typical active passive winch used for HC, where the hydraulic motors are speed-controlled to compensate for the vessel motion.

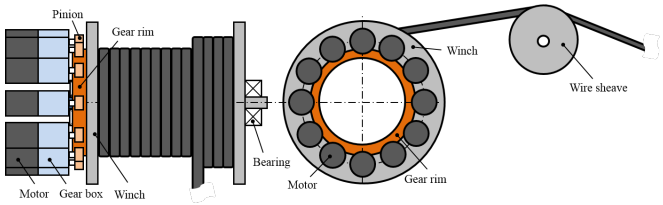

Figure 2: Basic components of AHC winch [1].

The main idea behind this paper is twofold: firstly, to present the challenges of AHC systems with fixed motor displacement, and secondly, to introduce a semi-secondary-control (SSC) method that takes advantage of the variable motor displacement with a view to meet the challenges. Limited work has been done on combining primary and secondary control. In [9], primary, secondary and combined control laws are developed and simulated for hydrostatic transmissions. The design criteria are response time and energy efficiency and it is shown that the combined method yields the best performance. However, no emphasis is on oscillatory behavior and in this work it is shown that the advantage of combined primary-secondary control also includes improved dynamic performance in this respect. One of the main challenges with the current AHC system is poor dynamic performance at low motor displacement leading to reduced controllability. In this work several in-field results combined with simulations from a high-fidelity model are used to highlight the oscillatory nature of the current system. More specifically, the proposed controller increases the motor displacement at low speeds

to improve the dynamic performance of the AHC system without affecting the demand for installed pump capacity. This method is related to the ones used for speed control of mobile machines with closed loop hydraulic systems, where the standard speed control is divided into three stages [10]. The first step is to increase the pump displacement, then the motor displacement is reduced, and at last additional speed is applied by increasing the rotational speed of the pump. The AHC winch is equipped with constant speed pumps and the proposed SSC method is a combination of the two first stages in [10]. The measurements and simulations are carried out on an AHC winch system developed by National Oilwell Varco (NOV) which is a world leading manufacturer of AHC cranes. The simulation model is based on a state-of-the-art model developed at NOV and adjusted to accommodate the proposed SSC method.

CONSIDERED SYSTEM

The HC system investigated in this paper corresponds to one of the most common National Oilwell Varco (NOV) offshore cranes with a nominal lifting capacity (safe working load = SWL) of 150 metric tonnes. It is a closed-loop hydraulic system and it is known as an active/passive system that is designed as two separate hydraulic loops connected to the winch, see Fig. 3, by means of variable displacement motors. The passive system is a constant pressure secondary control system designed and controlled to balance the nominal weight of the load. The active system is connected in parallel with the passive system through a common gear rim.

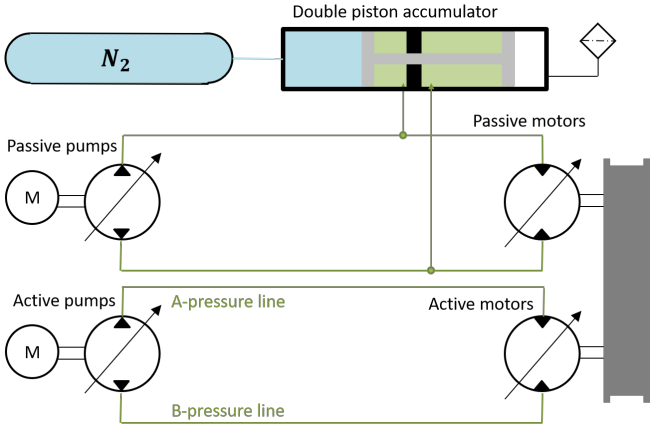

Figure 3: Simplified winch system overview.

The active system represents the AHC part of the HC system and it is used for position control of the winch so that it meters wire in or out in accordance with the input from the crane operator while compensating for the motion of the vessel. The displacement of the active pumps is controlled based on the input from a motion sensor that picks up the position, velocity, and acceleration (motion reference unit = MRU) of the vessel upon which the crane is mounted together with the feedback from the actual winch motion. The active system absorbs all the remaining forces which mainly include mechanical and hydraulic friction and acceleration of inertia. The displacement of the motors is only controlled as a function of the winch layer and the selected mode, high-speed (HS) or normal-speed (NS). The active motor displacement is held fixed to avoid jeopardizing the position control which is allowed to work as a single input – single output (SISO) system in this way.

In NS mode the displacement of the active motors is set to a value so that the active motors can deliver a certain percentage of the SWL. For this crane this is 30% of the SWL, or 45 metric tonnes, and this value is based on best practice developed over many years that saying that the active motors must be able to deliver 30% of the static load to handle friction and acceleration loads without compromising the position control. Since the active motor displacement is held fixed this gives a conservative design for situations where the load is less than the SWL. This is shown in Fig. 4, where the range of operation for NS is indicated. It is clear that the obtainable maximum wire speed in NS, $U_{max}^{(NS)}$, is substantially smaller than the maximum obtainable winch speed, U_{max}, where the latter corresponds to minimum active motor displacement and maximum active pump displacement. If the active motor displacement were continually adjusted to be 30% of the actual load rather than of the SWL, then the operational range would correspond to that of the NS mode plus the triangle shown in Fig. 4.

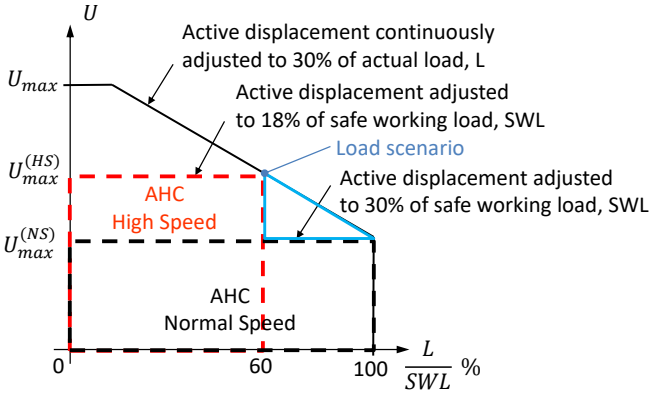

Figure 4: Operational range for the HC system. The wire speed is referred to as U and the actual load as L. The two rectangles indicates the operational range of NS and HS mode.

To access some of the unused wire speed potential without compromising the SISO control strategy, the HS mode is available, which simply corresponds to a reduced setting of the active

motor displacement. It is desired that loads up to 60% of the SWL are handled in HS to maximize operational weather window. Therefore, according to the best practice at NOV the active displacement is adjusted to withstand 18% (30% of 60%) of the maximum SWL, or 36 metric tonnes. This mode is chosen when it is known that the actual load will remain well below the SWL and it introduces a new operational window as shown in Fig. 4 with higher possible wire speed.

The overall control system block diagram for the new proposed controller is shown in Fig. 14. The classical controller is identical except for the active motor displacement calculations marked with red boxes. In the classical controller the motor displacement is only changed due to the operators choice between high-speed mode and normal-speed mode and the amount of wire layers on the winch.

System challenges

The design of the hydraulics and of the control system produces two main challenges. These challenges are confirmed and validated throughout this section with real life field measurements.

1. The SISO concept with fixed active motor displacement poses a limitation on the maximum wire speed that is only partially solved with the two different speed modes.
2. The biggest contributor to control error in AHC is when the winch motion changes direction of rotation. The error contribution from the stick slip behaviour is not seen as critical if it is kept to a minimum. However, experience shows that the motor displacement in the active system has a significant impact on zero/low speed performance. Lowering the displacement due to the winch layer or to the chosen speed mode reduces the smoothness of the winch speed, especially at low speed motions.

Challenge number one is mainly due to system and control design. The second challenge is a result of the combination of the control system and the system dynamics. The result is due to several dynamic and physical properties of the system. Firstly, the nominal pressure in the system will increase due to the lowered displacement. Therefore, a higher start-up pressure will be needed to overcome the stiction in the winch system. The increased start-up pressure will cause larger oscillations of the pressure in the hydraulic circuit that will need longer time to be cancelled out. A side effect of the need for higher start-up pressure is that the pump will use more time to build up the necessary pressure. In addition, the leakage will increase due to the increased pressure. The relative leakage compared to the nominal flow will increase because of the lowered displacement. The extra leakage and delay in pressure build up will cause two things. Firstly, the dead band of the pump signal versus the winch movement will increase. Secondly, because of the increase in dead band the control signal will be less smooth due to a dominant feed forward signal from the crane tip speed, see Fig. 14, that does not consider a varying signal dead band. Additionally, the displacement setting has a significant impact on the eigenfrequency of the system. Therefore, the overall bandwidth is reduced with reduced displacement. To sum up there are three main effect of reduced motor displacement; increased pressure peak at start, increased deadband of pump vs winch movement, and reduced system bandwidth. This phenomenon is visualized in Fig. 5 and Fig. 6 where a repeated ramp up of the winch speed is performed with four different motor displacements.

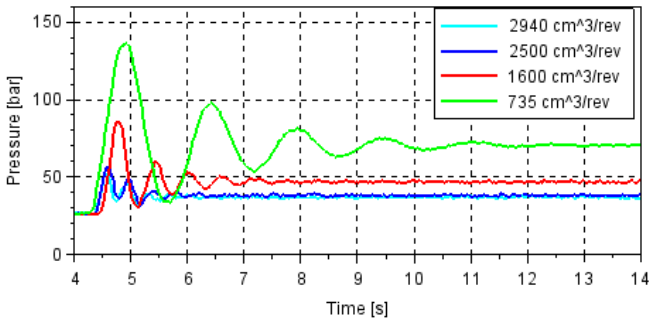

Figure 5: A-side pressure while ramping up the winch speed.

The system is a closed loop hydraulic system with the speed controlled by variable displacement axial piston pumps. The system has 12 variable axial piston motors with a maximum displacement of 250 cm^3/rev per motor. For each test the motor displacement is kept constant. The periodic oscillation time is increasing from 0.4 second at 2940 cm^3/rev to 1.5 seconds at 735 cm^3/rev. It is also seen that when the displacement is lowered the dampening of the control pressure is reduced. The lowered eigenfrequency and lowered damping is giving a significant impact on the winch speed when the displacement is reduced to 735 cm^3/rev, causing heavy oscillations in winch speed (see Fig. 6).

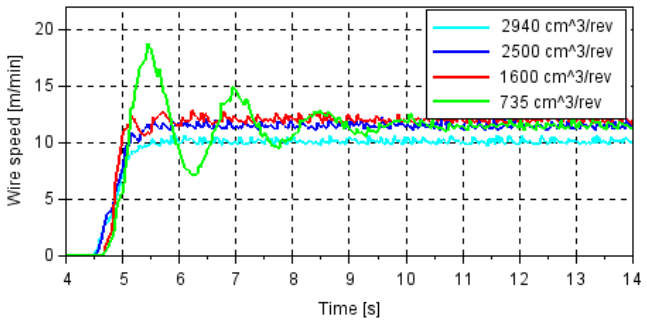

Figure 6: Winch speed for different motor displacement settings. Maximum is 250 cm^3/rev per motor (total of 3000 cm^3/rev)

Table 1: DISPLACEMENT IMPACT

Motor displacement	Period	Effect on winch speed
2940 cm^3/rev	0.4s	No
2500 cm^3/rev	0.4s	No
1600 cm^3/rev	0.7s	Yes
735 cm^3/rev	1.5s	Yes

In the examination of the results (see table 1) shown in Fig 6, the displacement is shown to have a significant impact on the oscillation frequency. Oscillation frequency period is measured as the time between first and second peak and is significantly increased in the two measurements with 1600 cm^3/rev and 735 cm^3/rev. In normal crane operation (not AHC) the challenges visualized in Fig. 5 and Fig. 6 are solved by a winch controller that only allows the motors to be at the maximum displacement setting when the winch speeds are low. A similar control strategy is missing for AHC which results in a very sensitive winch at low speeds and reduced displacement of the motors. One of the most significant difference is how the crane performs in low speed AHC for active/passive systems. Winch stiction is significant and initiate oscillations. Thus, the system dynamics will be important.

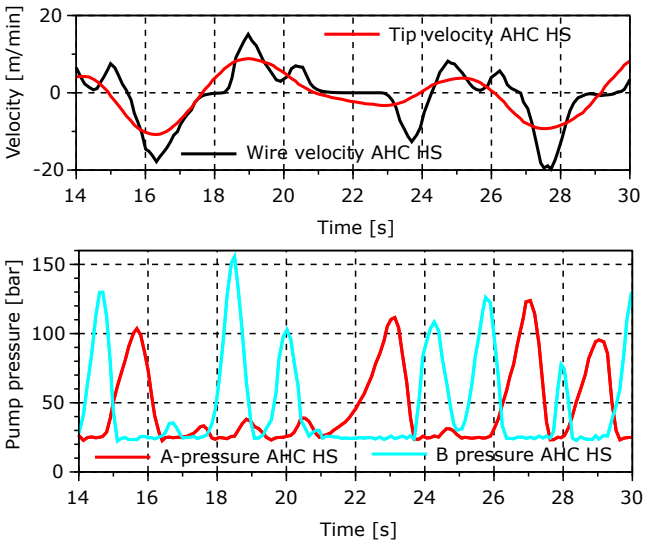

Figure 7: Boom tip velocity (reference speed), and actual wire speed in AHC. Lower plot shows the corresponding A-side and B-side pump pressure, which is located according to A and B line in Fig. 3. Displacement is 162 cm^3/rev on each active motor.

In Fig. 7 to Fig. 8 some measurements taken offshore with a 165 tons crane is displayed. The measurements were taken in November 2016 in the Gulf of Mexico. The hook load for these measurements is 4 tons (in water). The crane has three active motors with a maximum of 250 cm^3/rev per motor.

It can be seen by comparing Fig. 7 and Fig. 8 that low displacement gives significantly more oscillations in the pressure, and it also affects the winch speed control.

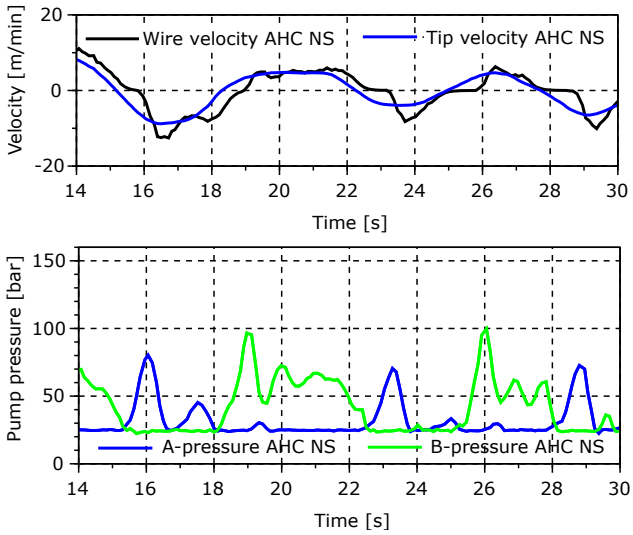

Figure 8: Boom tip velocity (reference speed), and actual wire speed in AHC. Lower plot shows the corresponding A-side and B-side pump pressure, which is located according to A and B line in Fig. 3. Displacement is 245 cm^3/rev on each active motor.

Linear model of the hydraulic system

The reduced winch speed control and the increase in pressure oscillations is a result of the changes in the hydromechanical system. One of the main advantages with a high motor displacement around zero velocity is the reduced pressure build required to overcome stiction and other non-linearities in the system friction. Another obvious effect, is the change in hydro-mechanical resonance frequency. To explain the mathematics behind the phenomena, an evaluation of the simplified hydraulic circuit (Fig. 9) is performed.

System equation:

$$\frac{V_1}{\beta} \cdot \Delta\dot{p} = D_{P,max} \cdot \alpha_P \cdot \omega_P - C_1 \cdot \Delta p - D_{M,max} \cdot \alpha_M \cdot \omega_M, \quad (1)$$

$$p_2 = constant$$

Where the external leak on the pressure side of pump and motor and the internal leakages across pump and motor are merged to-

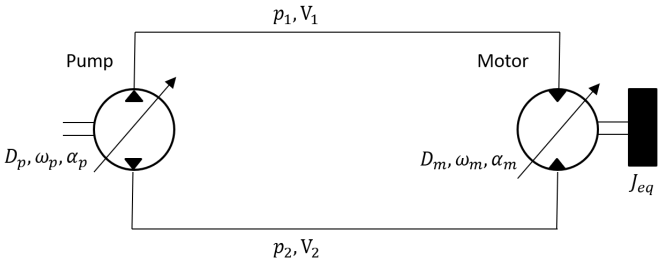

Figure 9: Simplified closed loop hydraulic circuit.

gether and represented as an internal leakage, $C_1 \cdot \Delta p$. V_1 is the total volume between motor and pump.

$$J_{eq} \cdot \dot{\omega}_M = -B_v \cdot \omega_M + D_{M,max} \cdot \alpha_M \cdot \Delta p - T_L - T_{CF} \tag{2}$$

The linear model for the hydraulic system is represented on the standardized form seen in Eqn. 3 and Eqn. 5:

$$\dot{\mathbf{x}} = \mathbf{A}\mathbf{x} + \mathbf{B}u + \mathbf{G} \tag{3}$$

$$\begin{bmatrix} \Delta\dot{p} \\ \dot{\omega}_M \end{bmatrix} = \begin{bmatrix} \frac{-C_1\beta}{V_1} & \frac{-D_{M,max}\alpha_M\beta}{V_1} \\ \frac{D_{M,max}\alpha_M}{J_{eq}} & \frac{-B_v}{J_{eq}} \end{bmatrix} \begin{bmatrix} \Delta p \\ \omega_M \end{bmatrix} + \begin{bmatrix} \frac{D_{P,max}\omega_P\beta}{V_1} \\ 0 \end{bmatrix} \alpha_P + \begin{bmatrix} 0 \\ \frac{-T_L - T_{CF}}{J_{eq}} \end{bmatrix} \tag{4}$$

$$y = \mathbf{C}\mathbf{x} + \mathbf{D}u \tag{5}$$

$$y = \begin{bmatrix} 0 & 1 \end{bmatrix} \begin{bmatrix} \Delta p \\ \omega_M \end{bmatrix} + [0]\,\alpha_P \tag{6}$$

As a simplification the external forces such as Coulomb friction (T_{CF}) and load (T_L) were treated as a disturbance and neglected in the analysis. Derived with Laplace transformation the transfer function with input U and output Y is set:

$$\frac{Y(s)}{U(s)} = \mathbf{C}\left[\mathbf{I} \cdot s - \mathbf{A}\right]^{-1}\mathbf{B} + \mathbf{D} \tag{7}$$

$$\frac{Y(s)}{U(s)} = \frac{\frac{D_{M,max} \cdot \alpha_m \cdot D_{P,max} \cdot \omega_P \cdot \beta}{V_1 \cdot J_{eq}}}{s^2 + \left(\frac{B_v}{J_{eq}} + \frac{C_1 \cdot \beta}{J_{eq}}\right) \cdot s + \left(\frac{\beta \cdot D_{M,max}^2 \cdot \alpha_M^2}{J_{eq} \cdot V_1} + \frac{B_v \cdot C_1 \cdot \beta}{J_{eq} \cdot V_1}\right)} \tag{8}$$

$$\omega_0 = \sqrt{\frac{\beta \cdot D_{M,max}^2 \cdot \alpha_M^2}{J_{eq} \cdot V_1} + \frac{B_v \cdot C_1 \cdot \beta}{J_{eq} \cdot V_1}} \tag{9}$$

The derived eigenfrequency formula in Eqn. 9 shows that a reduction in the motor displacement will decrease the eigenfrequency. This corresponds well with the observations from test and simulation model results.

SIMULATION MODEL

To address and visualize the aforementioned issues, a simulation model of the active-passive system has been developed for a 150 ton crane. The model overview is given in Fig 11. The upper half of the model can be identified as the active system, where an equivalent active pump and an equivalent active motor are implemented (1 and 3, respectively). The pumps and motors in the passive system are identified as 2 and 4. The passive system also has a double piston accumulator (6). Marked with identifier 5 there are three submodels used to calculate the friction in active motors, passive motors and the remaining system friction from gears, bearings, wire sheaves etc. These submodels are based on previous investigations of motor and winch friction [1] [11]. The crane model has an integrated control system (7) that is verified to be working in the same way as the real control system implemented in the PLC on the full size real crane. 9 includes a submodel for calculating the equivalent mass moment of inertia of both the winch and the wire. In addition, it calculates what layer number the and layer-diameter of actual winch layer. 8 encapsulates a submodel meant for calculating the load dynamics based on the wirelength, the load geometry and the sea conditions.

Pumps (1-2)

The winch systems pumps are modelled with equivalent sizes to represent the same amount of flow capacity. The crane size described investigated in this paper has 2 active and 2 passive pumps. The pump shaft speed is simulated as load independent and is constant. For the pumps an important factor to include is the swash plate response. In the simulation model a second order response is included and fitted to results taken from the field. Small differences between pump sizes can be found, but the variations for the measured pump sizes are low and neglected in the model.

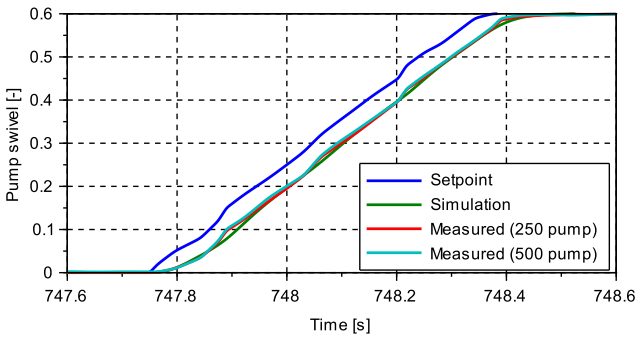

Figure 10: Swivel response test of A4VSG pumps on a 165 ton crane with the control setup that NOV uses. Pump size $500cm^3/rev$ and $250cm^3/rev$ are tested.

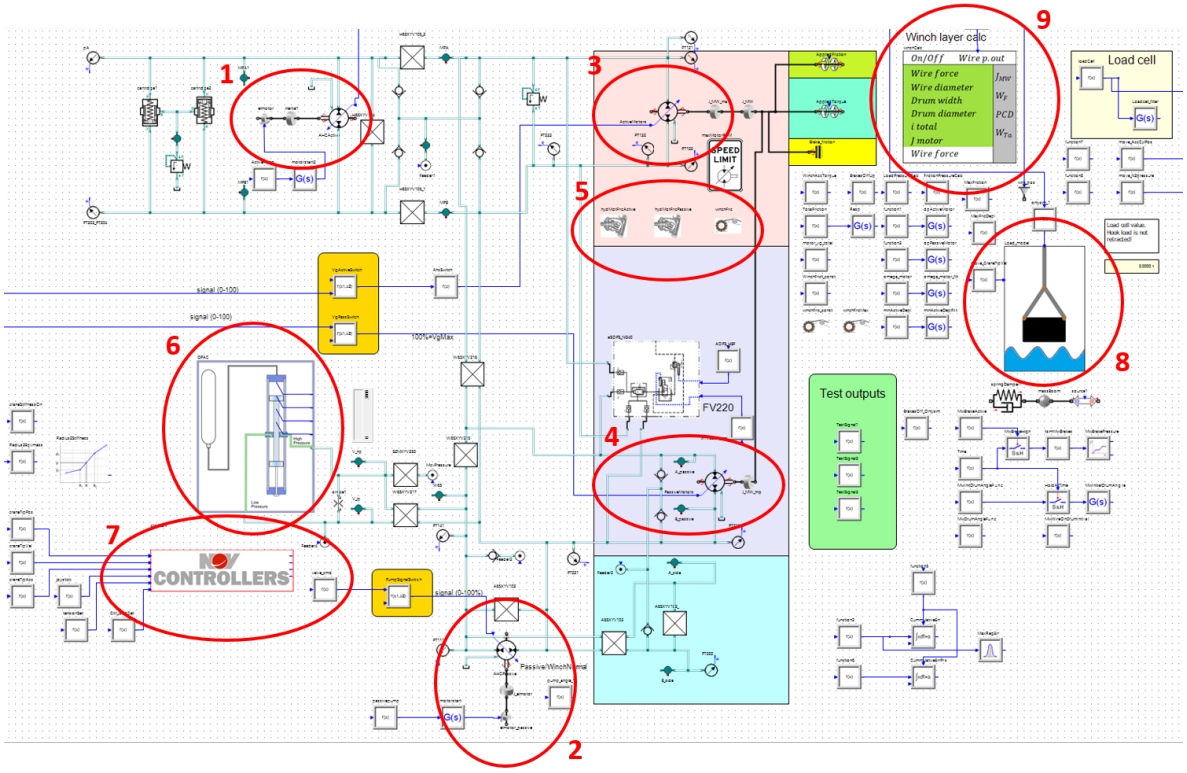

Figure 11: Overview of the high fidelity model built in SimulationX.

In Fig. 10 and in Fig. 12 a comparison between measured and simulated results is displayed. The comparison includes pump sizes, 250 and up to $500cm^3/rev$ and indicates that the variations in pump response are insignificant. The chosen pump model (Eqn. 10) for the winch model shows a good fit with the measured results.

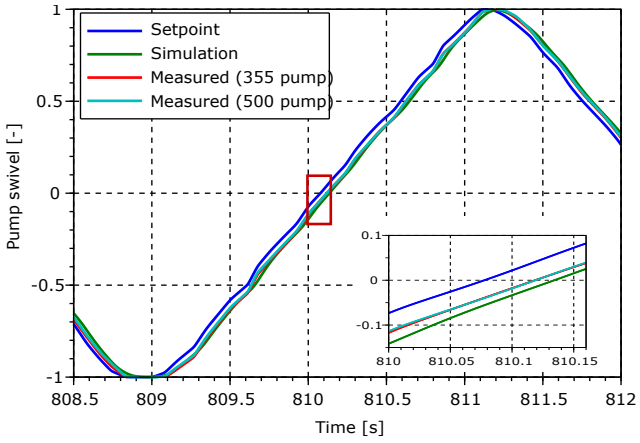

Figure 12: Response test of A4VSG pumps using a sinusoidal reference signal on a 150 ton crane with the control setup that NOV uses. Pump size $500cm^3/rev$ and $355cm^3/rev$ are tested.

$$G_{pump} = \frac{\omega_n^2}{s^2 + 2 \cdot \zeta \cdot \omega_n \cdot s + \omega_n^2} \tag{10}$$

Where the undamped natural frequency, ω_n, equal $31s^{-1}$, and the damping ratio, ζ, equal 0.9.

Motors (3-4)

The real system under investigation has 3 active and 8 passive variable-displacement motors A6VM 215. In the model, the set of motors have been merged into two equivalent units. The response of the motors is assumed to obey a second-order model like the one in Eqn. 10, with an undamped natural frequency of $5s^{-1}$ and a damping ratio of 0.99. This result in about 1s response time from zero to maximum motor displacement. The response time of a motor varies with control pressure, control settings, size of motor, and direction. Thus, the simulated behaviour is a simplification. The motor response is, accordingly to the experience and to the supplier data, varying from 0.7s to 3.5s depending on the aforementioned variables.

Friction (5)

Friction is included as parametric models. Three models are included, one for the active motors, one for the passive motors and one for the remaining system friction. The models are based on the authors previous work [11] [1].

Double piston accumulator (6)

The double piston accumulator is important to include in the simulation model to get the correct limitations. In AHC, the maximum compensation distance during a wave cycle is directly limited by the size of the accumulator. Friction is included as viscous friction, that is function of the piston speed, while the leakages between the high-pressure and low-pressure side are simulated to get a realistic pump demand from the passive-side pumps. However, these parameters have minor impact on system performance and they are mainly concerning the passive system performance whereas the focus of this paper is the active system.

Controller (7)

This sub block consists of controllers developed in NOV for winch control and includes control of active motors, passive motors, active pumps and passive pumps. The new controller addressed in this research replaces the control of the active motors and pumps.

Load and wire dynamics (8)

The wire is simulated as a single linear spring and damper. The spring stiffness is found by using Eqn. 11, were A is the effective steel area of the wire. E, is the E-modulus of steel and L is the wire paid out.

$$k = \frac{E \cdot A}{L} \tag{11}$$

As dampening coefficient, the wire is assumed to be slightly underdamped with a dampening ratio of 0.95.

Subsystem for winch calculations (9)

This block includes functions for calculating parameters related to the wire and to the winch drum. This includes variables such as current wire-layer diameter, wire layer and current total winch inertia due to the wire on the drum and drum itself. The fixed input parameters are crane specific and involve the drum inertia retrieved from a 3D-cad model, the wire diameter, the full wire on the drum, the wire mass properties, and the drum geometry.

PROPOSED CONTROLLER

The controller modifications presented in this paper are limited to the active system. The active system has two control inputs for active heave compensation, namely the pump and the motor displacement control signals. The pump is controlled with classical feed-forward signal and a linear feedback controller. This control setup is not changed with the new controller. The existing controller is not actively controlling the motors during heave compensation. Instead the motors are controlled due to a mapping based on how much wire is left on the drum and the selected speed mode. The relative wire paid out during an AHC operation is limited, thus the motor displacement is constant. The new controller introduces a dynamic control of the winch motors dependent on the winch load and the feed-forward pump signal. It is of interest to remove, or to mitigate, the oscillatory behavior. Based on the findings, an important factor related to these oscillations is the displacement of the motors. The goal for the new controller is therefore to maximize the motor displacement. The new controller aims to have maximum displacement whenever the winch is switching direction and the speed is low. This will improve performance at low and zero speed. To be able to reach high speed operations, the controller will reduce the motor displacement when the speed demand increases above a certain threshold.

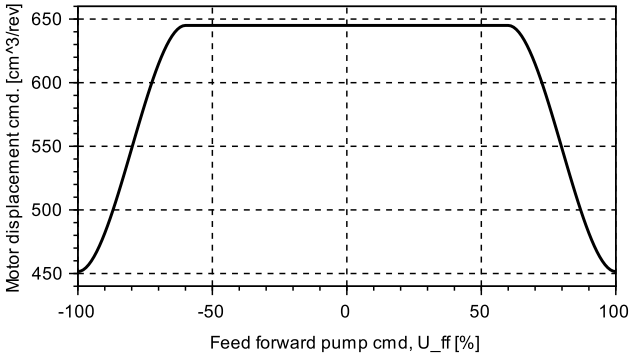

Figure 13: Motor displacement reduction dependent on pump control feed forward signal.

The modifications done to the new proposed controller are related to the motor control. Instead of being mapped dependent on speed mode and wire on the drum, it is now more dynamic and depends on the wire on the drum, on the motor displacement and on the pump control feed forward signal (U_ff). Figure 13 displays how the reduction of motor displacement adjusted controlled.

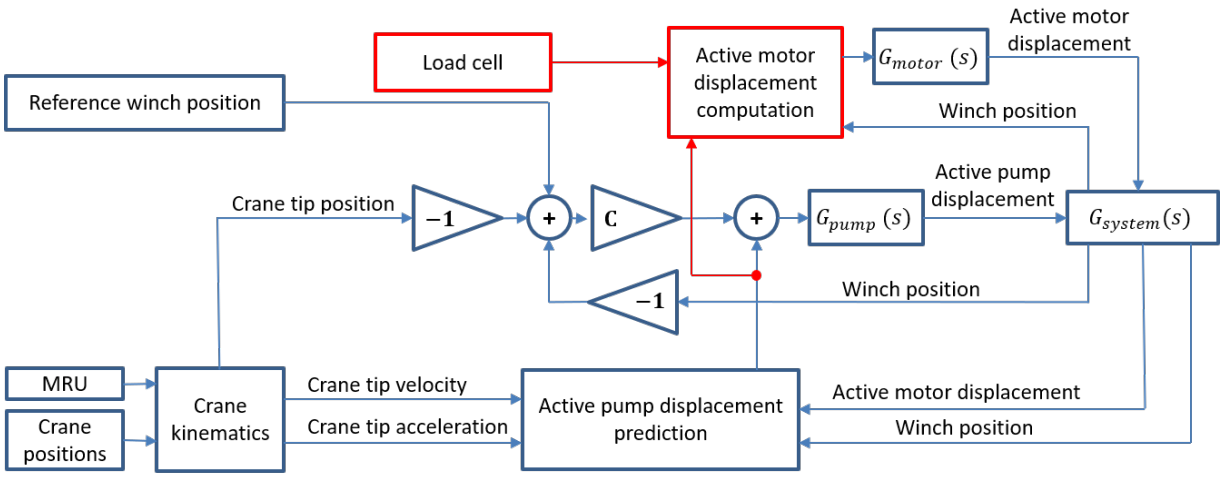

Figure 14: Control block diagram of the new proposed controller.

The reduction is ramped up with a third order polynomial function when the feed forward signal surpasses the threshold of $u_t = 60\%$.

$$u_{ff} = -(K_1 \cdot v_{tip} + K_2 \cdot a_{tip}) \cdot \frac{D_M}{D_{M,max}} \tag{12}$$

Where v_{tip} and a_{tip} are the crane tip velocity and acceleration.

$$\begin{aligned} &if \quad |u_{ff}| > u_t \quad then \\ &K_{red} = -31.25 \cdot |u_{ff}^3| + 75 \cdot u_{ff}^2 - 56.25 \cdot |u_{ff}| + 13.5 \\ &else \quad K_{red} = 0 \quad end \end{aligned} \tag{13}$$

At a 100% feed-forward (u_{ff}) signal the displacement is reduced to the minimum allowable dependent on the load case. For the proof of concept the minimum displacement is set to a fixed value, 30% below maximum displacement of the active motors.

$$u_M = D_{M,max} - K_{red} \cdot \left(D_{M,max} - D_{M,min}\right) \tag{14}$$

$$D_{M,min} = D_{M,max} \cdot 0.7 \tag{15}$$

In general the minimum displacement setting will be a function of winch layer diameter, winch load and speed limitations for the different winch components. As a result the simulations performed to test the controller are only performed on a fixed winch layer with a constant load. For further use and implementation on a real winch the minimum motor displacement will have to be calculated based on these system limitations:

1. The minimum displacement must ensure enough available torque without exceeding the maximum system pressure. The active motor torque must overcome friction, load dynamics and inertia accelerations.
2. Maximum allowable winch speed must be considered. The variable axial piston motors have a variable maximum speed depending on displacement setting. This will have to be included in the controller to avoid over speeding the motors and the gear transmission.

RESULTS

The controller is tested and validated in the simulation model of a 150 tons crane. In the validation, a load scenario with 90 tons hook load on the outer winch layer and boom tip velocities up to 90m/min is investigated.

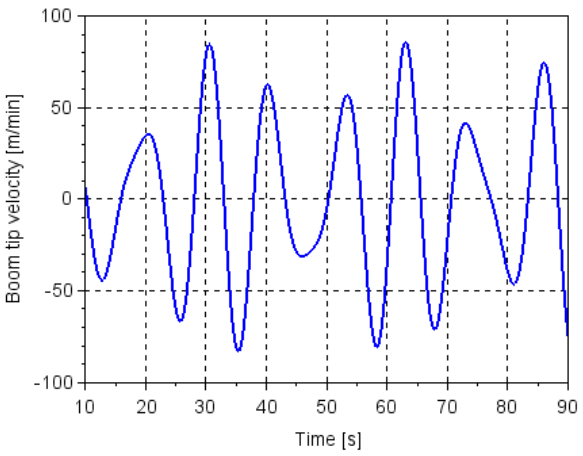

Figure 15: Boom tip velocity.

The load scenario are of high interest because the load con-

dition is in the boundary of where the operator must select high-speed mode and the hook load of 90 ton is the maximum allowable. The load scenario chosen is at a point where the classical controller is meeting its full potential. Reaching a maximum speed of $90m/min$ with a 90t winch load which is the maximum load in the high speed mode for the chosen crane. The load scenario is depicted in Fig. 4, where the crane SWL is 150t and the $U_{max}^{HS} = 90m/min$. The load scenario is simulated on the outer layer. On the outer layer the classical controller typically commands higher displacement to the motors than on the inner layers. The displacement command is often reduced towards the inner layer to make the winch able to maintain the same speed. Thus, the best performance of the classical controller is assumed to be on the outer layer and the comparison will be conservative.

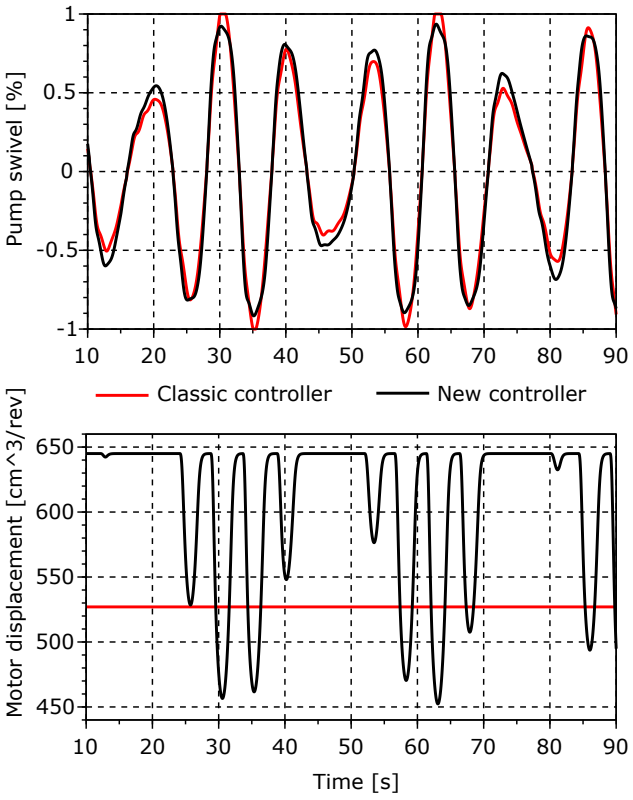

Figure 16: Pump swivel feedback and motor displacement (active system).

In Fig. 15 to Fig. 17, the simulated results are shown for both the classic and new controller. The simulations have been executed with the exact same wave pattern related to boom tip velocity elucidated in Fig. 15. The required speed is peaking 90m/min, thus the full pump displacement is used when applying the classic controller. When using the new controller, the pumps are only reaching 90% (see Fig. 16).

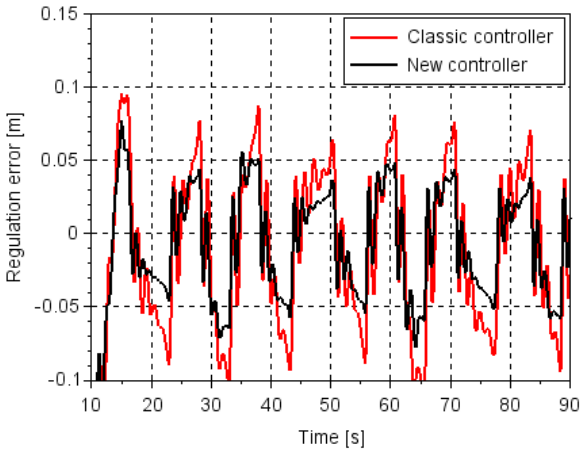

Figure 17: Control error in meters of wire paid out by the winch.

Figure 17 show a reduced control error of approximately 30%. An advantage with the new controller is that the system is forced to work with maximum motor displacement during low speed. A direct result of this is that the pressure levels are reduced in the low speed region.

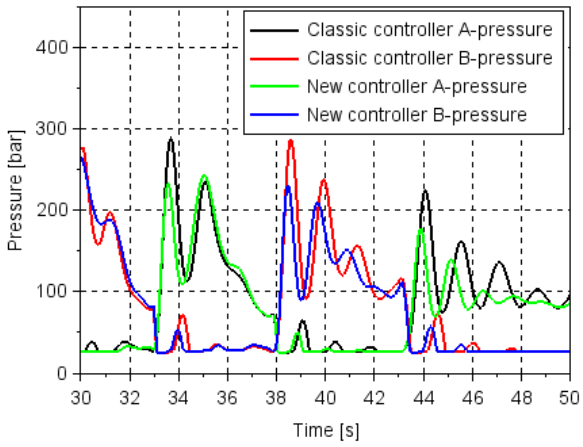

Figure 18: Closed loop hydraulic A-pressure and B-pressure in the active system.

In Fig. 18, the pressure levels from the classical controller and the new controller are compared and show an expected reduction of pressure peaks. The pressure measurements also show that pressure oscillations are dampened out earlier than with the classical controller. The maximum pressure peaks in Fig. 18 are shown to be reduced by approximately 20% when applying the

new controller. The exact amount of reduction will vary, but in general the classical controller is reducing the active motor displacement towards inner wire layer. This test was performed on outer layer where the motor displacement for the classical controller is at its highest, thus the relative reduction of the pressure level is assumed to be even more when the winch is working on the inner wire layers.

CONCLUSION

This paper addresses a challenge with the low displacement on hydraulic motors in a winch system. The system properties at low motor displacement have been visualized through measurements and theory have been used to understand and explain the changes in the dynamic system. The motor displacement is shown to have significant impact on the dynamics of the closed loop hydraulic systems. Reducing the motor displacement means decreasing the system bandwidth and makes the winch system more sensitive to pressure oscillations. Furthermore, the classical winch controller of the hydraulic winches does not account for these dynamical changes. The issue is not unknown, but the low displacement is often related to motion compensation in higher velocities, thus the low speed performance is ignored. A new control design has been proposed and validated to better deal with the dynamical changes. The new controller actively changes the displacement on the active motors when the pump demand is increased above a critical threshold. The result is that the motors are kept at maximum displacement in all cases where the speed demand is low. The pressure peaks due to start up friction and inertia accelerations are mitigated. Another benefit is that the reduced pressure oscillations are dampened out faster in comparison to the baseline system. Simulations show that the new controller allows the system to reach the maximum velocity with lower peak pressure than with the classical controller and with 10% less use of active pump capacity. Applied work and simulations show that the new controller affects the winch system in five main areas:

1. Maximum displacement at low speed: the system pressure oscillations at low speed is reduced
2. No need for two different AHC modes: this increase the usability in addition to lowering the test time.
3. Higher speeds: loads that previously were too high for AHC HS, but still lower than maximum SWL will be able to reach higher velocities with the new controller. For the 150t crane investigated it means that loads above 90t get the speed capacity increased up to 30%.
4. Peak pressure: lower peak pressure is good for component lifetime, it may reduce installed power demand, and it is beneficial for reducing load oscillations. The pressure peaks were reduced up to approximately 20%.
5. Control error: The regulation error is reduced for high speed scenarios by approximately 30%.

REFERENCES

[1] Moslatt, G. A., and Hansen, M. R., 2018. "Modeling of Friction Losses in Offshore Knuckle Boom Crane Winch System". In 2018 Global Fluid Power Society PhD Symposium, GFPS 2018.

[2] Padovani, D., and Ivantysynova, M., 2015. "The Concept of Secondary Controlled Hydraulic Motors Applied to the Propulsion System of a Railway Machine". In The 14th Scandinavian International Conference on Fluid Power.

[3] Padovani, D., and Ivantysynova, M., 2015. "Simulation and Analysis of Non-Hybrid Displacement-Controlled Hydraulic Propulsion Systems Suitable for Railway Applications". In ASME/BATH 2015 Symposium on Fluid Power and Motion Control, p. 11.

[4] Nikolaus, H., 1977. Antriebssystem mit hydrostatischer Kraftubertragung.

[5] National Oilwell Varco Norway, 2019. National Oilwell Varco, Cranes.

[6] Bosch Rexroth AG, 2014. Drive and control solutions for marine engineering : Reliable , efficient , durable.

[7] Huisman, 2015. Cranes, Huisman product brochure.

[8] TTS Group, 2019. Winches, hydraulic.

[9] del Re, L., Goransson, A., and Astolfi, A., 1996. "Enhancing Hydrostatic Gear Efficiency Through Nonlinear Optimal Control Strategies". *Journal of Dynamic Systems, Measurement, and Control,* ***118***(4), pp. 727–732.

[10] Vanwalleghem, B., Dousy, C., Pinte, G., and Vanseveren, B., 2012. "Optimization of the efficiency of hydrostatic drives". In 8th International Fluid Power Conference, Dresdem, Germany.

[11] Moslått, G.-A., Hansen, M. R., and Karlsen, N. S., 2018. "A model for torque losses in variable displacement axial piston motors". *Identification and Control,* ***39***(2), pp. 107–114.

D Practice for determining friction in hydraulic winch systems

Modeling, Identification and Control, Vol. 41, No. 2, 2020, pp. 109–120, ISSN 1890–1328

Practice for determining friction in hydraulic winch systems

G-A. Moslått [1] M.R. Hansen [2]

[1] *Department of Lifting and Handling, National Oilwell Varco, N-4630 Kristiansand, Norway.*
E-mail: geir-arne.moslaatt@nov.com

[2] *Department of Engineering, University of Agder, 4879 Grimstad, Norway.*
E-mail: michael.r.hansen@uia.no

Abstract

This paper presents a method for estimating friction in hydraulic active heave compensated (AHC) offshore winches. The method is a two-step approach where the first step is to model the friction loss in the hydraulic motors based on data from the sub-supplier. The second step requires real-life testing, where the remaining friction losses in the winch system is identified and modeled. In this context, a practice is characterized by obtaining a friction loss estimation with the highest possible accuracy over the widest possible range of operating conditions with a limited amount of experimental work. The method benefits from the use of parametric models, sub-supplier data, and real-life measurements on a 150 t AHC crane from National Oilwell Varco Norway (NOVN). The work is an important part of developing a simulation model that can be used actively in virtual testing and verification of crane operations at NOVN. A friction loss model developed from the proposed method was implemented in a NOVN simulation model. Computed and measured hydraulic pressures showed deviations of less than 10 % from measured results for a 150 t crane operating in AHC.

Keywords: Hydraulics, torque loss, winch system, offshore knuckle boom cranes.

1 Introduction

Offshore heave compensated winches are high-end equipment that is designed to operate under harsh conditions subjected to loads that are not easily reproduced either in laboratories or even during installation. Therefore, there is a huge demand for simulation models that can predict performance under any conditions. The main benefits from having simulation models available for behavior prediction have been more thoroughly described in Moslått et al. (2018) but they may be divided into:

- minimization of equipment costs by using model based design to reduce the level of conservatism in component selection.
- added value to equipment as a behavioral prediction tool useful for planning expensive and complicated operations.
- minimization of testing costs by using virtual testing to reduce level of full-scale testing.

One of the main challenges when predicting behavior is the friction, both in the hydraulic actuation system as well as in the mechanical system. An added challenge is that the winch systems, normally, are tailor-made to customers, giving a large amount of different combinations of motors, gear ratios, wire dimensions, drums sizes and wire sheaves. Therefore, a useful behavior prediction requires a modeling technique that handles both the difficulties of setting up friction models of hydraulic-mechanical systems as well as handling

doi:10.4173/mic.2020.2.6

the use of different components within the same topology. In this paper the focus has been to investigate the winch friction in offshore knuckle boom crane winch systems as the one shown in Fig. 1. An active passive system is divided into two main hydraulic circuits, see Fig. 2. The passive system is designed and controlled to hold the passive weight of the winch load. The passive system is a typical secondary controlled system working under constant pressure connected to an accumulator with a pump that is only used for leakage compensation during operations. The torque needed to hold the passive weight is obtained by use of the variable displacement motors. The active system uses the pump as a primary controller for motion control of the winch. The active system is expected to absorb all remaining loads related to acceleration, load dynamics and friction forces. Friction forces are a significant contributor among these forces and good knowledge and estimates are essential. Experimental validation is crucial for friction modeling, however, it is extremely costly to set up a test scheme that covers the entire operational range of an active-passive winch system. The most common practice today when estimating friction is to use simple constant efficiency factors. This method is based on values provided by sub-suppliers combined with empirical values. This type of modeling has many advantages in that it is simple and easily implemented in early design phases, however, it has obvious limitations in accuracy and does not meet any of the three potential benefits mentioned earlier.

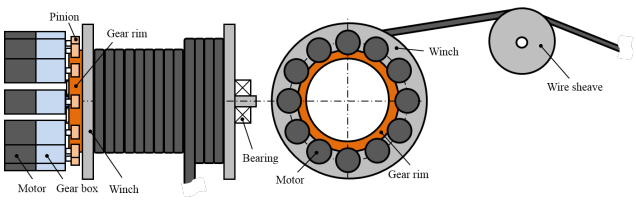

Figure 1: Simple sketch of a winch system.

The friction losses appear in the hydraulic power supply to the hydraulic motors, in each motor, in each gearbox, in each gear-rim connection, in the drum bearings, in the wire and in the sheaves. The friction losses in hydraulic motors have been subjected to research for several decades without any unified recommended practice model appearing. One of the first efficiency models of hydraulic motors were made by Wilson (1948). His model included torque dependent dry friction losses, viscous friction and a constant loss. The model was later used as a base for many other studies with different modifications. Schlösser (1961) modified it in 1961 , and added terms including fluid acceleration. In 1969 Jean Thoma included terms to include variable displacement, and the same was done by Pacey et al. (1979). In the following years there were many attempts on improving the loss models and in 1997 Huhtala and Villenius (1997) made a comparison of several models including Wilson, Schlösser, Zarotti, Thoma, Rydberg, Dorey, and their own model. They stated that the accuracy of previous models where inadequate to estimate losses in the full range of hydraulic motors. Huhtatala presented a totally empirical model based on curve fitting. The model was significantly more complex and the details for adapting it to variable displacement motors are unclear. Ortwig came a couple of years later with an in-depth study of several loss mechanisms in the hydraulic motor Ortwig (2002). The study included laminar and turbulent flow losses, pulse losses, churning losses, roller bearing losses, mixed bearing friction, seal losses, valve plate losses and dry friction. He probably saw the downside of having all these terms and made a simpler numerical expression to cover all the loss terms with a similar accuracy. The model was, however, only meant for fixed displacement motors. While Huhtala ended up with a numerical expression, Jeong and Kim (2007) did a similar approach in 2007. But instead of transforming it to a numerical equation, they kept the analytic aspect of the terms and merged them together in one equation. Unfortunately, this work also only considered fixed displacement motors. In 2018 citeMoslatt2018 took the model made by Jeung and Kim, and adapted it for variable displacement and, simultaneously, simplified it. The model showed substantial improvement from the old variable displacement models from Thoma and Pacey, but it also compared favorably with the newer model from Ortwig. The motor type used for that study was axial piston variable displacement motors, with efficiency data given by Bosch Rexroth AG (2010). The hydraulic motors that are easily identified as those

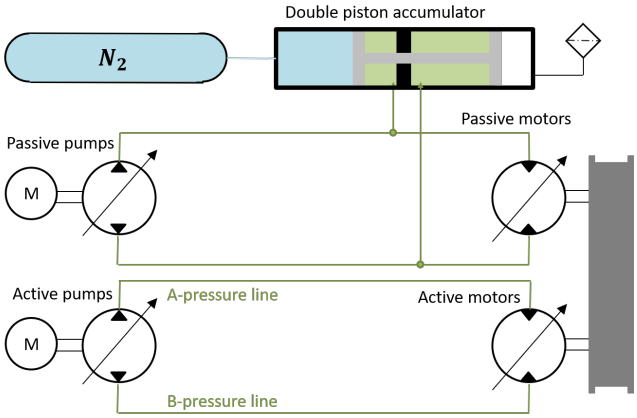

Figure 2: Simplified schematics of an active/passive hydraulic active heave compensated system

with the most complex friction loss pattern including both mechanical, viscous, and turbulent friction. The idea put forward in this paper is to combine a motor model based on sub supplier data with a model for the friction in the remaining system. The idea is that the friction of the remaining system can be modeled in a simpler way as compared to the motor. The main advantage of this method is that it reduces experimental work while yielding a friction loss model that covers the entire operational range of the winch system.

2 Method

The overall method to estimate the friction of a specific hydraulic winch system is carried out in four main steps.

1. Use an established model for axial piston variable displacement motors and obtain the needed parameters for the specific motors in the system.
2. Do friction measurements of the system with several different settings so that measurements capture a wide spectrum of working conditions.
3. Estimate the remaining friction in the system based on the measurements.
4. Use the estimation of the remaining friction to develop a model and specify its parameters.

The steps are described throughout the following sub-sections.

2.1 Step 1; Model of hydraulic motors

The sub-suppliers friction data is a table of efficiency values given for a range of operating conditions. There are basically two main ways to use this data. Either using the whole set of data as a map with some kind of interpolation, or fitting a parametric model to represent it. The data given covers most cases but lacks information about low torque, and low speed situations. Also, a parametric model is more easily adapted to situations where the working conditions (mainly fluid viscosity) at the actual plant differs significantly from those of the sub-supplier in-house testing. The parametric model which is mostly based on analytic terms is assumed to be able to cover the blind areas in a better way than an extrapolation of the existing data. This is assumed because the friction-changes in those areas are non-linear and costly to predict with extrapolation. A mapping model compared to a parametric model has the advantage of being simple to generate and will give very accurate results in the range of operating conditions that are given from the supplier. On the other hand the parametric will have a clear advantage when operating outside the operating conditions given by the supplier due to the analytically determined terms. It is also efficient to use and in many cases easier to implement because only an analytical expression is needed instead of a whole map of data. The main downside of having a parametric model is that the parameters will have to be obtained through system parameter identification routines and that a deviation between the desired data and the model have to be expected and accepted.

For parametric friction modeling the model presented in Moslått et al. (2018) is chosen. In equation 1 it is assumed that the fluid density and viscosity are constant. Normally, the investigated winch systems have relatively small temperature variations within normal working conditions, however, variations in viscosity at low speed can, potentially, have significant impact on behavior due to mixed lubrication films in the motor. The typical working temperature in the hydraulic oil of the investigated system is in the range of 40° to 60° Celsius. This corresponds to a variation in viscosity from 47 cSt to 34 cSt for the standard hydraulic fluid Rando HD46, used by NOVN in these winches.

$$\begin{aligned} T_{fm} = K_1 \cdot |\omega_m| + K_2 \cdot \omega_m^2 \cdot D_m^3 \\ +K_3 \cdot \Delta p_m \cdot D_m + K_4 + K_5 \cdot {\Delta p_m}^2 \end{aligned} \tag{1}$$

We can identify the K_1 term as the viscous friction. This type of loss can be found as viscous losses in bearings, churning losses for the cylinder block, viscous slipper friction and viscous friction between barrel and port plate. The K_2 term is mainly covering the turbulent losses in the inlet port plate. A minor part of the term is covering the churning losses from pistons and slippers although these losses would normally not have the same relationship to displacement setting as the inlet flow loss. The K_4 term represents the Coulomb friction in motor. The K_5 term represents mixed lubrication at high pressures. The K_3 term simply represents a general pressure dependant loss that was introduced to improve correlation between the model and the sub-supplier data.

The model parameters were obtained by means of minimization, using the numerical complex algorithm Box (1965)Krus et al. (1991) with a squared error as cost. The complex method was chosen due to the ease of implementation and that the full code was open and accessible for changes if needed. The cost function considered rotational motor speed from 400 to 2500 rev/min, displacements from 50 to $D_{m,max}$, and motor pressure differences of 50 to 350bar.

For the 150 t crane (Fig. 4) investigated in this pa-

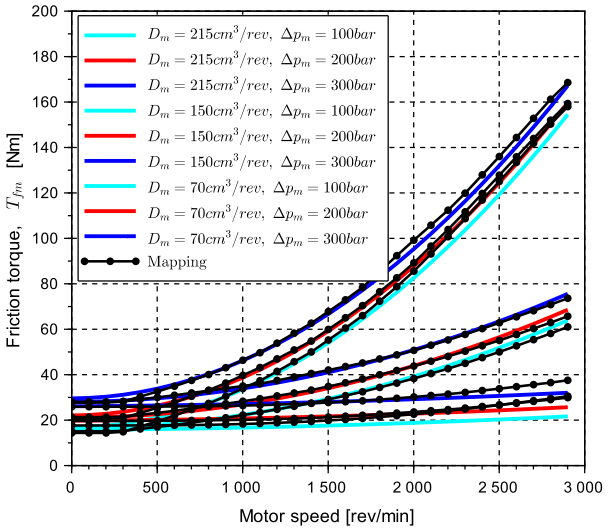

Figure 3: Parametric friction model vs a mapping with linear interpolation of the sub-suplier data for an A6VM (71 series) 215 cm^3/rev from Bosch Rexroth.

Figure 4: Photo of the crane used for testing.

per, the winch is equipped with 11 pcs of 215 cm^3/rev variable displacement axial piston motors. The friction torque for this motor is shown in Fig. 3. The deviation between mapping and parametric model is overall small, but the deviation is increasing at low displacements and high speeds. To improve confidence in the model parameters, the parameters for a set of three motors were found. The obtained model parameters show a good correlation and some small expected changes dependent on motor size. Following parameters where found for a set of Bosch Rexroth A6VM (71 series) hydraulic motors:

Table 1: Friction model parameters for Bosch Rexroth A6VM hydraulic motor.

$\mathbf{D_{m,max}}$	280 cm^3/rev	215 cm^3/rev	170 cm^3/rev
$\mathbf{K_1}[Nm \cdot s]$	$8.38 \cdot 10^{-3}$	$4.05 \cdot 10^{-3}$	$2.48 \cdot 10^{-3}$
$\mathbf{K_2}[\frac{N \cdot s^2}{m^8}]$	$2.58 \cdot 10^{10}$	$3.69 \cdot 10^{10}$	$5.01 \cdot 10^{10}$
$\mathbf{K_3}[-]$	0.00519	0.0050	0.0049
$\mathbf{K_4}[Nm]$	18.1	14.0	11.0
$\mathbf{K_5}[\frac{m^5}{N}]$	$1.47 \cdot 10^{-14}$	$1.16 \cdot 10^{-14}$	$0.925 \cdot 10^{-14}$

2.2 Step 2; Full size friction tests

A full size active heave compensated crane with up to 150 t SWL was tested (Fig. 4).

To obtain the total winch friction, the setup like the one explained in Moslått and Hansen (2018) was used. To calculate the winch system losses, the winch is driven at constant speed up and down with an intention to avoid transient behavior. This test is performed with several speeds, loads, and motor displacements variations. For each case, the winch speed, pump displacement, and system pressures are measured. All the data is logged in realtime from the crane PLC. A simplified schematic of the winch system hydraulics that is tested is shown in Fig. 5.

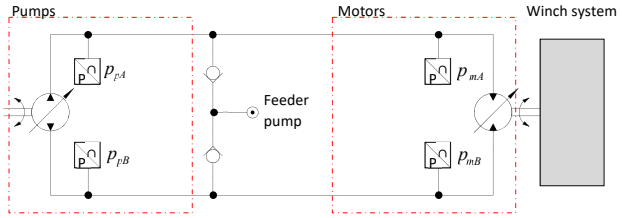

Figure 5: Simplified diagram of the investigated closed loop winch system

In Fig. 6, a typical test sequence is shown that demonstrates that a wide range of the pump capacity is covered.

For every test cycle like this (see Fig. 6), the steady state pressure and winch speed values are retrieved when having constant speed/pump displacement. The values between all these measurement points are estimated based on linear interpolation. The pressure values are used together with the motor displacement

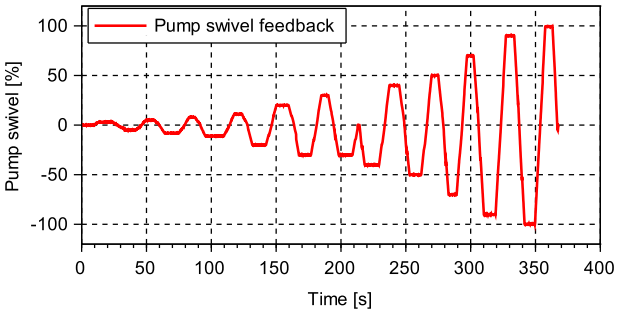

Figure 6: Typical pump displacement for a test sequence used for determining winch friction.

signal to estimate the friction. To calculate the friction loss the first step is to set up the function for pressure difference across the motor (Δp_m) when driving up vs down. Note that drag forces on the moving load is neglected since the test is performed with the load in air.

$$\Delta p_m = p_{mA} - p_{mB} \tag{2}$$

$$\Delta p_m^{(wu)} = \Delta p_L + \Delta p_F \quad \text{(winch up)} \tag{3}$$

$$\Delta p_m^{(wd)} = \Delta p_L - \Delta p_F \quad \text{(winch down)} \tag{4}$$

Where $\Delta p_m^{(wu)}$ is the pressure drop across the motor when hoisting and $\Delta p_m^{(wd)}$ is when lowering. Δp_F is the total friction losses, and Δp_L is the pressure difference due to winch load. Calculated friction losses such as pressure (5) is derived from equations (2-4).

$$\Delta p_F = \frac{\Delta p_m^{(wu)} - \Delta p_m^{(wd)}}{2} \tag{5}$$

The pressures are measured during the test from transmitter p_{mA} and p_{mB} (see Fig. 5). The friction torque (6) is derived by multiplying with the motor displacement.

$$T_{ft} = \Delta p_F \cdot D_m \tag{6}$$

, where D_m is the displacement and T_{ft} is the friction loss referred to as torque on the motor shaft. Each calculation is performed for measurements with the same winch speed. Due to leakage in the hydraulic system, the winch speed for lowering and hoisting will not be the same. Thus the interpolated pressure values are used to be able to compare pressure values at equal winch speed.

The crane operation sequence is shown in Fig. 6 and was performed for multiple load and displacement scenarios. All test scenarios used for friction determination are listed in Table 2

The measured results calculated as friction are seen in Fig. 7.

Table 2: Evaluated test scenarios

Name	**Motor displacement (total/single)**	**Winch load**
Test 1	2365/215 cm^3/rev	0 t
Test 2	2365/215 cm^3/rev	77 t
Test 3	2365/215 cm^3/rev	107 t
Test 4	1800/164 cm^3/rev	0 t
Test 5	1800/164 cm^3/rev	77 t
Test 6	1800/164 cm^3/rev	107 t
Test 7	2200/200 cm^3/rev	0 t

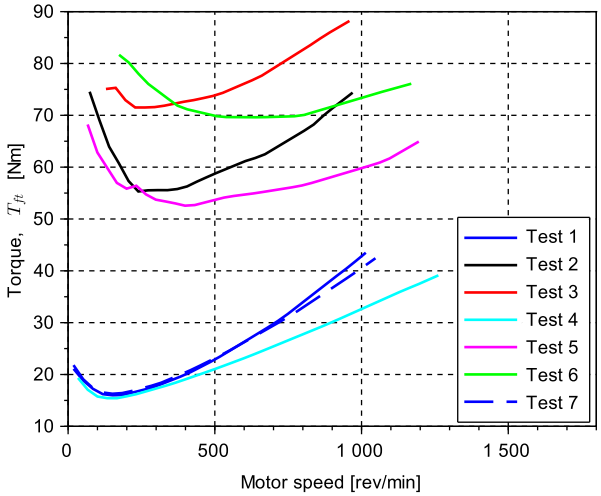

Figure 7: Calculated total winch friction based on measurements. The total torque is divided on 11 motors.

2.3 Step 3; Estimating remaining system friction

From the measurements taken, the total winch friction (T_{ft}) was calculated. The calculations are explained in detail in section 2.2. Based on the results, the motor torque loss is calculated based on the MJ4 model Moslått et al. (2018). The difference between the calculated MJ4 and the total losses gives the remaining torque loss in the winch system. A model to represent these remaining losses is then implemented, and parameters are identified for optimal results. The remaining system friction is found by subtracting the motor friction from the total measured friction.

$$T_{fs} = T_{ft} - T_{fm} \tag{7}$$

2.4 Step 4; Determine a model for remaining friction

Based on previous results by Moslått and Hansen (2018), equation 8 was chosen to represent the remaining system friction. It includes torque dependent Coulomb and Stribeck terms, and a viscous friction term dependent on winch speed.

$$T_{fs} = (C_1 \cdot T_d + C_3) \cdot e^{\frac{-|\omega_m| \cdot 60}{C_4 \cdot 2\pi}} + C_2 + C_5 \cdot \omega_m + C_6 \cdot T_d \quad (8)$$

The model has a Stribeck shape to describe the dry friction at 0rev/min and the exponential curve to account for any mixed lubrication at low speed, a Coulomb and viscous friction term. The first and second are load-dependent, and the third depends on the rotational speed of the drives.

The parameters C_{1-6} were optimized based on test data from the crane. The data used to optimize the model parameters are the tests mentioned in table 2. The parameters were identified by means of minimization of the deviation between measured and modeled friction. All seven test cycles were considered during the optimization (test=1,2..7). For every test the error was calculated over the whole range of measured velocities (from i_{min} to i_{max}) with an iteration step of 25 rev/min. The total cost, E, was calculated according to (9).

$$E = \sum_{test=1}^{7} \sum_{i=i_{min}}^{i_{max}} (T_{ft} - (T_{fs} + T_{fm}))^2 \quad (9)$$

The non gradient based complex method Box (1965)Krus et al. (1991) was used with a population of 36 designs. For every iteration in the optimization routine, the population is adjusted by taking the worst design and mirror it with a factor of 1.3 across the center of gravity of the population. Table 3 shows the optimized parameters for the crane investigated in this paper (Crane 2) and previous results from a similar crane (Crane 1) investigated in a previous paper, Moslått and Hansen (2018).

Similar as for Crane 1, the optimization routine showed no need for a term representing Coulomb friction, C_2, hence the overall system model is simplified to:

$$T_{fs} = (C_1 \cdot T_d + C_3) \cdot e^{\frac{-|\omega_m| \cdot 60}{C_4 \cdot 2\pi}} + C_5 \cdot \omega_m + C_6 \cdot T_d \quad (10)$$

Figure 8 shows how the distribution between Coulomb, stiction, and viscous friction is within the system friction model for Crane 1 and Crane 2. The friction is estimated based on both cranes having a hanging load of 100 t of a maximum 150 t. The calculated system friction is shown as the torque applied on each motor shaft (Crane 1 and Crane 2 have a total of 11 motors).

Table 3: Optimized system friction parameters

Model	**150 t crane Crane 1**	**150 t crane Crane 2**
$\mathbf{C_1}[-]$	$328 \cdot 10^{-7}$	$155 \cdot 10^{-7}$
$\mathbf{C_2}[Nm]$	0.0	0.0
$\mathbf{C_3}[Nm]$	3.15	0.562
$\mathbf{C_4}[\frac{rev}{min}]$	157	229
$\mathbf{C_5}[Nm \cdot s]$	0.00851	0.00943
$\mathbf{C_6}[-]$	$121 \cdot 10^{-7}$	$162 \cdot 10^{-7}$
E	NA	1345

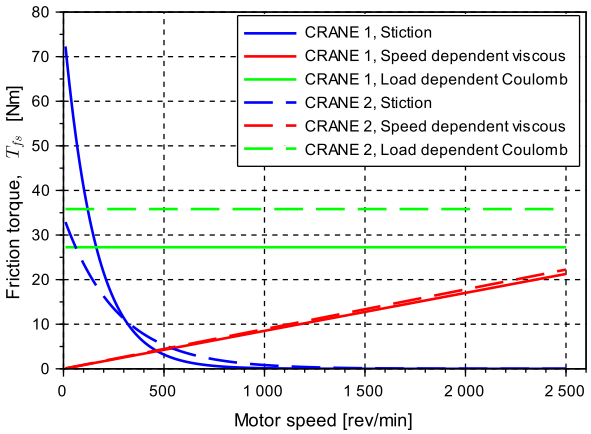

Figure 8: Comparison of modeled friction in Crane 1 and Crane 2. Crane load is 100 t.

3 Model modifications

One of the benefits of using parametric models is that the parameters can be modified to better fit the experimental data from the system investigated. The method up til now has been to define hydraulic motor parameters based on sub-supplier data, then defining system friction parameters based on measured results (ref. first and second box in Fig. 9). To see if results can be further improved a simple iterative optimization is performed (see Fig. 9). An additional loop of optimizing the model parameters is added were the system friction parameters were locked and the motor friction parameters opened, and this time optimized

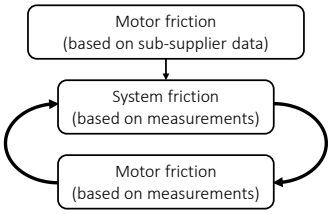

Figure 9: Iterative optimization loop of friction parameters.

based on the measured results instead of data from the sub-supplier. Next the motor model parameters will be locked again and new system friction parameters will be determined. In principle, this could be performed in several loops, however, results revealed that significant improvements were only obtained in the first loop.

Table 4: Optimized friction parameters

Model	**Crane 2, first loop**	**Crane 2, second loop**
$\mathbf{K_1}[\mathrm{Nm \cdot s}]$	$4.05 \cdot 10^{-3}$	$0.0 \cdot 10^{-3}$
$\mathbf{K_2}[\frac{\mathrm{N \cdot s^2}}{\mathrm{m^8}}]$	$3.69 \cdot 10^{10}$	$4.5 \cdot 10^{10}$
$\mathbf{K_3}[-]$	0.0050	0.012
$\mathbf{K_4}[\mathrm{Nm}]$	14.0	12.8
$\mathbf{K_5}[\frac{\mathrm{m^5}}{\mathrm{N}}]$	$1.16 \cdot 10^{-14}$	$0.0 \cdot 10^{-14}$
$\mathbf{C_1}[-]$	$155 \cdot 10^{-7}$	$141 \cdot 10^{-7}$
$\mathbf{C_2}[\mathrm{Nm}]$	0.0	0.0
$\mathbf{C_3}[\mathrm{Nm}]$	0.562	2.38
$\mathbf{C_4}[\frac{\mathrm{rev}}{\mathrm{min}}]$	229	270
$\mathbf{C_5}[\mathrm{Nm \cdot s}]$	0.00943	0.0089
$\mathbf{C_6}[-]$	$162 \cdot 10^{-7}$	$159 \cdot 10^{-7}$
E	1345	938

Doing the extra step of optimization affects the deviation between simulated and measured results used for optimization. This can be seen from the cost function, E, which is reduced by 30 % (4). From the changes, it is observed that viscous losses ($K_1 = 0$) and high-pressure losses ($K_5 = 0$) in motor friction have been practically eliminated, but instead, the parameter for turbulent losses has increased (K_2 parameter increased with 22%). In the system friction model, there are only smaller changes except for the C_3 parameter, which has quadrupled in size. However, even if the increase is relatively significant, the added 2 Nm does not significantly impact the overall stiction loss.

When looking at the motor model changes in Fig. 10, it can be seen that the turbulent losses are increased. This is seen by the increase in high speed, high displacement friction. The modification has also led to a significant decrease in friction at low displacements. It has to be taken into consideration that the test scenarios used for the optimization of parameters do not include displacement settings lower than 160 cm^3/rev.

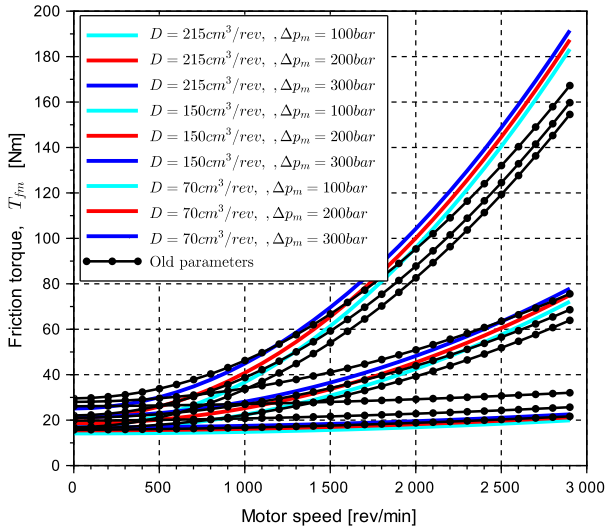

Figure 10: New motor parameters compared to old.

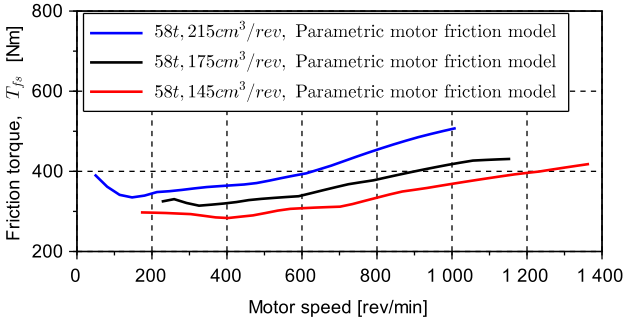

Figure 11: System friction derived from measurements.

An observation when analyzing the measurements is that similar working conditions for the mechanical system result in different values of the calculated system friction. An example is when the winch is operated with the same load at the same speed, but with different motor displacement. With a perfect motor friction model, these values should be the same, and the curves in Fig. 11 should be coincident. The estimation difference at 1000 rev/min is approximately 100 Nm, when comparing the 145 and 215 cm^3/rev displacement setting (see Fig. 11). The estimation error indicates that there are unmodeled friction losses in the hydraulic motors.

The additional set of tests with 107 t and 77 t (see Fig. 12) show the same tendencies as seen for the 58

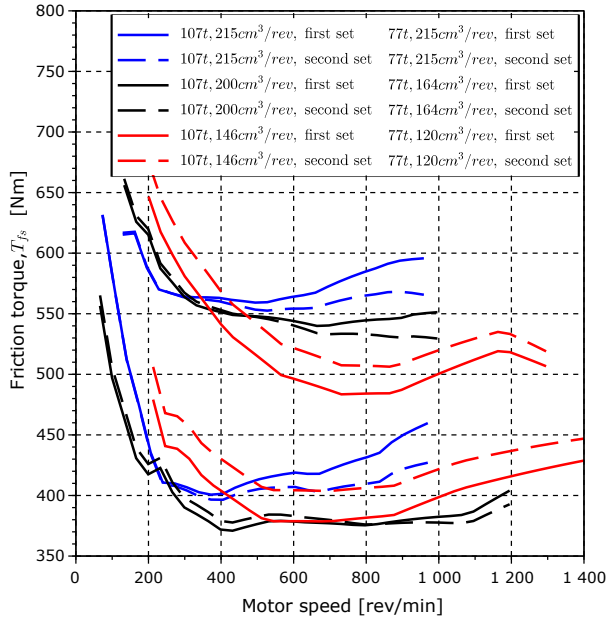

Figure 12: Calculated total system friction for tests with 77 and 107t load.

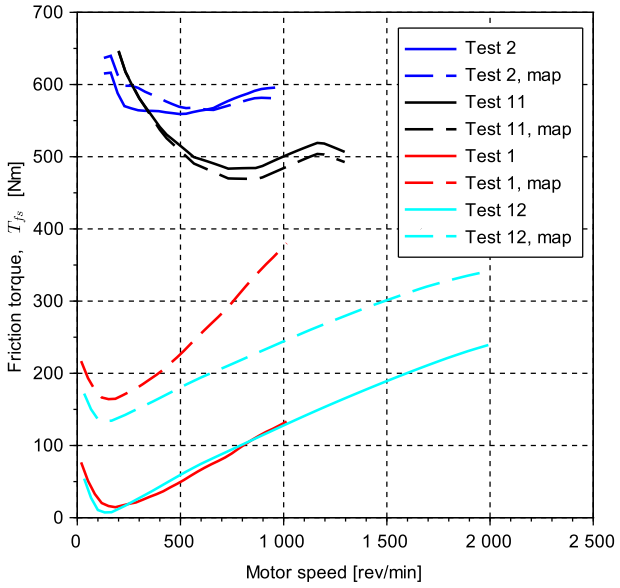

Figure 13: System friction calculated based on model versus efficiency map from supplier.

t test in Fig. 11, indicating that there are unmodeled friction losses in the hydraulic motors. A solution to this problem could be introducing a second optimization loop and modifying the motor friction model based on the measurements. In Fig. 12, the system friction is derived from measurements using both the first optimization loop and the second. The results are slightly better, but the deviation is still approximately 100 Nm, indicating that there are variations that the model cannot cover. The unmodeled friction is not a result of the parametric model's ability to represent the measurements from the sub-supplier. This is shown in Fig. 13, where the system friction is derived based on a black-box (map) friction model of the motors. The black-box model is based on the sub-suppliers efficiency map, using linear interpolation. The use of the black-box does not show any significant improvement, and at low loads (Test 1 and Test 12), the parametric model is significantly better. Overall it must be expected that the sub-supplier data will not necessarily be transferable to other situations.

The effect of a second optimization loop was also checked for the low load scenario with 0 t hook load (Fig. 14). The results are not particularly improved with the second optimization loop. This is not unexpected since low load scenarios are not highly prioritized in the second optimization loop. Unlike the other load cases, this one shows quite small variations of the estimated system friction, which indicates that the motor model is working quite well under these conditions.

The two parameter-sets were also compared in a

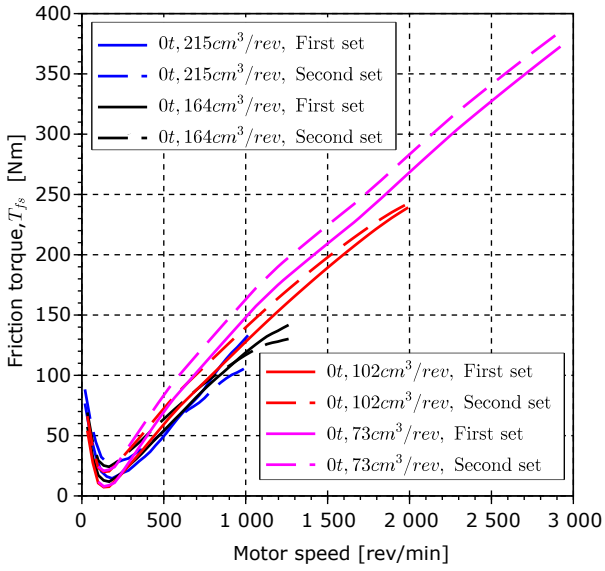

Figure 14: Calculated system friction for tests with 0 t hook load (hook weighs approx 2t).

simulated AHC scenario replicating the real test mentioned in section 4 (see Fig. 15). Each active side motor is set to 215 cm^3/rev, and the winch load is 55 t on the outer wire layer.

The implementation of a second optimization loop did not show any significant improvement of the results when looking at the test done with simulated waves and activated AHC (Fig. 15). During the optimization, the cost was significantly reduced, which

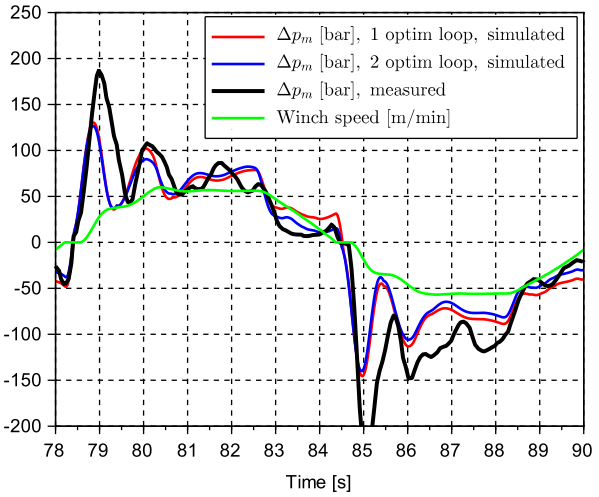

Figure 15: Measured and simulated pressure drop.

should comply with better results. An explanation for not getting this improvement is assumed to be that the measurements, which are used as a reference for the second optimization of motor model parameters and the system friction parameters, do not include any low displacement settings. In the verification test performed, the eight passive motors are set to 70 cm^3/rev and the three active motors are set to 215 cm^3/rev. Conclusions are difficult to extract from these results, but previously performed tests on similar systems have had the same tendency that the calculated system friction differs when the motors' displacement is changed (ref. Crane 1, which was investigated in Q1 2018 Moslått and Hansen (2018)). The deviation is slightly decreased with the second optimization loop, and for the displacement changes shown in Fig. 12, the deviation is less than 10 % from the average value. The results indicate that motor friction has some additional losses dependent on displacement and probably also some system-dependent variables like oil properties and working temperature since these losses are not captured in the sub-supplier data. The overall friction is not affected too much since the system friction model is anyway fitted to the remaining friction. The deviation is not insignificant, but it has to be considered that the system friction will have to cover this deviation, leading to a nonperfect distribution between motor friction and system friction.

4 Verification

The verification process was divided into three parts:

- Checking deviation between the measured data and the friction model.
- Checking the actual difference in pressure drop in a simulation model vs. measurements (normal winch mode).
- Checking the actual difference in pressure drop in a simulation model vs. measurements (Active heave compensated winch mode).

4.1 Measured vs. modeled friction

Three further tests (Test 8, 9, and 10), see Table 5, were added and combined with tests 2, 3, and 5 from Table 2, yielding a set of high load tests. The high load scenarios are prioritized because they most often are the critical design parameter for system design.

Table 5: Evaluated test scenarios

Name	Motor displacement (total/single)	Winch load
Test 8	2200/200 cm^3/rev	107 t
Test 9	1600/146 cm^3/rev	77 t
Test 10	1320/120 cm^3/rev	77 t
Test 11	1600/146 cm^3/rev	107 t
Test 12	1120/102 cm^3/rev	0 t

Figure 16 shows a comparison between the modeled total winch system friction versus the measured. The torque is referred to the motor shaft but represents the total loss of all 11 motors and associated components. The results shown in Fig. 16 look promising, and the maximum deviation is approximately 50 Nm. In general, there is a good correlation between the model and measurements on both the shape as well as the percentage deviation. However, the low speed below 200 rev/min is more inaccurate, which can be seen in Fig. 17, where the deviation between the results (error) is shown in percentage of the nominal system torque.

4.2 Normal winch mode scenario

The test is executed in what is called normal mode, which is a manually operated mode where the crane operator controls the winch with the joystick. A simulation model of the winch system was developed in the commercial modeling and simulation software SimulationX^{TM}. For example, the measured and simulated pressure drop across the motors are shown for Test 3 in Fig. 18. The results shows a good correlation between estimated pressure in the model and real measured values from the tests. However, the results also indicate that the friction model underestimates the losses when the displacement setting is low, and the speed is high.

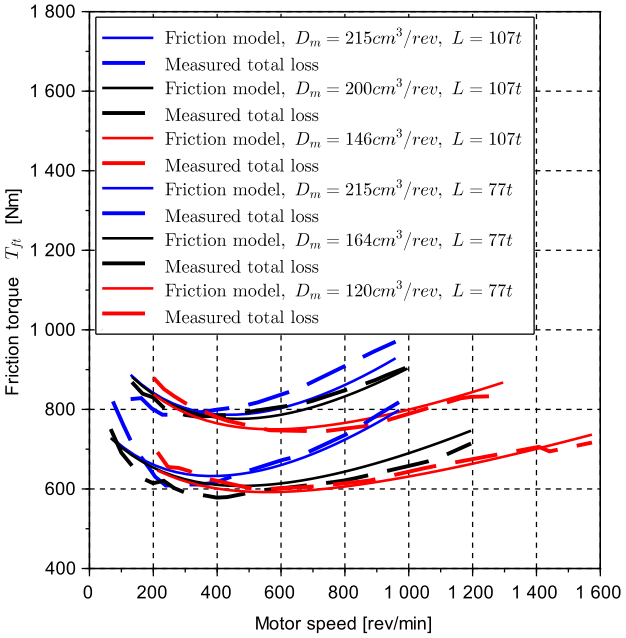

Figure 16: Compared model versus measured results.

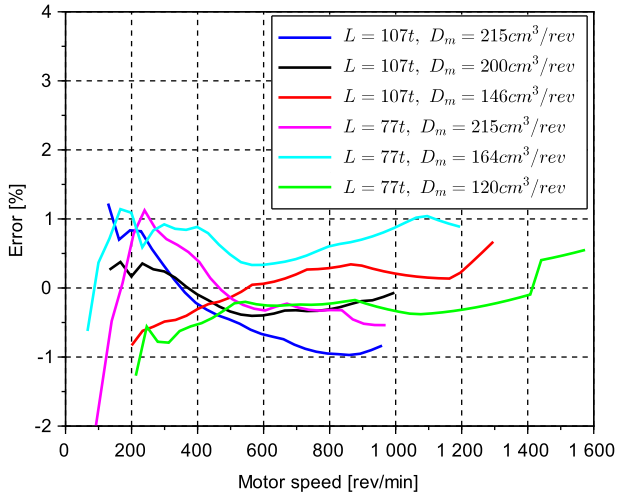

Figure 17: Model error in percentage of the nominal system torque.

4.3 AHC scenario

As a third step of verifying the model, it is of interest to look at a situation in AHC. For that purpose, a specially designed onshore test had to be conducted without the actual heave motion but still moving the load in reference to an artificially generated wave motion. An important thing to notice is that when the winch system is configured for AHC, all friction is absorbed by the active side motors. This friction includes friction generated from both the passive and the active

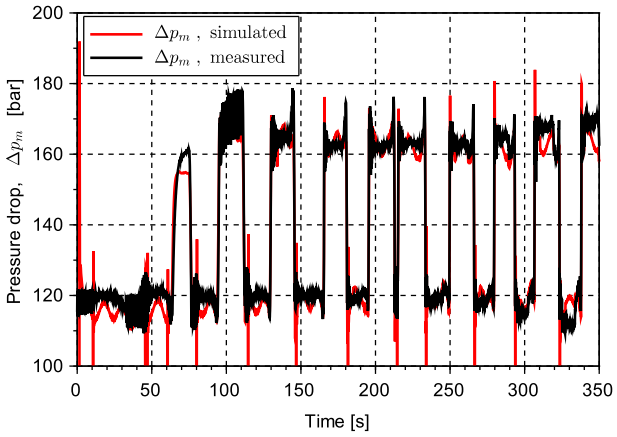

Figure 18: Comparison of measured versus simulated pressure drop across the motors for Test 3.

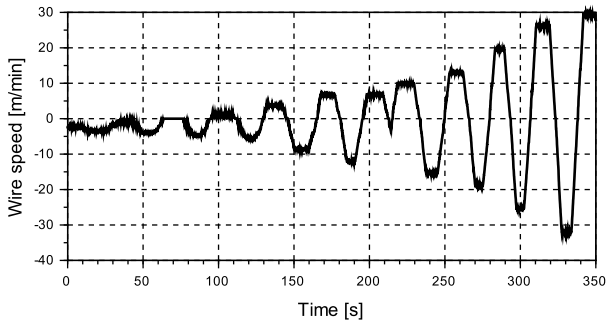

Figure 19: Winch speed profile for the test results shown in Fig. 18

side of the winch system. The passive side will not have the same displacement setting and pressure levels as in the active loop. Thus the total friction will reflect a combination of different motor displacements and pressures.

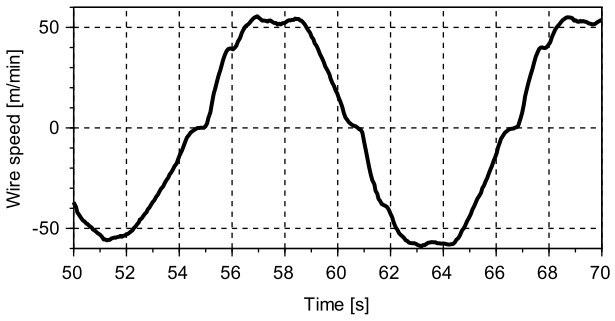

Figure 20: Winch speed profile for Fig. 21

In Fig. 21, the winch is operated in AHC at the outer layer with an attached load of 55 t. The active side motors are set to 215 cm^3/rev. The pressure estimated by simulations shows a decent accuracy. When paying

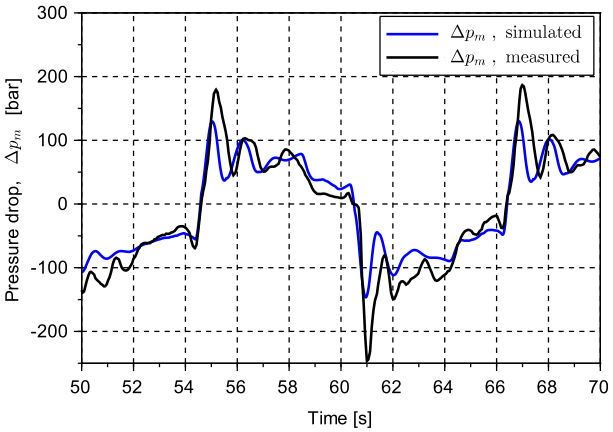

Figure 21: Measured and simulated pressure drop across the motors (active side), with winch speed according to Fig. 20.

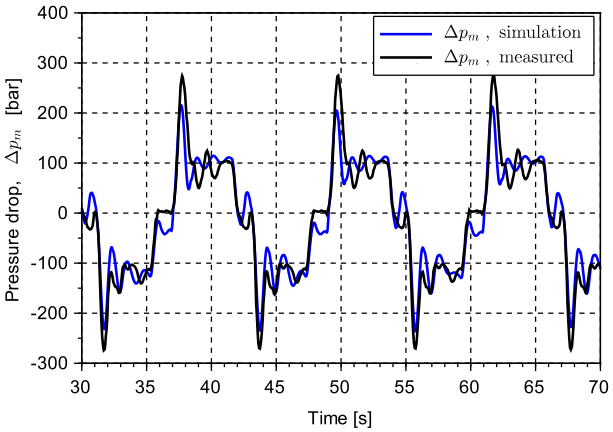

Figure 23: Measured and simulated pressure drop across the motors (active side), with winch speed according to Fig. 22.

out wire, the error is approximately 20 bar, and when pulling in, the error is significantly lower and close to zero. This implies an overall deviation of 10 bar of the actual 130 bar. In the next test scenario (Fig. 22), the motor displacement on the three active motors is set to 160 cm^3/rev, and the load is kept the same.

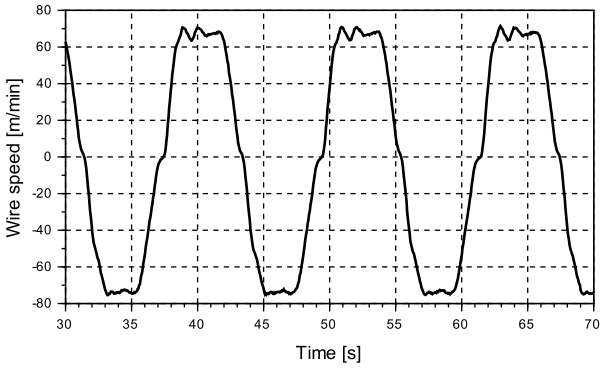

Figure 22: Winch speed profile for Fig. 23

Results are shown in Fig. 23 show about the same or better accuracy as the results with 215 cm^3/rev, with a pressure deviation of ±10 bar at the areas constant velocity (low-pressure disturbance by load dynamics). The passive side is in both scenarios in Fig. 21 and 23, pressurized with a more or less constant pressure drop across the motors of approximately 275 bar. The displacement is balancing the load at approximately 70 cm^3/rev per motor. For these two scenarios, a 10 bar deviation gives a resulting 3 and 4 % (160 cm^3/rev and 215 cm^3/rev) error in the estimated loss (in percentage of the nominal winch torque). This is more than what was measured at the previous tests in normal winch mode, where the results gave up to 1 % error.

5 Conclusions

The method for friction estimation shows friction estimation results within 1 % of the nominal load at speeds higher than 250 rev/min, which is acceptable. An additional test to verify the model in an active/passive heave compensated setup was performed in AHC with a 55 t winch load. The model gave an error average of 10 bar giving a relative error of approximately 10 % of the measured pressure. The verification test was done with a 55 t load on a crane designed for a maximum of 150 t. Tests with higher loads would be preferred, but unfortunately not possible at this point. Despite this, the confidence in the model is quite good since the model structure is divided into two parts. One for the hydraulic axial piston motors and one for the remaining mechanical system. The motor model was made by the use of sub-supplier datasheets and covered a large part of the motors operating conditions with respect to displacement settings, pressure, and speed. The second part of the model was estimated based on several tests done on the full-size crane. The tests were done with a wide spectrum of loads, speeds, and displacement settings. The loads in these tests reached a maximum at 107 t, which is over 70 % of the maximum safe working load (SWL). An additional test to see if the modification/optimization of the motor friction model parameters could improve the overall results was looked into. A second optimization loop was added to improve the model parameters for motor friction based on the real measurements done on the crane (not by using the sub-supplier data). The second optimization loop resulted in an improved result of the cost function. It was seen

that the new set of parameters gave a more realistic estimation of the system friction (based on measurements and motor friction model), which indicates an improved motor friction model. Although the model parameters seem to be improved, it leaves some uncertainty about the complete range of the model with respect to load and motor displacement. The second optimization loop is likely to give a better distribution between motor friction and system friction, but the uncertainty increases due to a limited range of data to use in the optimization routine. The improvement is shown to be most significant at high loads (see fig. 12).

References

Bosch Rexroth AG. Sales Information, Axial Piston Units. 2010.

Box, M. J. A New Method of Constrained Optimization and a Comparison With Other Methods. *The Computer Journal*, 1965. 8(1):42–52. doi:10.1093/comjnl/8.1.42.

Huhtala, K. and Villenius, M. Comparison of Steady-State Models of Hydraulic Pump. 1997.

Jeong, H. S. and Kim, H. E. A novel performance model given by the physical dimensions of hydraulic axial piston motors: Experimental analysis. *Journal of Mechanical Science and Technology*, 2007. 21(4):630–641. doi:10.1007/BF03026968.

Krus, P., Jansson, A., and Palmberg, J.-O. Optimization for Component Selection Hydraulic Systems. In *Fourth Bath International Fluid Power Workshop*. 1991.

Moslått, G.-A. and Hansen, M. R. Modeling of Friction Losses in Offshore Knuckle Boom Crane Winch System. In *2018 Global Fluid Power Society PhD Symposium, GFPS 2018*. IEEE, pages 1–7, 2018. doi:10.1109/GFPS.2018.8472316.

Moslått, G.-A., Hansen, M. R., and Karlsen, N. S. A model for torque losses in variable displacement axial piston motors. *Modeling, Identification and Control*, 2018. 39(2):107–114. doi:10.4173/mic.2018.2.5.

Ortwig, H. New Method of Numerical Calculation of Losses and Efficiencies in Hydrostatic Power Transmissions. *SAE International Off-Highway Congress*, 2002. 1418(724). doi:0148-7191.

Pacey, D. A., Turnquist, R. O., and Clark, S. J. The development of a coefficient model for hydrostatic transmissions. In *In: Proc.35th Nat.conf.on Fluid Power*, volume 33. 35th National Conference in Fluid Power, Chicago, pages 173–178, 1979.

Schlösser, W. Mathematical model for displacement pumps and motors, part 1. *Hydraulic Power Transmission*, 1961. pages 252–269.

Wilson, W. Performance criteria for positive displacement pumps and fluid motors. In *ASME Semi-annual Meeting*, paper No. 48-SA-14. 1948.

E Performance Improvement of a Hydraulic Active/Passive Heave Compensation Winch Using Semi Secondary Motor Control: Experimental and Numerical Verification

energies

MDPI

Article

Performance Improvement of a Hydraulic Active/Passive Heave Compensation Winch Using Semi Secondary Motor Control: Experimental and Numerical Verification

Geir-Arne Moslått [1,*], Michael Rygaard Hansen [2] and Damiano Padovani [2]

[1] Department of Lifting and Handling, National Oilwell Varco, 4639 Kristiansand, Norway
[2] Department of Engineering Sciences, University of Agder, 4879 Grimstad, Norway; michael.r.hansen@uia.no (M.R.H.); damiano.padovani@uia.no (D.P.)
* Correspondence: geir-arne.moslaatt@nov.com

Received: 28 April 2020; Accepted: 18 May 2020; Published: 25 May 2020

Abstract: In this paper, a newly developed controller for active heave compensated offshore cranes is compared with state-of-the-art control methods. The comparison is divided into a numerical part on stability margins as well as operational windows and an experimental validation of the expected performance improvement based on a full-scale testing on site with a crane rated to 250 metric tons. Such a crane represents the typical target for the new control method using a combination of active and passive hydraulic actuation on the main winch. The active hydraulic actuation is a hydrostatic transmission with variable-displacement pumps and variable-displacement motors. The new controller employs feedforward control of the motors' displacement so that the window of operation is increased and, simultaneously, oscillations in the system are markedly reduced.

Keywords: active heave compensation; winch; hydrostatic transmission

1. Introduction

There are high demands for motion compensated offshore cranes today, mostly related to oil and gas, but also the offshore wind industry. The purpose of motion compensation is to decouple the vessel motion from the connected payload. There are two main categories of compensation. The first is a full 3D compensation (horizontal and vertical plane), while the second is a 1D compensation (vertical plane alone). The most common solution is equipping the crane with a 1D compensation system, and the vessel with a dynamic positioning system keeps the position in the horizontal plane. This approach works very well for most subsea operations since the payload motion in the horizontal plane due to the vessel's roll, pitch, and yaw becomes insignificant by the dampening effect when the payload is below the sea surface. If 1D or 3D compensation is used, the most common methods for the vertical compensation of the motion are controlling the wire speed in the winch or using a passive motion compensator mounted directly on the crane's hook. The wire's speed control can be done with the drum directly or with a dedicated cylinder [1]. When the system is drum controlled, it is usually done with a hydraulic transmission that can be categorized into five types [1–4]:

1. Primary controlled systems with variable-displacement pumps and fixed-displacement motors (VPFM) operated in the closed-circuit configuration.
2. Primary controlled systems with variable-displacement pumps and variable-displacement motors (VPVM) operated in the closed-circuit configuration.
3. Secondary control with a VPVM system operated in closed-circuit configuration with an in-line accumulator ensuring constant pressure.

4. Active/passive hydraulic systems (also known as "hybrid") with two VPVM systems where one of them is secondary controlled, and the other one is primary controlled.
5. Open-circuit systems with a power supply and a pressure-compensated proportional valve.

The active/passive systems dominate the market when looking at crane sizes with lifting capacity above 100 tons. Pure secondary controlled systems are also an option and could be equipped with both analog or digital displacement motors. Although digital displacement motors are not a mature solution at the moment [5], these systems are well suited for the recuperation of energy when subjected to negative loads [3,6,7]. The secondary control units benefit from higher speed capabilities, and improved system response compared to the classic primary pump-controlled systems. Secondary control was introduced in 1977 [8] for hydraulic systems but has still not obtained widespread use in the offshore crane market. The main disadvantage is the demand for expensive components such as over-center hydraulic motors or digital displacement hydraulic motors. The active/passive system is chosen for further investigation in this paper due to its widespread use. Specifically, the active circuit has untapped improvement potential [9]. In the active part of an active/passive system, the motors are equipped with an adjustable displacement. However, the most common active heave compensation strategy is to utilize the motors as if they were fixed-displacement units (like a VPFM system). This approach results in the pumps used as the control element, while the motors' displacement is not adjusted continuously but simply set to fixed values based on the number of wire layers on the drum. When VPFM systems are used in active heave compensation (AHC), the maximum exploitable speed for the winch is limited because the fixed-displacement motors are set based on the high-torque scenarios. As a result, systems that use this classic control method often have different modes to cover a greater speed range. Typically, different modes comprise a normal-speed mode that allows full load capacity, and a high-speed mode. The high-speed mode operates with reduced motors' displacement; therefore, the winch gets a lower allowable safe working load (SWL).

Linear control approaches for hydrostatic transmission (HST) systems, like classic PID controllers, are still commonly used in industrial applications. However, the HST is a nonlinear system, and researchers have tried to address this for several years. One of these strategies utilizes nonlinear backstepping methods [10,11]. Others strategies introduce adaptive control techniques [12–17], or model-based control [18–22]. Some attempts directly towards active heave compensated systems have also been investigated, like fuzzy PI or PID controller [23,24], position controller with tension feedback [25,26], and cascade controllers [27]. To control the winch-drives, one should consider the use of fault-tolerant control (FTC) approaches [12,28]. There are two main categories of FTC [29], namely, active and passive. The cranes from National Oilvell Varco are, in principle, equipped with parts from both, but should, in general, be seen as a system equipped with passive FTC. The AHC controller is a robust linear controller, which is a type of passive FTC. However, the cranes could also be equipped with systems that detect critical errors, such as sensor faults or power loss. In the event of a power failure, the crane uses parameter reconfiguration in the controller, which is a type of active FTC. E.g., if one of the three hydraulic power units shuts down, the fault is detected, the unit gets isolated, and the control parameters are reconfigured (the process is done on-the-fly without stopping the AHC operation). Further, it has been some interest regarding the vessel's motion prediction [30,31] that can be used to improve the controller performance or to predict future events. However, all the aforementioned research is concerned with system performance optimization by exclusively focusing on either the primary control unit or the secondary control unit. In [32] such a dual approach was introduced, and it was shown that optimized control of the pumps' and motors' displacement could yield a better trade-off between response speed and efficiency. The results were, however, not experimentally verified. Another strategy to improve the performance of an HST system for an AHC winch system was introduced in [9]. It highlighted that the dynamical properties of the winch system are highly affected by the motors' displacement, and maximizing them at low speed would result in significant improvements in pressure-peaks and control error. The proposed control strategy actively adjusts the motors' displacement and, at the same time, keep the classic primary

pump-controller. Thus, the system is a mix of secondary control and primary control and called semi secondary control (SSC). Since the displacement in SSC is active and also load sensitive, the need for two or more operational modes is removed as well as the corresponding limitations on the SWL. The results from simulations showed increased performance with regards to the maximum winch velocity and permitted load. It also improved the dynamic response of the winch, which resulted in a smaller control error and smoother winch motion.

Even though the SSC system has been introduced, no systematic evaluation of the new system has been put forward, and no full-scale experimental verification of the improved performance has been presented. Both these aspects are, therefore, addressed in this paper. A description of the hydraulic and mechanical winch system is given in the next section, together with a portrayal of the new controller. In the third section, the new controller's effect on stability is reviewed. Then, in section four, a comparison of the classic control method and the new SSC approach are compared in a simulation model. Section five continues with more comparisons that originated from field tests, followed by the conclusions in section six.

2. Control Algorithm and System Description

The VPVM system under investigation consists of these main components: three over-center variable-displacement pumps for the active side and three for the passive side, five active motors, sixteen passive motors, and a large double piston accumulator connected to nine pressure vessels. The motors are attached to a two-stage gear-transmission, followed by a pinion connected to a ring-gear on the rotating drum. A simplified schematic of the hydraulic transmission is shown in Figure 1, and the total sizes of the main components can be seen in Table 1.

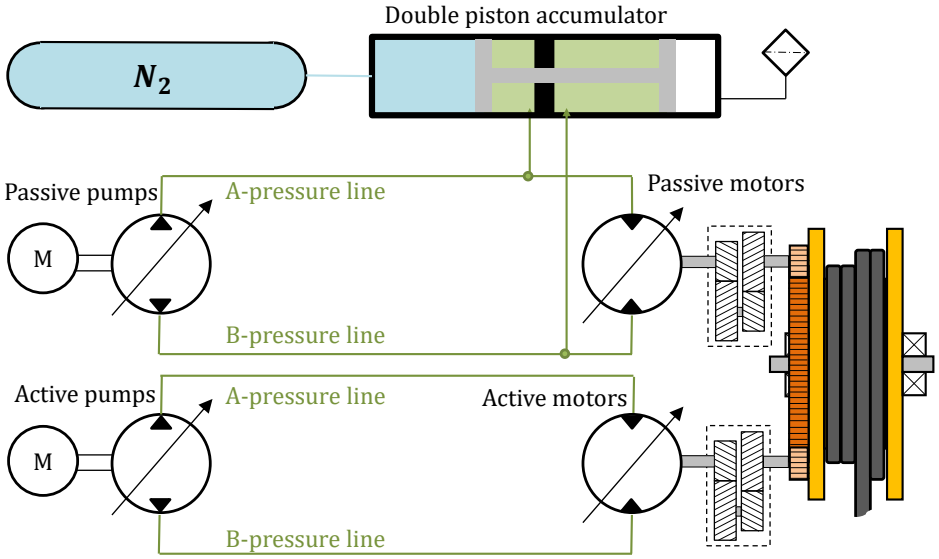

Figure 1. Simplified schematic for a hydraulic active/passive winch system.

The classic AHC controller works as a VPFM system where the motors' displacement is only adjusted when the drum layer is changed. The new controller introduced in [9] suggests an active control of the motors' displacement. The control input is basically a feedforward signal based on the amount of wire on drum, crane's tip velocity, crane's tip acceleration, and motors' displacement.

Table 1. Main component data.

Description	Total Size
Active motors	1075 cm^3/rev
Passive motors	3440 cm^3/rev
Active pumps	1355 cm^3/rev
Passive pumps	1210 cm^3/rev
Gearbox ratio	35.4
Pinion ring-gear ratio	14.17
Drum diameter (without wire)	2.8 m
Drum width	1.9 m
Wire diameter	96 mm

The control structure is depicted in Figure 2, where the parts marked in red represent changes from the classical PVFM controller.

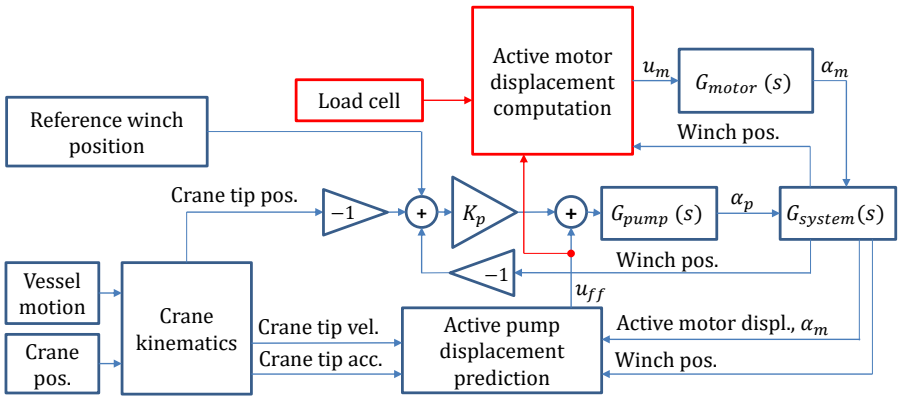

Figure 2. The new control structure.

The classic system's control uses a conservative fixed value of the motors' displacement to be able to cope with the required operation, winch stiction, and winch acceleration. The resulting torque peaks when the winch is switching direction (i.e., scenarios with low speed and high acceleration). The new controller is expected to improve the performance compared to the classical controller. One of the main reasons is that the motors are set to maximum displacement whenever the winch is passing zero velocity. This decision will ensure a higher system stiffness and high torque capacity. As a result, lower amplification of the system resonance and smaller pressure peaks are achieved. Considering that the feedforward signal is the most significant part of the pumps' command signal, it is clear from Figure 3 that the motors' displacement will be at the maximum value when the pump is passing zero displacement.

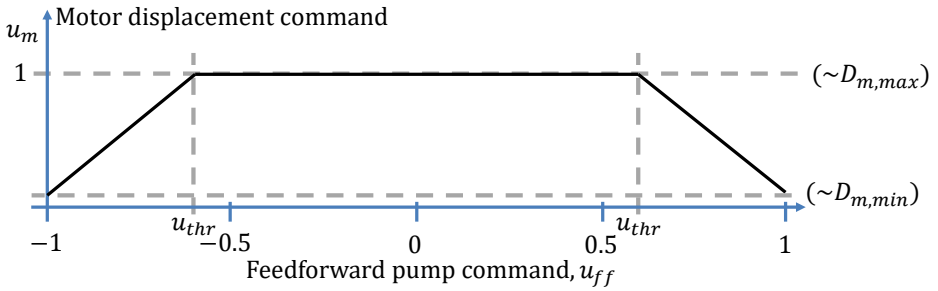

Figure 3. Motor displacement control due to u_{ff}.

Thus, the motors' displacement is controlled according to Equations (1)–(3):

$$u_m = 1 - k_{vgred} \cdot \frac{D_{m,max} - D_{m,min}}{D_{m,max}}, \tag{1}$$

$$k_{vgred} = \begin{cases} \frac{1}{1-u_{thr}} \cdot |u_{ff}| - \frac{u_{thr}}{1-u_{thr}}, & |u_{ff}| \geq u_{thr} \\ 0, & |u_{ff}| < u_{thr} \end{cases}. \tag{2}$$

The relative reduction of the motors' displacement between the maximum and a dynamically set minimum (load dependent) is referred to as k_{vgred} (Equation (2)). If $k_{vgred} = 1$, it implies that the motors' displacement is reduced to its minimum allowable displacement, $D_{m,min}$. The factor, k_{vgred}, is controlled by the feedforward command, u_{ff}, which is based on the vessel movement, actual displacement, and the exit diameter of the wire on the drum. The threshold-value, u_{thr}, defines at what point the motors' displacement should start to be reduced.

The second major benefit of using the variable motors' displacement control is the increased maximum speed of the winch. At higher speed demand, the torque needed for acceleration is less, and the motors' displacement can be reduced with low risk of exceeding the admitted pressure levels. The reduction of the displacement dictates a higher velocity capacity as a direct outcome. To ensure that the displacement is not reduced too much, the new controller uses the loadcell sensor (i.e., a measure of the winch load) to calculate a minimum displacement level, $D_{m,calcMin}$. Additionally, an absolute minimum, $D_{m,absMin}$, is also set to avoid exceeding the speed limitations of the winch components. The maximum setting of the two defines $D_{m,min}$ (Equation (3)).

$$D_{m,min} = max(D_{m,absMin}, D_{m,calcMin}) \tag{3}$$

Due to the dynamic adjustment of the motors' displacement, the new controller will be able to reach higher wire velocity without saturating the pumps. An example of this feature is shown in Figure 4. The amount of extra speed that can be obtained will mainly depend on the winch load and minimum allowed motors' displacement.

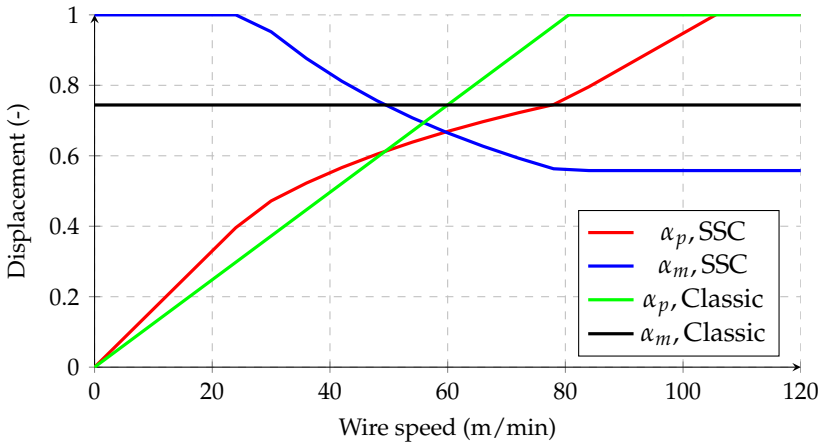

Figure 4. Steady-state motors' and pumps' displacement setting (α_m and α_p).

3. System Stability

An analysis of both the closed-loop system's transfer function and the tuning parameter, K_p, was performed to investigate the influence of the system changes that the new controller introduces. The system's governing equations listed in Equations (1)–(11) are the non-linear, time-domain equations. These equations are based on a simplified equivalent hydraulic system representing

the active part in the active/passive hydraulic system seen in Figure 1. The controller algorithm described in Equations (1) and (2), where Equation (1) defines the motors' control signal, u_m.

$$u_{ff} = (k_1 \cdot v_{tip} + k_2 \cdot a_{tip}) \cdot K_{wire} \cdot \alpha_m \tag{4}$$

$$e = \int (v_{tip} - \frac{\omega_m \cdot d_{D,max}}{i_{hD} \cdot 2 \cdot K_{wire}}) \cdot dt \tag{5}$$

$$u_p = u_{ff} + K_p \cdot e \tag{6}$$

$$\ddot{\alpha}_m = w_{nm}^2 \cdot (u_m - \alpha_m) - 2 \cdot \zeta_m \cdot w_{nm} \cdot \dot{\alpha}_m \tag{7}$$

$$\ddot{\alpha}_p = w_{np}^2 \cdot (u_p - \alpha_p) - 2 \cdot \zeta_p \cdot w_{np} \cdot \dot{\alpha}_p \tag{8}$$

$$v_w = \frac{\omega_m \cdot d_{D,max}}{i_{hD} \cdot 2 \cdot K_{wire}} \tag{9}$$

$$J_{meff} \cdot \dot{\omega}_m = D_{m,max} \cdot (p_A - p_B) \cdot \alpha_m - B_v \cdot \omega_m \tag{10}$$

$$\frac{V_A}{\beta} \cdot (\dot{p}_A - \dot{p}_B) = D_{p,max} \cdot \omega_p \cdot \alpha_p - \alpha_m \cdot D_{m,max} \cdot \omega_m - K_{leak} \cdot (p_A - p_B) \tag{11}$$

The motors' control signal depends on the feedforward control signal, u_{ff}, from the crane's tip motion and winch geometry shown in Equation (4). The position control error, calculated in Equation (5), is used with a proportional controller and a feedforward command to control the pumps (Equation (6)). The second-order equations in Equations (7) and (8), describe the response of the pumps' and motor's displacement. Equations (9)–(11) represent the dynamics of the hydromechanical system.

When linearizing the above-mentioned set of equations, it is assumed that $u_{thr} < u_{ff} < 1$, and the low-pressure side, p_B, is kept constant. Since a linearization is performed around a steady-state velocity, the a_{tip} will naturally disappear.

$$U_m = -\frac{1}{1 - U_{thr}} \cdot |U_{ff}| \cdot \frac{D_{m,max} - D_{m,min}}{D_{m,max}} \tag{12}$$

$$U_{ff} = k_1 \cdot v_{tip}^{(ss)} \cdot K_{wire} \cdot A_m + k_1 \cdot V_{tip} \cdot K_{wire} \cdot \alpha_m^{(ss)} \tag{13}$$

$$s \cdot E = V_{tip} - \frac{W_m \cdot d_{D,max}}{i_{hD} \cdot 2 \cdot K_{wire}} \tag{14}$$

$$U_p = U_{ff} + K_p \cdot E \tag{15}$$

$$s^2 \cdot A_m = w_{nm}^2 \cdot (U_m - A_m) - 2 \cdot \zeta_m \cdot w_{nm} \cdot s \cdot A_m \tag{16}$$

$$s^2 \cdot A_p = w_{np}^2 \cdot (U_p - A_p) - 2 \cdot \zeta_p \cdot w_{np} \cdot s \cdot A_p \tag{17}$$

$$V_w = \frac{W_m \cdot d_{D,max}}{i_{hD} \cdot 2 \cdot K_{wire}} \tag{18}$$

$$J_{meff} \cdot s \cdot W_m = D_{m,max} \cdot (p_A^{(ss)} - p_B) \cdot A_m + D_{m,max} \cdot \alpha_m^{(ss)} \cdot P_A - B_v \cdot W_m \tag{19}$$

$$\frac{V_A}{\beta} \cdot P_A \cdot s = D_{p,max} \cdot w_p \cdot A_p - \alpha_m^{(ss)} \cdot D_{m,max} \cdot W_m - w_m^{(ss)} \cdot D_{m,max} \cdot A_m - K_{leak} \cdot P_A \tag{20}$$

$$G_v(s) = \frac{V_w}{V_{tip}} \tag{21}$$

By the parameter-variation and use of the Routh-Hurwitz criterion on the transfer function $G_v(s)$, the K_p for a marginally stable system was found, $K_p^{(ms)}$. The added motor control is implemented as a pure feedforward, hence stability is not affected as long as the internal displacement controller of the motors are stable (which is assumed in this case). Therefore, the motors' natural frequency and damping ratio, ω_{nm} and ζ_m, have no effect on the system stability. As seen in Figure 4, the new controller could lead to situations with lower displacement settings than the classic controller. Based on parameters from Table 2, Figure 5 shows the relationship between $K_p^{(ms)}$ and motor displacement.

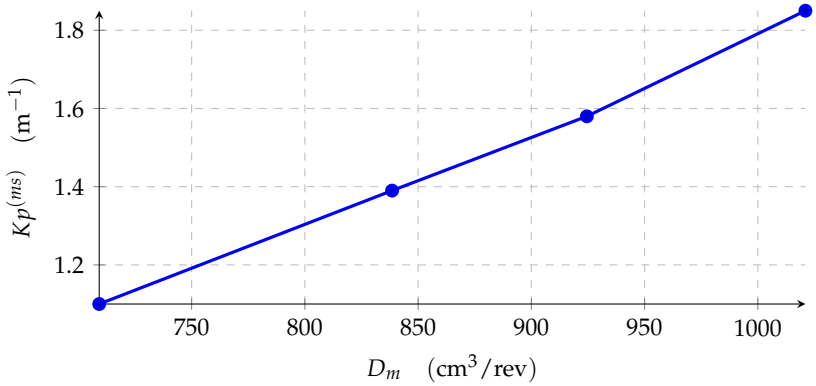

Figure 5. Variation of the motor displacement with all other system parameters fixed.

Table 2. Parameters.

$d_{D,max}$	5.1 m	J_{meff}	4.1 kg/m^2	β	17,500 bar
V_A	80 l	i_{hD}	501.6	ζ_p	0.9
$D_{m,max}$	1075 cm^3/rev	$D_{m,min}$	645 cm^3/rev	ω_{np}	31 rad/s
K_p	0.16 m^{-1}	U_{thr}	0.6	ζ_m	1
K_1	0.68 s/m	B_v	2.1 $\frac{\text{Nm·s}}{\text{rad}}$	ω_{nm}	5 rad/s
K_{leak}	0.4 $\frac{\text{l}}{\text{min}}$/bar	ω_p	1800 rev/min	K_{wire}	1

Compared to the classical control strategy, the main difference with the SSC system is that the displacement is adjusted actively. The displacement in the classical controller is held constant, while in the SSC, the displacement is adjusted due to the winch's speed command. In Figure 4, the steady-state command signals are plotted for both pumps and motors. It is seen that for most operating conditions, the motors' displacement will be higher for most wire-speed scenarios. However, the curves will cross at some point, and the SSC will demand a lower motor displacement than the classical controller. The lower motor displacement will reduce the $K_p^{(ms)}$ compared to the classically controlled system. However, this characteristic is not seen as critical because, in an active heave compensation scenario, the speed demand will be cyclic, and in every cycle, the speed will return to zero. Zero speed demand will give maximum motor displacement and, therefore, also the highest stability margin. In that way, the system will never stay for many seconds in a scenario with low or negative stability margins. Additionally, these systems do not usually demand high K_p, and a slight reduction in the stability margin is not seen as a problem.

4. Comparison of the Classic and New Controller

A simulation model is built and verified with field measurements. Further, it is used to compare the two different strategies. The model allows for testing the complete operating range of the winch, which is not always possible to test on the real crane. A map of different load scenarios was created and compared. The load scenarios include loads from 20% to 100% of the SWL, and crane's tip velocity profiles with peak velocities from 10 m/min to 120 m/min. The performance is reviewed based on three different characteristics, namely the control error, peak pressures, and settling time.

4.1. The Control Error

The test sequence is a representative velocity profile like the one shown in Figure 6. The profile is scaled up and down to match the desired peak velocities so that different conditions are explored. The control error is calculated as the peak-to-peak control error over 20 s (see Figure 7).

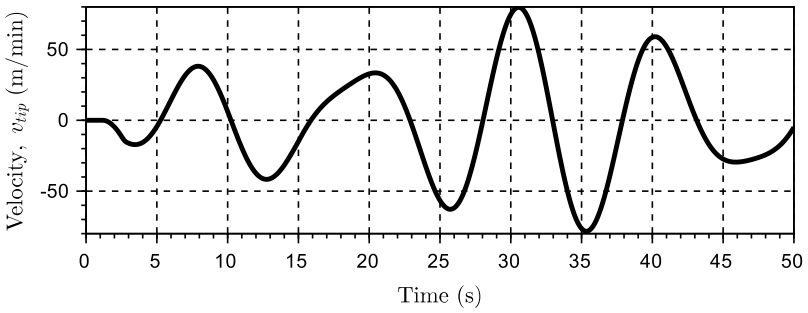

Figure 6. Velocity reference (the first 10 s are neglected due to the model initialization).

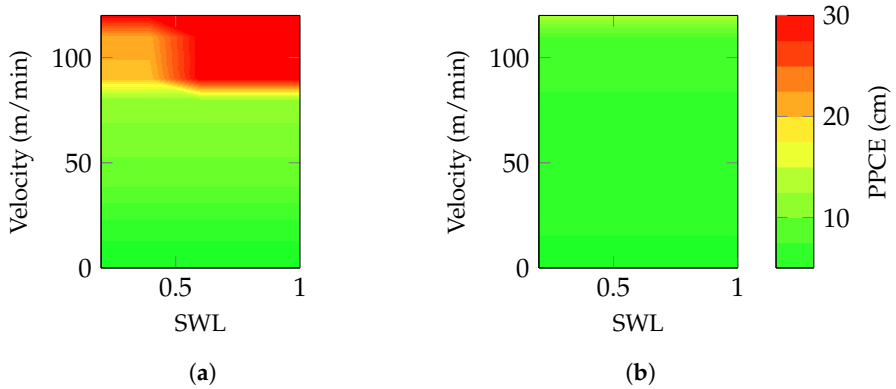

Figure 7. Maximum peak-to-peak control error (PPCE) during the test sequence: (**a**) Classic; (**b**) SSC.

The results in Figure 7, show that the classic controller has significantly reduced performance in the high-speed scenarios, and the dark-red areas displays areas where the classic controller is not applicable. In contrast, the SSC strategy show a stable and consistent performance in the whole range.

4.2. The Peak Pressures

The peak pressures taking place in the hydraulic system were monitored during the same cycle used for investigating the control error (see Figures 6 and 7). The maximum peak pressure depicted in Figure 8 show that for most cases the differences are small, but in favor of the SCC. The most significant peak pressure reductions are found at velocities above 80 m/min.

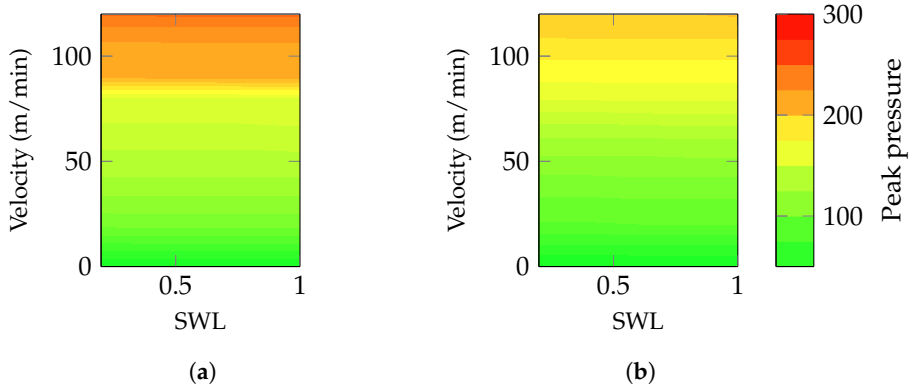

Figure 8. Maximum peak pressure during test sequence: (**a**) Classic; (**b**) SSC.

4.3. The Settling Time

Due to the increased motor's displacement at low speed, the winch is expected to run smoother and give lower settling times. The settling time is tested by setting a fixed wire velocity reference and then step up the reference velocity by 5 m/min. The settling time is defined as the amount of time between the step command and the instant where the velocity is settled close to the target value within

a certain tolerance. In this case, this tolerance is 2% of the step size (i.e., 0.1 m/min) as reported in Figure 9.

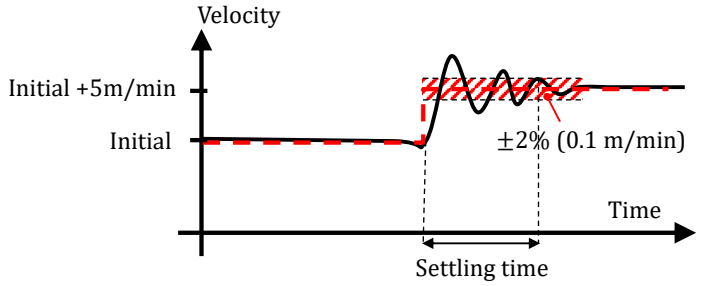

Figure 9. Description of the test for the settling time.

The results in Figure 10 show a significant improvement when the SSC is applied. The corresponding motors' displacement, in Figure 11, substantiate the assumptions that improved performance at low speed is highly affected by the motors' displacement. Additionally, the large displacement variations when using SSC is illustrated compared to the classic controller with only two fixed displacement settings.

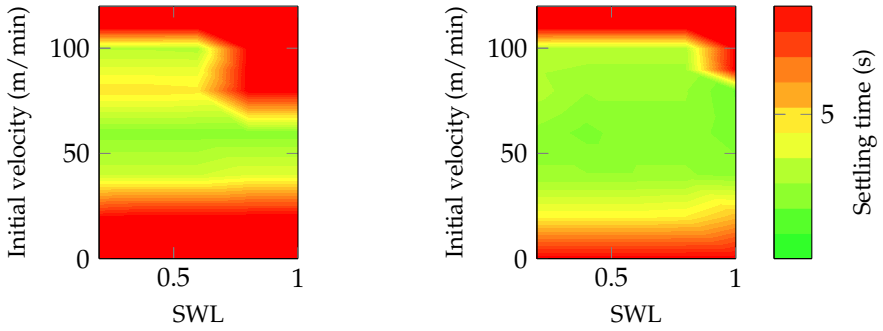

Figure 10. Settling time within 2% after a 5 m/min step increase of the reference velocity: (**a**) Classic; (**b**) SSC.

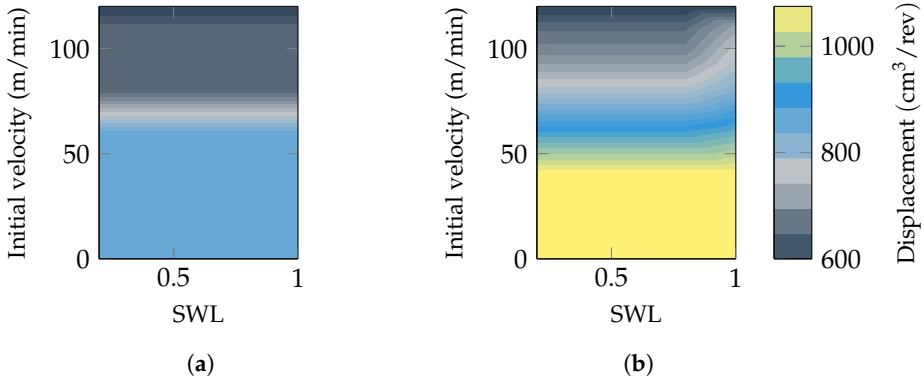

Figure 11. Motors' displacement for the results shown in Figure 10: (**a**) Classic; (**b**) SSC.

As expected, low-speed settling time characterizes the new controller. It is also seen that the new controller performs better at higher speeds and covers part of the map that the classical controller did not. Additionally, it is seen that in the area where the classical controller is close to the speed limitation of the normal-speed mode, around 80 m/min, the SSC performs better.

5. Experimental Results

The full-scale tests performed on a real crane were divided into two main parts. First, the system was tested along a quayside with an empty hook to ensure that the overall functionality and safety could be approved. This step included checking the motors' displacement response and running the winch in AHC with the simulated crane's tip motions. Next, a second experiment was conducted offshore with loads up to 200 tons.

5.1. The Quayside Test

The quayside test was conducted with low winch load and simulated crane's tip motions. The chosen scenario reduces the risk of potential damages to an absolute minimum. Further, the test should reveal how the control of the motors' displacement performs on the real system and if any unforeseen challenges occur. The test was performed with approximately 15 m of wire paid out and the hook hanging freely in air (Figure 12).

Figure 12. A 250t AHC crane from National Oilwell Varco placed on a vessel.

5.1.1. The Control of the Motors' Displacement

Depending on the particular crane, the inner control of the motors' displacement is done in closed-loop (CL) with displacement feedback, or open-loop (OL) without feedback. For the optimal displacement control, the CL approach needs to be used. However, due to cost or retrofit limitations, the other options can be preferred. If OL control is used, but the displacement feedback is available, the overall control accuracy is not affected since the actual displacement is always known and can be fed into the heave compensation controller. The downside is that the actual displacement has significant error compared to the displacement reference, affecting the maximum speed capacity. A third option is the OL without feedback. This method undermines the maximum speed capacity compared to the OL with feedback and affects the control error. The control error is now affected because the feedforward command in the heave compensation controller now has to use the motors' displacement command instead of the measured displacement. Hence, an offset between the actual wire velocity and the desired velocity should be expected. In the crane under investigation, the motors

were controlled in OL with feedback, i.e., there is always a certain discrepancy between the commanded and measured displacement, even at steady-state (Figure 13a).

Several tests were conducted to ensure that the motors can change displacement fast enough to track the commanded setting. The motors are generally reacting faster when the CL is used, so the OL control was chosen being the most conservative way to evaluate the new control method. The results with the OL were satisfactory since sufficient displacement variation was achieved in less than one second (Figure 13b). For comparison in a worst-case scenario, the AHC may have to react to a sinusoidal wave with a peak velocity of 110 m/min and the winch working on the outermost layer. If u_{thr} is set to 0.6, there will be a duration of 1.1 s from when the variable motor control is active to the point of maximum velocity. Therefore, the response time of approximately 1 s is considered more than adequate.

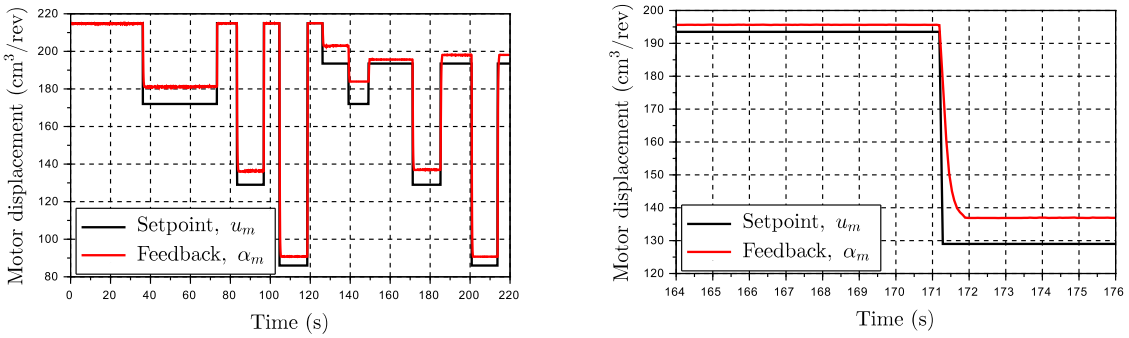

(**a**) Results with open loop displacement control. (**b**) Close view of (**a**).

Figure 13. Response of the motors to a displacement variation.

The downside of the OL control is represented by the hysteresis and offset between desired and actual displacement. The offset is not critical since all the motors have a displacement feedback sensor. It introduces some challenges when the system is trying to reach its full capacity, i.e., maximum pumps' and minimum motors' displacement. If the motors have not reached the desired displacement, the maximum speed capacity is reduced. It is, however, not seen as critical for the planned tests that the system is not be able to reach its maximum capacity, and it is of little consequence in the evaluation of the new control method. During the test shown in Figure 13b, the motor was standing still and with an idle pressure of 25 bar on the A and B port. The displacement controller was running on a fixed pilot pressure of 150 bar to ensure good controllability. This scenario is representative of the motors operating under normal conditions. It is seen that the displacement has an offset of approximately 5–10% and a noticeable hysteresis.

A more realistic scenario was tested by running the winch with the new controller and a simulated crane's tip motion. This crane's tip motion was a pure sine wave, and the test was carried out with two different patterns. The first was a 12 s period with 3.2 m amplitude, while the second involved a 6 s period and 1.2 m amplitude (see Figure 14).

The main issue to notice from those tests was the offset between feedback and setpoint. The offset is up to 20 cm^3/rev, resulting in a reduced potential for the winch speed. However, the winch could easily meet the speed requirements for these wave-profiles. The tests were performed on the outer layer and wave periods down to 6 seconds. This is the worst-case scenario for the motors because the amount of time where the motors have to reduce and increase their displacement is minimized. One of the reasons the $u_{thr} = 0.6$ is preferred to a smaller value, for example 0.4, is that 0.6 results in the winch operating more often at maximum motors' displacement. As the previous analyses have shown, working at maximum displacement improves the overall winch performance.

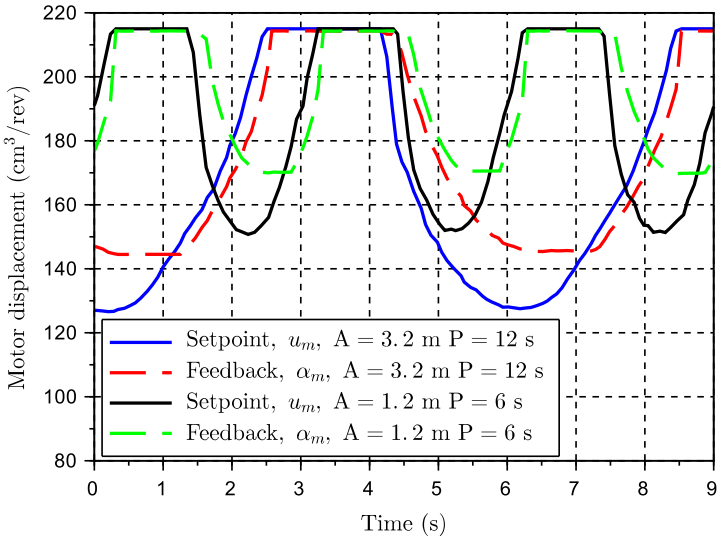

Figure 14. Simulated sinusoidal motion with 12 s period and 6 s period. The motors' displacement controller runs in open-loop.

5.1.2. The Winch Performance

From earlier simulated results, by Moslått et al. [9], some of the significant benefits enabled by the new controller is a smoother winch control and lower pressures, especially at low-speed. Three different test scenarios are performed, including high and low wire velocities. Within these three test scenarios, a direct comparison between the classic control and the new SSC control is made. All scenarios were compared under the same conditions.

Scenario 1

The scenario 1 can be defined as a low-speed operation with a peak velocity around 30 m/min, see Figures 15–18.

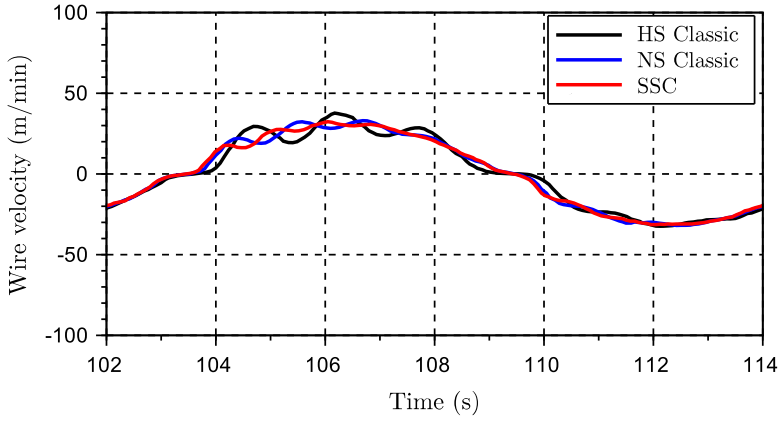

Figure 15. Wire velocities for scenario 1.

The VPFM methods are clearly more oscillatory in the velocity pattern (Figure 15), and more pronounced in the pressure pattern (Figure 16). The oscillations increase the control error that is kept to a minimum by the proposed method (Figure 17).

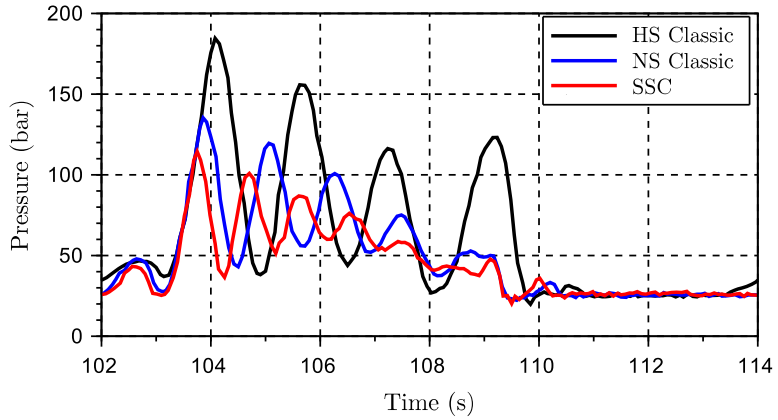

Figure 16. Pressure levels on the A-side of the active system for scenario 1.

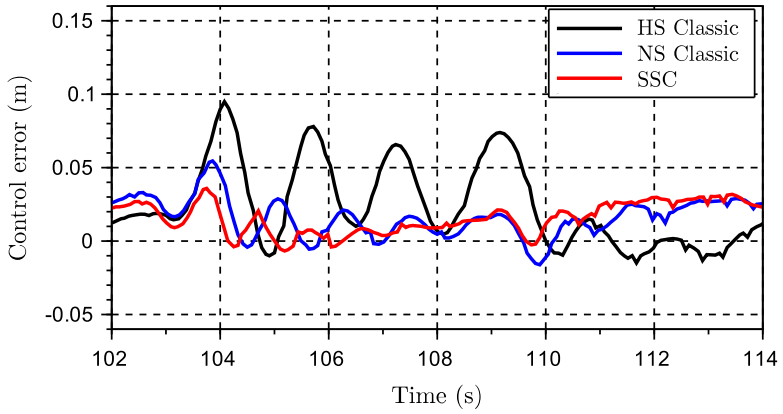

Figure 17. Control error for scenario 1.

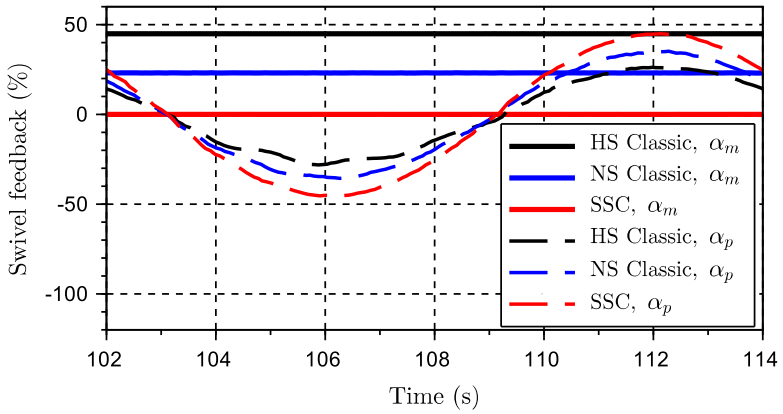

Figure 18. Pump and motor displacement settings for scenario 1 (0% for the motor means maximum displacement).

Scenario 2

In the second scenario the peak velocity is increased to the maximum capacity for the AHC normal speed (Figure 19).

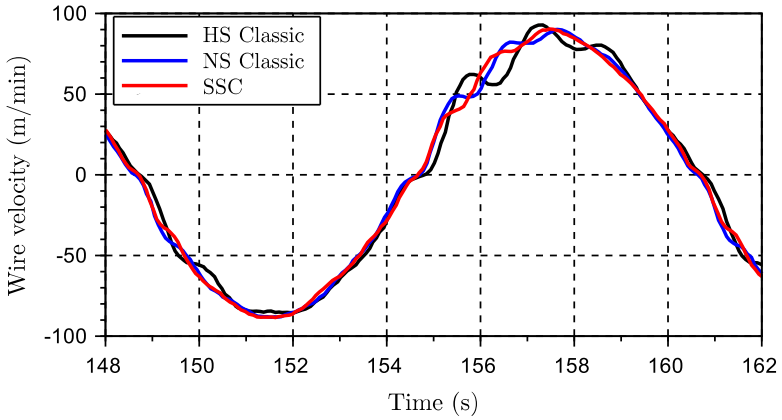

Figure 19. Wire velocities for scenario 2.

The velocities are so high that the high speed (HS) mode would be the chosen option from a lift planner perspective. Comparing the proposed method (i.e., the AHC SSC) to the HS mode, the pressure peaks are now reduced by more than 120 bar (Figure 20), that is a significant achievement. Additionally, the control error remains within 10 cm compared to more than 20 cm for the HS mode (Figure 21). The normal speed mode is also performing adequately, but with higher pressures than the AHC SSC. When addressing the classic normal speed (NS), it is worth mentioning that this mode reaches its full capacity, while the AHC SSC still has 10% pump capacity left in addition to a potential motors' displacement reduction of more than 20% (see Figure 22).

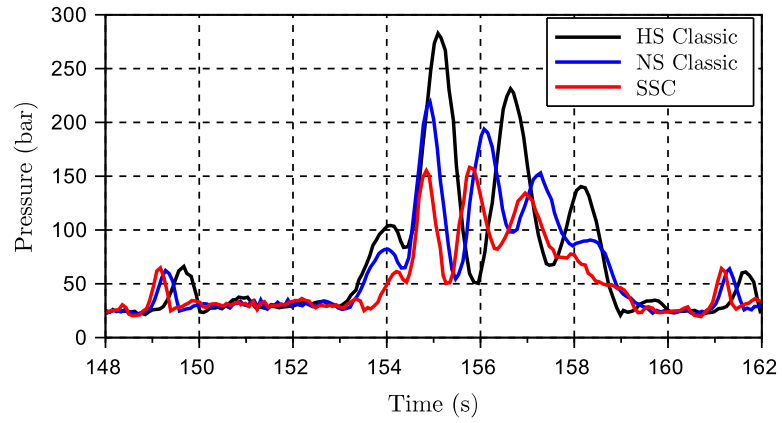

Figure 20. Pressure levels on the A-side of the active system for scenario 2.

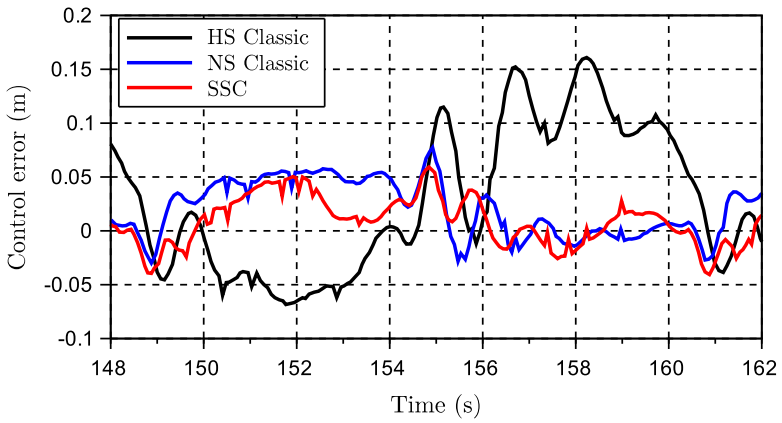

Figure 21. Control error for scenario 2.

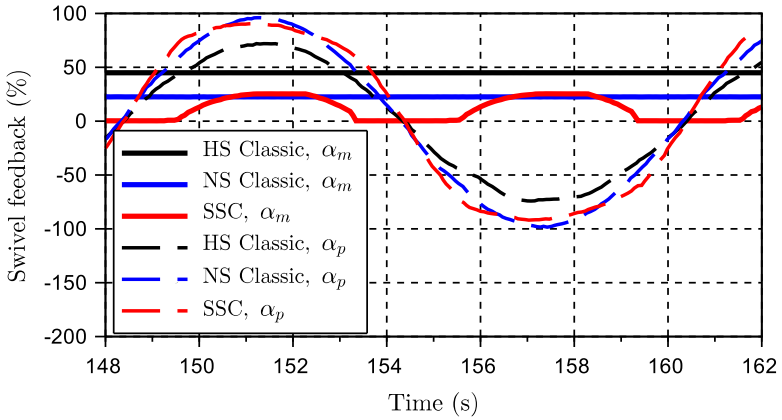

Figure 22. Pump and motor displacement settings for scenario 2 (0% for the motor means maximum displacement).

Scenario 3

Finally, a third scenario was tested (Figures 23–26). The classic AHC HS controller is compared again with the AHC SSC controller.The wave pattern is made more complex with two overlying sine waves.

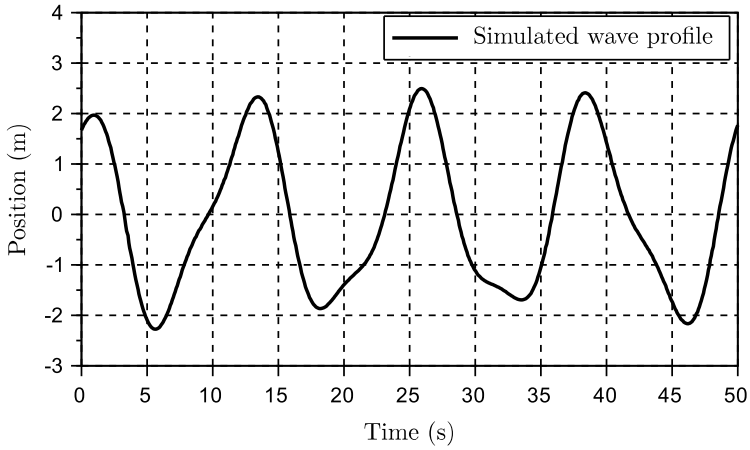

Figure 23. Crane's tip position for scenario 3.

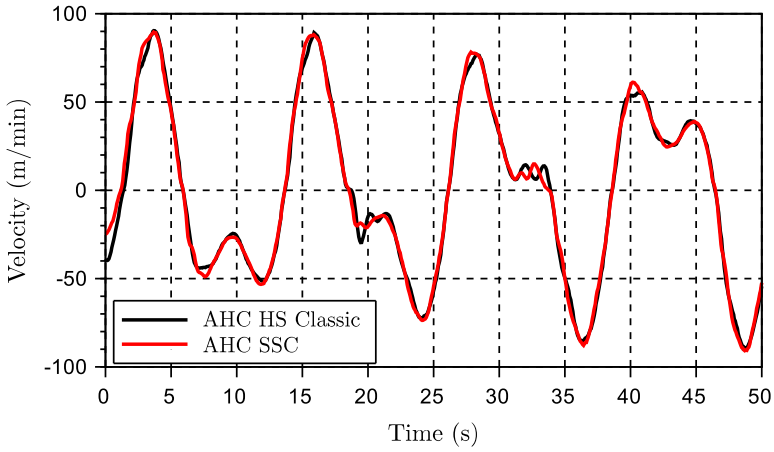

Figure 24. Wire velocities for scenario 3.

The purpose of this modification was exploring the systems' performance under a scenario closer to a real-life operation. Typically, the vessel has at least two dominant frequency components.

One frequency for large swells, often related to the pitch of the vessel, and another one with a bit smaller amplitude but higher frequency. The second frequency is, in many cases, related to the vessel roll. In this case, it was simulated as a 0.5 m amplitude with a 6 s period time on top of a 2 m amplitude with a 13 s period time.

The results from scenario 3 are in line with the previous ones and confirm that the AHC SSC has obvious advantages concerning controllability in the form of reduced oscillations for most conceivable working scenarios. The pressure levels are lowered (Figure 25), and the control error (Figure 26) is minimized.

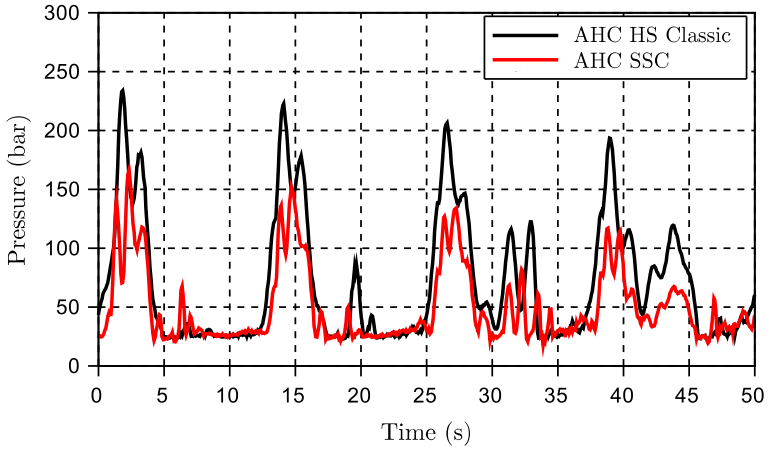

Figure 25. Pressure levels on the A-side of the active system for scenario 3.

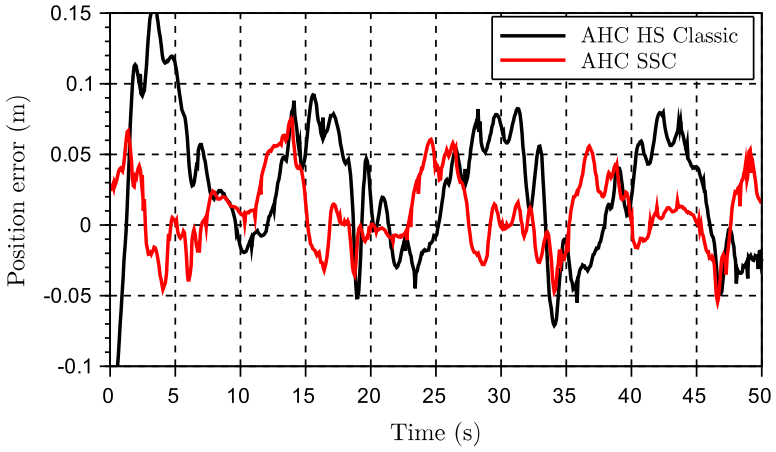

Figure 26. Control error for scenario 3.

5.2. Discussion of the Results

The results from the field tests are shown to be very much in line with the previously simulated results. From the empty hook tests at the quayside, the motors' displacement control was confirmed to behave sufficiently well due to the acceptable response time. The positive effects of keeping a high displacement setting at low speed were confirmed since the classic controller lead to higher and more oscillatory pressures and winch motion, especially at low speeds shown in Figures 16 and 17. This trend was also confirmed with the mapped results from simulations in Section 4. From the different maps, it is seen that the new controller expands the range of the AHC system in terms of both high velocity and high load scenarios. The performance has also been slightly improved, where normal speed mode is working close to its maximum velocity potential. Further, it is discovered that the peak pressures are reduced, especially for scenarios with high wire velocities. Additionally, the low-speed performance is improved (it was measured by the use of the settling time after a step

command in the velocity reference). Concerning the crane tested in field, it was not possible to gain any extra speed compared to the classic HS controller due to gearbox speed limitations. Nevertheless, the AHC SSC controller enables higher load capacity and better winch performance. For the offshore testing, the results were similar, although it was not possible to compensate with higher velocities than 40m/min due to the weather conditions (40 m/min is below 50% of the rated winch capacity). The the results were still positive leading to reduced peak pressures and reduced oscillations. The classic HS mode was also tested offshore. The tests, not displayed in this paper, confirmed the same satisfactory behavior that was seen during the quayside tests.

6. Conclusions

The newly developed semi secondary control (SSC) method for offshore heave compensated winches has been investigated and compared to the current state-of-the-art approach with a fixed setting of the motors' displacement. Firstly, it has been shown that the SSC leads to variations in the marginal stability because of the variations in the motor displacement, but, higher stability margins are achieved compared to the the classical control method at low speeds. Secondly, the increased window of operations expected from the SSC has been verified by comparing the peak-to-peak position error, peak pressure, and settling time for variations in both the payload and reference motion. Finally, the improved dynamic performance has been experimentally verified by means of full scale tests on a 250 ton crane.

In general, the active heave compensated (AHC) SSC system is shown to be the preferred control strategy. Based on the experimental and simulated results, the SSC show better performance in terms of control error and dynamics with significantly fewer oscillations and lower pressure levels (Figure 27). The fact that the new controller covers the whole operational area of both the AHC NS and the AHC HS, clearly suggests that the AHC SSC can succefully replace the two modes. Also, the AHC SSC controller allows higher velocities with more hook load than before and only requires one set of tuning parameters.

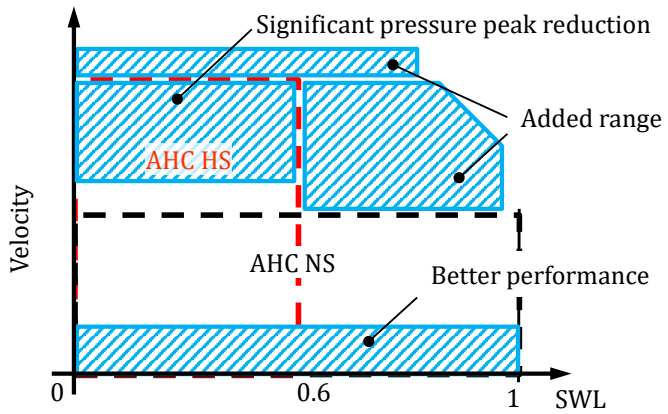

Figure 27. Significant findings from comparison between the classic controller and the SSC.

Author Contributions: Proposal: Conceptualization, G.-A.M.; methodology, G-A.M., D.P., and M.R.H.; software, G.-A.M.; validation, G.-A.M.; formal analysis, G.-A.M.; investigation, G.-A.M.; data curation, G.-A.M.; writing—original draft preparation, G.-A.M.; writing—review and editing, M.R.H. and D.P.; visualization, G.-A.M.; supervision, M.R.H. and D.P. All authors have read and agreed to the published version of the manuscript.

Funding: This research was funded by the research council of Norway and National Oilwell Varco Norway, grant number 263525. The APC was funded by the University of Agder.

Acknowledgments: Thanks to Anders Meisfjordskar for good conversations on the topic and to National Oilwell Varco Norway (NOVN) for dedicating resources to perform the full scale field tests. An excellent effort was given by Andreas Reppen at NOVN to prepare the crane-software, and the experimental field tests were assisted by Øystein Kolrud and Andreas Reppen.

Conflicts of Interest: The funder, National Oilwell Varco Norway, had a role in the design of the study; in the collection, analyses, and interpretation of data; in the writing of the manuscript, and in the decision to publish the results.

Abbreviations

α_m	Motor displacement feedback
α_p	Pump displacement feedback
ω_m	Rotational velocity of motor shaft
ω_{nm}	Natural eigenfrequency of motor displacement control
ω_{np}	Natural eigenfrequency of pump displacement control
ζ_m	Damping ratio of motor displacement control
ζ_p	Damping ratio of pump displacement control
A_m	Laplace transform of α_m
A_m	Laplace transformed α_m
A_p	Laplace transform of α_p
A_p	Laplace transformed α_p
a_{tip}	Crane tip acceleration
$d_{D,max}$	Maximum drum diameter
$D_{m,max}$	Maximum motor displacement
$D_{m,min}$	Minimum allowable motor displacement
E	Laplace transform of e
e	Controller error
i_{hD}	Transmission ratio between hydraulic motor shaft rotation and drum
J_{meff}	Total inertia on motor shaft
k_1	Proportional gain for crane tip velocity in feedforward controller
k_2	Proportional gain for crane tip acceleration in feedforward controller
K_{leak}	Laminar leakage factor
K_p	Proportional gain for feedback control error
k_{vgred}	Factor for motor displacement reduction
K_{wire}	Drum diameter factor
P_A	Laplace transform of p_A
p_A	Pressure A side
p_B	Pressure B side
U_{ff}	Laplace transform of u_{ff}
U_{ff}	Laplace transformed u_{ff}
u_{ff}	Feedforward signal
U_m	Laplace transform of u_m
U_m	Laplace transformed u_m
u_m	Command signal for motor displacement control
U_p	Laplace transform of u_p
u_p	Command signal for pump displacement control
U_{thr}	Laplace transform of u_{thr}
u_{thr}	Threshold value for when to start reducing motor displacement
V_{tip}	Laplace transform of v_{tip}
V_{tip}	Laplace transformed v_{tip}
v_{tip}	Crane tip velocity
V_w	Laplace transform of v_w
V_w	Laplace transformed v_w
v_w	Wire velocity
W_m	Laplace transform of ω_m

AHC	Active heave compensation
AHC HS	Active heave compensation, high-speed mode
AHC NS	Active heave compensation, normal speed mode
FTC	Fault tolerant control
HST	Hydrostatic transmission
MPC	Model-based control
NOV	National Oilwell Varco
VPFM	Variable pumps and fixed motors
VPVM	Variable pumps and variable motors
SSC	Semi secondary control
SWL	Safe working load

References

1. Woodacre, J.K.; Bauer, R.J.; Irani, R.A. A review of vertical motion heave compensation systems. *Ocean Eng.* **2015**, *104*, 140–154, doi:10.1016/j.oceaneng.2015.05.004.
2. Feuser, A. *Hydrostatic Drives with Control of the Secondary Unit*; Mannesmann Rexroth GmbH: Lohr am Main, Germany, 1989; Volume 6.
3. Palmgren, G.; Rydberg, K.E. Secondary Controlled Systems—Energy Aspects and Control Strategies. In Proceedings of the International Conference on Fluid Power, Tampere, Finland, 24–26 March 1987.
4. Bosch Rexroth AG. *Drive and Control Solutions for Marine Engineering: Reliable, Efficient, Durable*; Rexroth Bosch B.V., Netherlands. Available online: https://dc-us.resource.bosch.com/media/us/products_13/product_groups_1/industrial_hydraulics_5/\pdfs_4/R999001175_2015-1.pdf (accessed on 24 May 2020).
5. Marien, M.; Wiig, K.E.; Ebbesen, M.K. Secondary Control of a Digital Hydraulic Motor for Winch Applications. Master's Thesis, University of Agder, Kristiansand S, Norway, 2018.
6. Padovani, D.; Ivantysynova, M. The Concept of Secondary Controlled Hydraulic Motors Applied to the Propulsion System of a Railway Machine. In Proceedings of the 14th Scandinavian International Conference on Fluid Power, Tampere, Finland, 20–22 May 2015.
7. Padovani, D.; Ivantysynova, M. Simulation and Analysis of Non-Hybrid Displacement-Controlled Hydraulic Propulsion Systems Suitable for Railway Applications. In Proceedings of the ASME/BATH 2015 Symposium on Fluid Power and Motion Control, Chicago, IL, USA, 12–14 October 2015; p. 11, doi:10.1115/FPMC2015-9509.
8. Nikolaus, H. Antriebssystem mit hydrostatischer Kraftubertragung. Patent number 27,399,684, 1977.
9. Moslått, G.A.; Padovani, D.; Hansen, M.R. A Control Algorithm for Active/Passive Hydraulic Winches Used in Active Heave Compensation. In Proceedings of the ASME/BATH 2019 Symposium on Fluid Power and Motion Control; American Society of Mechanical Engineers: Sarasota, FL, USA, 7–9 October 2019; p. 11, doi:10.1115/FPMC2019-1710.
10. Kaddissi, C.; Kenne, J.P.; Saad, M. Identification and Real-Time Control of an Electrohydraulic Servo System Based on Nonlinear Backstepping. *IEEE/ASME Trans. Mechatron.* **2007**, *12*, 12–22, doi:10.1109/TMECH.2006.886190.
11. Yao, J.; Jiao, Z.; Ma, D. Extended-state-observer-based output feedback nonlinear robust control of hydraulic systems with backstepping. *IEEE Trans. Ind. Electron.* **2014**, *61*, 6285–6293, doi:10.1109/TIE.2014.2304912.
12. Mahulkar, V.; Adams, D.E.; Derriso, M. Adaptive fault tolerant control for hydraulic actuators. In Proceedings of the American Control Conference, American Automatic Control Council, Chicago, IL, USA, 1–3 July 2015; Volume 2015, pp. 2242–2247, doi:10.1109/ACC.2015.7171066.
13. Yao, J.; Jiao, Z.; Ma, D.; Yan, L. High-accuracy tracking control of hydraulic rotary actuators with modeling uncertainties. *IEEE/ASME Trans. Mechatron.* **2014**, *19*, 633–641, doi:10.1109/TMECH.2013.2252360.
14. Yao, B.; Bu, F.; Reedy, J.; Chiu, G.T. Adaptive robust motion control of single-rod hydraulic actuators: Theory and experiments. *IEEE/ASME Trans. Mechatron.* **2000**, *5*, 79–91, doi:10.1109/3516.828592.
15. Yao, J.; Deng, W.; Jiao, Z. Adaptive control of hydraulic actuators with LuGre model-based friction compensation. *IEEE Trans. Ind. Electron.* **2015**, *62*, 6469–6477, doi:10.1109/TIE.2015.2423660.
16. Yao, J.; Jiao, Z.; Ma, D. A Practical Nonlinear Adaptive Control of Hydraulic Servomechanisms with Periodic-Like Disturbances. *IEEE/ASME Trans. Mechatron.* **2015**, *20*, 2752–2760, doi:10.1109/TMECH.2015.2409893.

17. Do, H.T.; Ahn, K.K. Velocity control of a secondary controlled closed-loop hydrostatic transmission system using an adaptive fuzzy sliding mode controller. *J. Mech. Sci. Technol.* **2013**, *27*, 875–884, doi:10.1007/s12206-012-1237-2.
18. Meller, M.; Kogan, B.; Bryant, M.; Garcia, E. Model-based feedforward and cascade control of hydraulic McKibben muscles. *Sens. Actuators A Phys.* **2018**, *275*, 88–98, doi:10.1016/j.sna.2018.03.036.
19. Chatzakos, P.; Papadopoulos, E. On model-based control of hydraulic actuators. *Proc. RAAD* **2003**, *3*, 7–10.
20. Rezayi, S.; Arbabtafti, M. A New Model-Based Control Structure for Position Tracking in an Electro-Hydraulic Servo System with Acceleration Constraint. *J. Dyn. Syst. Meas. Control* **2017**, *139*, doi:10.1115/1.4036878.
21. Guan, C.; Pan, S. Adaptive sliding mode control of electro-hydraulic system with nonlinear unknown parameters. *Control Eng. Pract.* **2008**, *16*, 1275–1284, doi:10.1016/j.conengprac.2008.02.002.
22. Zheng, S.; Wang, X.; Lu, Y.; Wang, Y. The sliding mode control for speed system of the variable displacement motor at the constant pressure network. In Proceedings of the 2013 International Conference on Intelligent Control and Information Processing, ICICIP 2013, Beijing, China, 9–11 June 2013; pp. 499–503, doi:10.1109/ICICIP.2013.6568126.
23. Liu, S.; Guo, Q.; Zhao, W. Research on active heave compensation for offshore crane. In Proceedings of the 26th Chinese Control and Decision Conference, CCDC 2014, Changsha, China, 31 May–2 June 2014; pp. 1768–1772, doi:10.1109/CCDC.2014.6852456.
24. Shi, M.; Guo, S.; Jiang, L.; Huang, Z. Active-Passive Combined Control System in Crane Type for Heave Compensation. *IEEE Access* **2019**, *7*, 159960–159970, doi:10.1109/ACCESS.2019.2950703.
25. Michel, A.; Kemmetmüller, W.; Kugi, A. Modeling and control of an active heave compensation system for offshore cranes. *At-Automatisierungstechnik* **2012**, *60*, 8–15, doi:10.1152/physiol.00038.2009.Phagocytosis.
26. Sanders, R. *Modelling and Simulation of Traditional Hydraulic Heave Compensation Systems*; Technical Report; University of Twente, Faculty of Engineering Technology: Enschede, The Netherlands, 2016.
27. Wu, J.; Wu, D. Integrated design of an active heave compensation crane with hydrostatic secondary control. In Proceedings of the OCEANS 2018 MTS/IEEE Charleston, OCEAN 2018, Charleston, SC, USA, 22–25 October 2018; pp. 1–7, doi:10.1109/OCEANS.2018.8604859.
28. Donkov, V.; Andersen, T.; Ebbesen, M.K.; Linjama, M.; Paloniitty, M. Investigation of the fault tolerance of digital hydraulic cylinders. In Proceedings of the 16th Scandinavian International Conference on Fluid Power, Tampere, Finland, 22–24 May 2019.
29. Dijoux, E.; Steiner, N.Y.; Benne, M.; Péra, M.C.; Pérez, B.G. A review of fault tolerant control strategies applied to proton exchange membrane fuel cell systems. *J. Power Sources* **2017**, *359*, 119–133, doi:10.1016/j.jpowsour.2017.05.058.
30. Küchler, S.; Mahl, T.; Neupert, J.; Schneider, K.; Sawodny, O. Active control for an offshore crane using prediction of the vessels motion. *IEEE/ASME Trans. Mechatron.* **2011**, *16*, 297–309, doi:10.1109/TMECH.2010.2041933.
31. Kusters, J.G.; Cockrell, K.L.; Connell, B.S.; Rudzinsky, J.P.; Vinciullo, V.J. FutureWaves™: A real-time Ship Motion Forecasting system employing advanced wave-sensing radar. In Proceedings of the OCEANS 2016 MTS/IEEE Monterey, OCE 2016, Monterey, CA, USA, 19–23 September 2016; pp. 1–9, doi:10.1109/OCEANS.2016.7761478.
32. Del Re, L.; Goransson, A.; Astolfi, A. Enhancing Hydrostatic Gear Efficiency Through Nonlinear Optimal Control Strategies. *J. Dyn. Syst. Meas. Control* **1996**, *118*, 727–732, doi:10.1115/1.2802349.

F Digital twin for lift planning with offshore heave compensated cranes

Geir-Arne Moslått[1]
Department of Lifting and Handling,
National Oilwell Varco,
Kristiansand N-4630, Agder, Norway
e-mail: geir-arne.moslaatt@nov.com

Damiano Padovani
Associate Professor
Department of Engineering,
University of Agder,
Grimstad 4879, Agder, Norway
e-mail: damiano.padovani@uia.no

Michael Rygaard Hansen
Professor
Department of Engineering,
University of Agder,
Grimstad 4879, Agder, Norway
e-mail: michael.r.hansen@uia.no

A Digital Twin for Lift Planning With Offshore Heave Compensated Cranes

This paper presents a state-of-the-art digital twin of a hydraulic actuated winch that is used for heave compensation in offshore applications. The digital twin is used as part of a larger simulation model that involves all necessary components to perform lift planning and, subsequently, determine the corresponding weather window. The winch simulation model is described and verified by means of full-scale measurements. In addition, a set of acceptance criteria are presented that should be used whenever verifying digital twins of heave compensating winches that are to be used for lift planning. [DOI: 10.1115/1.4048881]

Keywords: computational mechanics and design, offshore safety and reliability, offshore structures and ships in ice, digital twin, subsea technology

Introduction

Design engineers commonly use computer-based models for optimization, testing, development, and maintenance support [1–5]. For offshore cranes, the use of simulations in the design phase is of great value because any physical testing of equipment is costly, time-consuming, and, for some load cases, simply not feasible. There is a special need for models of offshore cranes that can be used in so-called lift planning. Complex offshore lift operations are bound through certification authorities to be engineered and planned before the actual lift takes place [6]. The critical phases that must be examined are typically the initial lift and overboarding, entering/exiting the splash zone, moving through varying water depths, and landing/lifting the object to/from the seabed or to/from a floating structure [7,8]. Examples of operations to be engineered are suctioning anchor deployment, lifting large equipment or structures between two floating vessels, and landing of subsea installations. The main output of the lift planning phase is defining the acceptable operating conditions for the lift. These conditions mainly refer to wind and waves and are commonly known as the weather window. The weather window is determined based on repeated simulations of the planned lift. The result is of high importance for the crane operators because a small weather window can be followed by a significant increase in operational costs. The lift planners who engineer the lift are building a simulation model capable of representing the planned operation. However, they have to use conservative estimates based on recommendations from the classification societies when accurate models are not available. This approach is often the case when it comes to offshore cranes, and such assumptions lead to a significant reduction in the weather window. For lift planners, there is a strong need for simulation models that are verified and constitute an acceptable representation of the physical system. These models are often referred to as digital twins. Digital twins have never been a more common engineering tool than today, and their importance as an essential engineering tool is expected to increase heavily in the future [9,10]. The digital twin is well known for being used as a tool for maintenance prediction [11], development, and process control [12]. A digital twin is a model (virtual twin) representing the physical twin that, typically, can have one or more decisions or recommendations fed back to the physical system. However, this is not the only feature that describes a digital twin. Many formulations can be found since the digital twin became a concept in 2002. Madni et al. [13] made an effort to divide the different digital twins into four levels based on how the user-interface is adapted and how the digital twin is updated (Table 1).

The definitions are wide, and cover everything from standalone models at level 1 and 2, to highly integrated and adaptable models in level 4. In 2019, the CIRP Encyclopedia of Production Engineering launched this definition [14]: "A digital twin is a digital representation of an active unique product (real device, object, machine, service, or intangible asset) or unique product-service system (a system consisting of a product and a related service) that comprises its selected characteristics, properties, conditions, and behaviors by means of models, information, and data within a single or even across multiple life cycle phases." In other words, digital twin has become an expression that, among others, covers what is also called: simulation model, model-based optimization, three-dimensional (3D)-model, and prototype-model. In a literature review by Jones et al. [15], some future research directions were identified, and they included benefits of digital twins, use-cases, and levels of fidelity.

From the lift planners' perspective, a verified model that is accessible offline and that can be integrated with other software engineering tools is needed. Based on the classification given by Madni, this corresponds to a level 2 digital twin. The discussion about levels and features of a digital twin are common topics, however, the actual quality requirement to a digital twin is rarely mentioned. In a panel discussion with the offshore companies TechnipFMC, Petoro, and DNV GL [16], this was said by Erlend Fjøsna

Table 1 Levels of digital twins [13]

Level	Name	Model sophistication	Data acquisition from physical twin
1	Pre-digital twin	Virtual system model	N/A
2	Digital twin	Virtual system model	Batch updates
3	Adaptive digital twin	Virtual system model with adaptive UI	Real-time updates
4	Intelligent digital twin	Virtual system model with adaptive UI and reinforcement learning	Batch and Real-time updates

[1]Corresponding author.

Contributed by the Ocean, Offshore, and Arctic Engineering Division of ASME for publication in the JOURNAL OF OFFSHORE MECHANICS AND ARCTIC ENGINEERING. Manuscript received June 10, 2020; final manuscript received October 16, 2020; published online November 20, 2020. Assoc. Editor: Zhen Gao.

(TechnipFMC), "TechnipFMC and DNV GL have recognized a need for a recommended practice to qualify the trustworthiness of a digital twin." This has also been recognized by NOV in Norway, which started a collaboration with a marine engineering company, CoreMarine, in 2019. The main target was to achieve acceptance for the use of digital twins in lift planning (presented at the conference: "Floating INsight 1.0", Oslo, Norway, Mar. 9, 2020).

Unlike the crane manufacturer, the lift planner needs information that, almost exclusively, has to be gathered from outside its own company (see Fig. 1). This key requirement includes environmental data such as wind, waves, and currents, wire data, vessel data, and data concerning the lifted object. Preferably, this information should be available as predefined models; however, this is typically not the case. This means that the lift planners will have to develop their own submodels.

Custom-made digital twins represent predefined models. Ideally, a lift planner has access to several digital twin models that can be combined in a simulation environment suited for weather window calculations. Simplifications and idealizations are accumulated when these models are linked, and it is crucial to maintain an overview of the assumptions and how they affect the entire simulation.

The most important simulation model is the digital twin of the crane's winch. Therefore, the crane manufacturer must be capable of producing a simulation model that considers transparency, accuracy, and computational costs in a balanced way. Also, the model must include a way of evaluating specific lift operations, i.e., a set of acceptance criteria. So far, there have only been a few reports on digital twins of active heave compensated crane systems. Among these, Ref. [17] discusses virtual prototyping for system design and operations and Ref. [18] focuses on on-board systems decision support for pre-operational planning. However, they do not include discussions about acceptance criteria and the performance of the models. In this paper, a digital twin of the hydraulically actuated winch is presented. The winch is connected to a knuckle boom crane and is used for active heave compensation (AHC). This digital twin is especially developed for lift planning. Emphasis is placed on the structure of the simulation model and the acceptance criteria needed to validate the model for lift planning analyses. The digital twin presented here is also a commercial unit that has reached a maturity level so that it is sold in parallel with the physical crane. This paper is part of a research project that has revolved around the model-based development and implementation of motion control of hydraulic actuated winches. In that context, the model development and the digital twin has proven invaluable for the virtual testing and allowed for the practical implementation and verification of the new control methods [3].

System Description

The system assumed as the physical twin in this paper is the winch system of an active heave compensated crane manufactured by National Oilwell Varco (NOV). These cranes are used on floating vessels, as depicted in Fig. 2.

The crane's control system continuously estimates the crane's tip motion to perform heave compensation accordingly. A motion reference unit is placed in the lower part of the crane pedestal. This unit feeds out the vessel heave, roll, and pitch values that combined with the current geometry of the knuckle boom crane are used to calculate the vertical motion of the crane-tip. The winch is controlled to pay in and out wire in the opposite direction to the vertical motion of the crane-tip so that the vessel motion is decoupled from the motion of the lifted object. Additionally, the operator can change the reference point relative to the fixed seabed by operating a joystick. The winch system could be of various types, e.g., electric, passive hydraulic, and active hydraulic. This paper addresses the most commonly used solution in NOV, which is the active/passive hydraulic system.

The hydraulic system is split into two subsystems, an active and a passive. Both subsystems are connected to the same winch through a gear rim. The passive subsystem is arranged in a closed-circuit configuration and is equipped with an accumulator that maintains a constant high pressure in the A-pressure line. The motor displacements are actively controlled to meet the torque level needed to hold the passive weight of the lifted object. This is done by measuring the wire force with a load cell and measuring the pressure level in the high pressure side of the passive system, and adjust the motor displacements accordingly.

Since the passive subsystem is torque-controlled to hold the payload, the remaining forces to be overcome by the active system are due to the winch acceleration, disturbances, and friction. The active subsystem is a classic primary controlled hydraulic system in closed-circuit configuration and performs the winch position control. More details about the system architecture are shared in Ref. [3].

The digital twin of such a system will be equipped with one output variable and three input variables. The single output variable is the wire velocity, and the three inputs will be the operator's joystick command, the vessel motion, and the measured wire tension (Fig. 4).

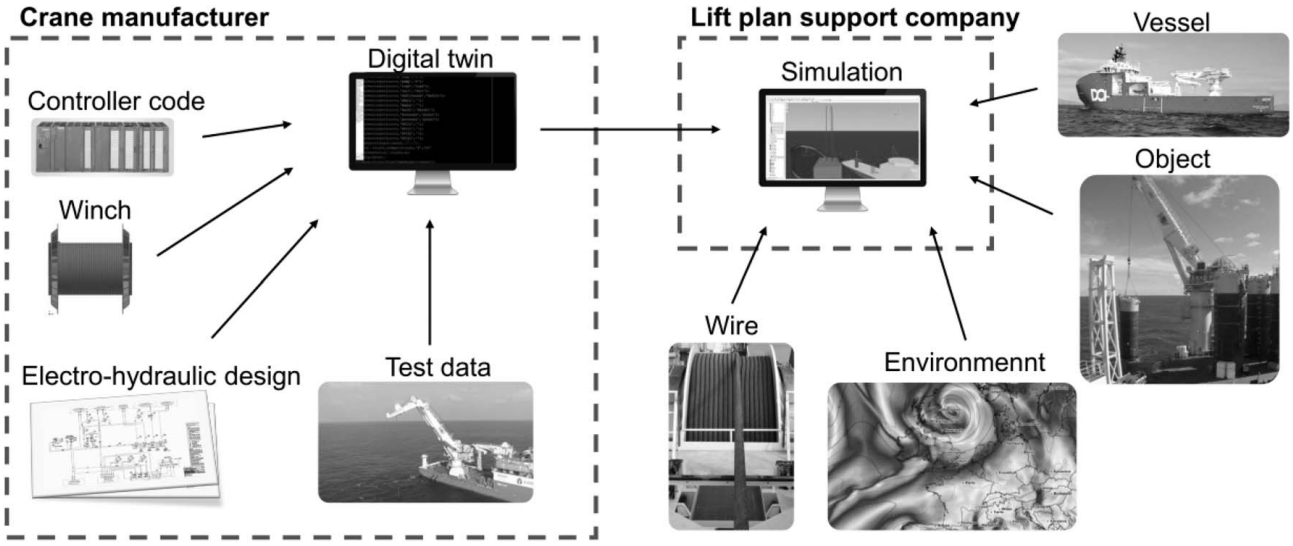

Fig. 1 Gathered data required for a simulation model

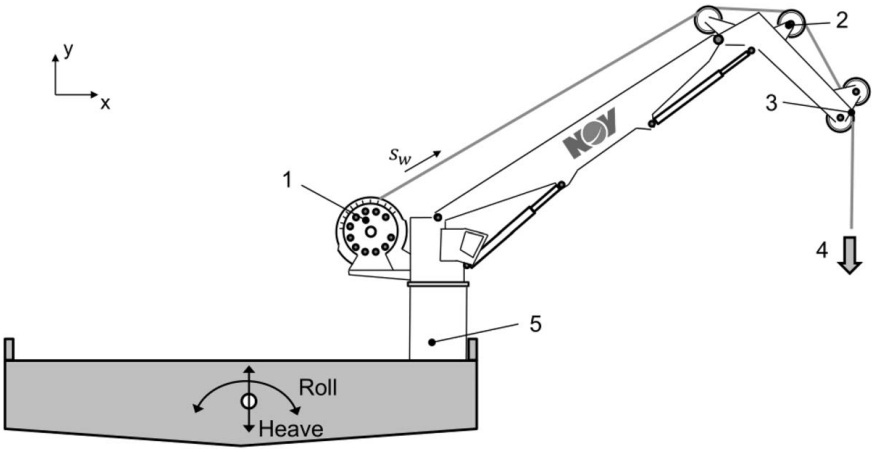

Fig. 2 Simplified overview of a crane that employs a hydraulic winch system: (1) winch system, (2) load cell, (3) crane-tip, (4) wire force, and (5) crane pedestal

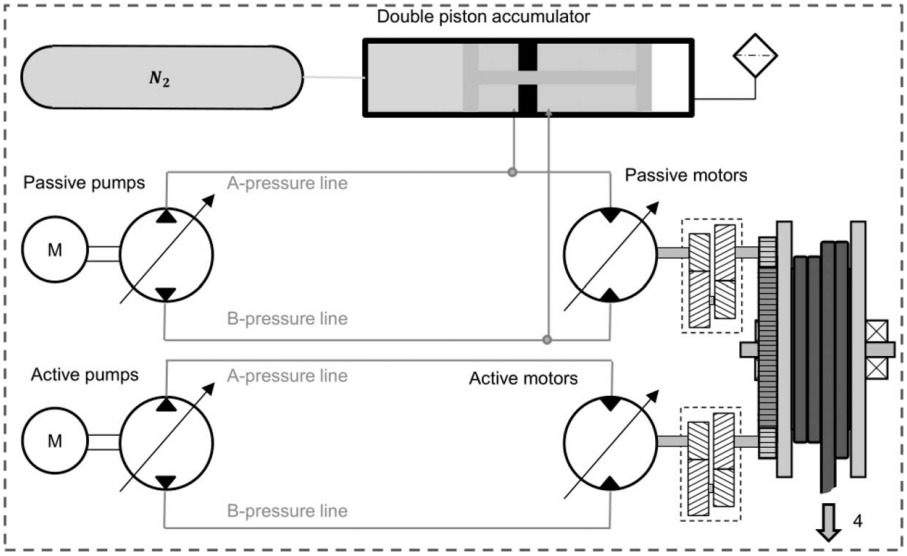

Fig. 3 Simplified sketch of the hydraulic and mechanical winch system

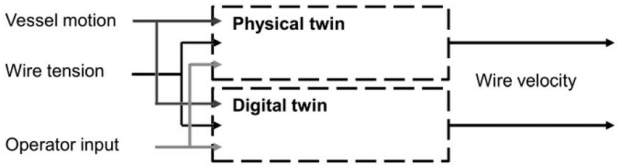

Fig. 4 Digital twin inputs and output

The two most common terms used to quantify the AHC performance are the control error and compensation efficiency. The control error is typically measured as the deviation between the desired, $s_w^{(ref)}$, and actual, s_w, wire payout displacement. If the crane-tip's deflection and the wire dynamics are both neglected; then, this error reflects the undesired movement of the lifted object during heave compensation. Denoting the control error with e_C, we have

$$e_C = s_w^{(ref)} - s_w \tag{1}$$

The control error is usually fluctuating around zero, and its instantaneous value does not reflect the quality of the heave compensation. Therefore, it is often more relevant to talk about the peak-to-peak control error, e_{Cpp}, over a period of time:

$$e_{Cpp} = e_{Cmax} - e_{Cmin} \tag{2}$$

where e_{Cmax} and e_{Cmin} are the maximum and minimum control error observed over a specific period. The compensation efficiency, η_C, is a term that quantifies e_{Cpp} relative to the absolute crane-tip motion as

$$\eta_C = 1 - \frac{e_{Cpp}}{s_{Tpp}} \tag{3}$$

where s_{Tpp} is the vertical peak-to-peak motion of the crane-tip.

Acceptance Criteria

Simulation fidelity and functionality are essential for any simulation model, but the ability to represent the real system is often overlooked or not handled systematically. The main considerations must be twofold, i.e., what parameters (digital and physical) should behave similarly and under what conditions.

Any digital twin is used for some decision support or decision making that is either set automatically or manually through a human interface. For this reason, it is crucial to know the quality

of the support expected from the digital twin, and to what extent it should be trusted. In this section, the acceptance criteria for digital twins of active heave compensated winches used for lift planning are proposed.

In crane operations where the payload is being lifted subsea and heave compensated, the compensation error is the predominant factor reflecting the variation in the wire tension. Hence, comparing the measured and simulated winch position error is the essential acceptance criteria used to validate the digital twin. The quality of the data acquired from real-life tests is crucial to ensure high confidence in the model. For this purpose, the data sets should apply to specific criteria. First, the data sets should cover multiple wire-paid-out lengths. This criterion ensures that the wire-layer-dependent calculations, such as the total drum inertia and the layer dependent controller outputs, are verified. Second, the verification should be performed with multiple winch loads. Further, the wave- and wind-induced motion applied to the vessel should ensure a variation in the crane's tip peak-to-peak motion, s_{Tpp}. Finally, it should be emphasized that the model addresses the dynamic response properly, i.e., transients should be investigated.

The position control error is chosen as the overall simulation parameter to assess the performance of the model. In this paper, the position control error refers to the one-dimensional deviation between the measured wire-paid-out and the wire-paid-out reference. Although the compensation efficiency is most useful for evaluating the crane performance, it is, nevertheless, suggested that the control position error is most useful for model verification purposes. The position error should be preferred to a velocity error because the measured winch velocity is derived from position measurements (measured with a tachometer), and the calculation involves differentiation based on internal time-steps and filtering techniques. Hence, the velocity estimation introduces higher uncertainties and tolerances, especially at low speeds which is always occurring in AHC. Although the winch velocity measurement could be of higher quality on other winch systems than the one investigated in this paper, the position control error is preferred. The position is, in any case, a state variable dependent on the velocity, and hence a qualification of one of them will implicitly qualify the other. The control error is chosen as a key identifier for AHC performance because it has a significant influence on wire tension variations. The control error will to a large extent determine how the lifted object moves with respect to the fixed seabed and how the wire resonance is amplified.

When evaluating the control error, a peak-to-peak error measured over a specific period should be used. The period should preferably cover at least 1-2 wave tops and 1-2 wave crests (see Fig. 10 for typical control error variations). The average deviation between the simulation model and real-life should be compared with the use of the calculated peak-to-peak control error.

The control commands to motors and pumps should be verified. It is possible to model the controllers with close to 100% accuracy. However, when the measured data is logged and reused as controller inputs, a perfect result is not possible. The logged data gathered from measurements does include some deviation due to data processing. Thus, a control command deviation must be accepted.

Saturation effects should be validated; however, the accuracy is not necessarily critical unless extreme scenarios are simulated. It is important in model development of regular heave compensation that little or no effort is put into modeling extreme scenarios except the ability to recognize the conditions for when they occur. Otherwise, the model will have to include non-linearities and stiff subsystems that can be detrimental to the cost-effectiveness of the computations. In summary, the following acceptance criteria are proposed:

(1) Data set
   (a) The data set should cover different wire-paid-out lengths.
   (b) The data set should embrace different winch loads.
   (c) A minimum heave range for the crane's tip should be covered.
   (d) The data sets should span a certain time interval.
(2) Control error
   (a) The difference between the simulated and recorded values of the maximum control error must be acceptable.
   (b) The average deviation between measured and simulated peak-to-peak control error should be compared.
   (c) The compared compensation efficiencies must reflect a low deviation at high crane's tip motions.
   (d) The simulated control error should be of similar shape to the measured one.
(3) Controller command
   Simulated controllers should be verified and compared to measurements.
(4) Extremes
   Pump saturation should be tested and evaluated.

To be able to measure and control that these criteria are fulfilled, some of them will need to be quantified. Together with lift-planning engineers, a part of the criteria has been quantified in Table 2.

These quantified criteria are the first of its kind for active heave compensated winch models. The criteria determine the performance that is expected and needed from the simulation model.

Simulation Model

General Information. The high-fidelity simulation model is built in SIMULATIONX®, which is a general purpose modeling software. The model overview is given in Fig. 5.

The upper half of the model can be identified as the active subsystem, where an equivalent active pump and equivalent active motor can be seen in areas 1 and 3, respectively. The pumps and motors of the passive subsystem can be seen in areas 2 and 4, respectively. The passive system also has a double-piston accumulator (area 6). Three submodels (area 5) calculate the friction in both the active and passive motors as well as in the gears, bearings, and wire sheaves. They are based on previous investigations of motor and winch friction [19,20]. The crane model has an integrated control system (area 7); it was verified that it behaves in the same way as the real control system implemented in the programmable logic controller (PLC) of the full-size crane. Area 9 includes a submodel for calculating the equivalent mass moment of inertia for both the winch and the wire. Additionally, it calculates the current layer number and layer diameter. Finally, the submodel (area 8) calculates the load dynamics based on the wire length, load geometry, and sea conditions. More insight into the modeling approach is given in the sequel.

Pumps (Areas 1 and 2). The pumps of the winch system are modeled as a single unit with equivalent displacement that is driven at constant speed. The dynamic response of the displacement adjustment system is a key aspect. A second-order transfer function was found sufficient to simulate the swash plate position [21,22]. It was fitted to the results taken from the field as displayed in

Table 2 Proposed criteria

No.	Description	Criteria
1a	Tested with different wire lengths	≥2
1b	Tested with different winch loads	≥2
1b	Highest winch load	>40% SWL
1c	Crane-tip motion range	0.5 – 2.0 m
1d	Total data set length	>1500 s
2a	Maximum error deviation across the complete data set	<5 cm
2b	Peak-to-peak calculation period	30 s
2b	The average peak-to-peak error deviation	<5 cm
3	Control command deviation	<3%

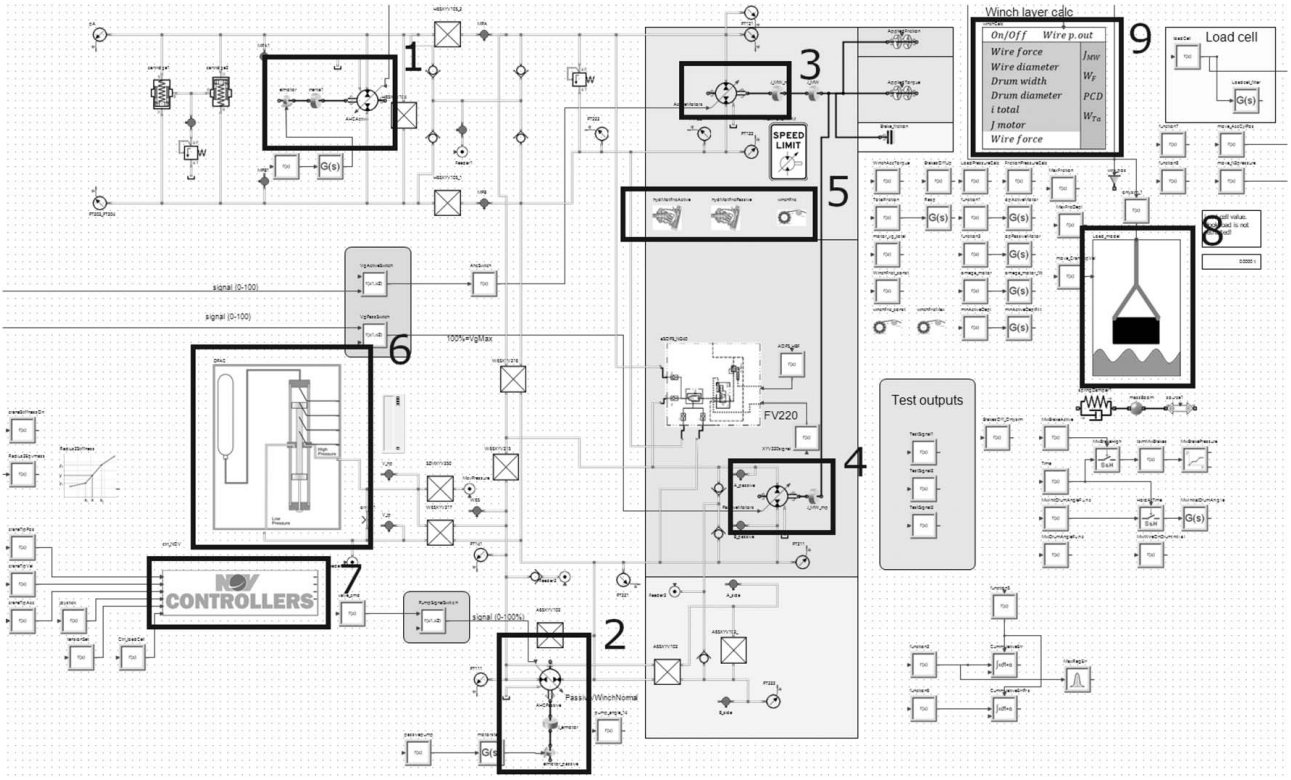

Fig. 5 Overview of the high-fidelity model built in SIMULATIONX [3]

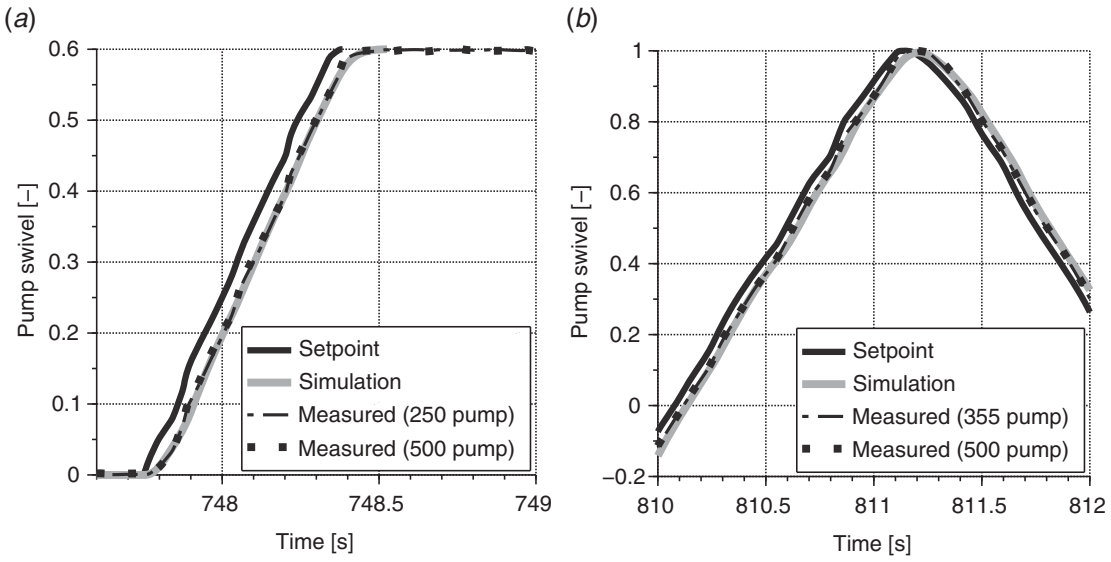

Fig. 6 Response test of the displacement adjustment system using A4VSG pumps: (*a*) results for a 500 cm^3/rev and a 250 cm^3/rev pump obtained by using a steep linear ramp as the reference signal and (*b*) results for a 500 cm^3/rev and a 355 cm^3/rev pump obtained using a sinusoidal as the reference signal

Figs. 6(*a*) and 6(*b*). The comparisons include pump displacements ranging from 250 cm^3/rev to 500 cm^3/rev and show excellent agreement between measured and simulated results.

The chosen model of the displacement adjustment system of the pumps (Eq. 4) provides a good fit of the measured results, where the undamped natural frequency, $\omega_n = 31$ rad/s, and damping ratio, $\zeta = 0.9$, are used

$$G_{pump}(s) = \frac{\omega_n^2}{s^2 + 2 \cdot \zeta \cdot \omega_n \cdot s + \omega_n^2} \tag{4}$$

Motors (Areas 3 and 4). The real system under investigation has four active and 15 passive variable-displacement motors. In the model, the motors have been merged into two equivalent units. The dynamic response of the motors' displacement adjustment system is assumed to obey a second-order model like the one in Eq. (4), with undamped natural frequency of 5 rad/s and damping ratio 1. As a result, about 1 s is needed to change the motor displacement from zero to full value. The response time of a motor varies with the control pressure, control settings, size of motor, and direction. Thus, the simulated behavior is simplified. The motor response can, according to the authors' experience and

the supplier data vary from 0.7 s to 3.5 s depending on the aforementioned variables.

Friction (Area 5). Friction in the winch system is addressed via parametric models. Three models are included, one for the active motors, one for the passive motors, and one for the remaining system friction. The models are based on earlier work on friction estimation in axial-piston motors and winch systems [19,20]. These friction models are based on a gray-box approach. Some terms are related to physical properties, while others are derived from verifications against real-life data. The effects of the fluid's temperature changes are neglected due to the active cooling and temperature control employed in all cranes (i.e., the fluid temperature remains substantially constant during standard operations).

Double-Piston Accumulator (Area 6). Including the double-piston accumulator in the simulation model is necessary in order to get the correct system limitations. During heave compensation, the maximum compensation distance in a wave cycle is directly limited by the size of the accumulator. Friction between the accumulator's moving parts is assumed to be viscous, and the internal leakages are tuned to obtain a realistic flow demand from the passive-side pumps. It is worth mentioning that these parameters have a minor impact on the performance of the system.

Controller (Area 7). This part consists of controllers developed by NOV for different types of winch control. It includes active control of the active motors, passive motors, active pumps, and passive pumps. The simulated controllers are built based on internal functional descriptions and reverse engineering of the controllers implemented on the crane. Additionally, the simulated model and controller are run on fixed-step solvers. Since the controller is not a direct copy of the controller and running with different step sizes, the simulated controller is validated with data from real-life to ensure maximum accuracy on the controller output. In general, the deviation in pump controller output is minimal and negligible compared to other dominating sources of deviation.

Subsystem for Winch Calculations (Area 9). This block includes functions for calculating parameters related to the wire and to the winch drum. This submodel returns variables such as current wire-layer diameter, wire layer, and current total winch inertia due to the wire on the drum and drum itself. The fixed input parameters are crane-specific and cover the drum inertia retrieved from the 3D-computer-aided design model of the winch, wire diameter, full wire on the drum, wire mass properties, and drum geometry.

Rotational Inertia of the Winch System. This submodel encompasses the rotational inertia dictated by the motors, gearboxes, drum, and wire. The impact of the different terms can be seen in Figs. 7(*a*) and 7(*b*), where values representative for a 150 t AHC crane are displayed.

All the included contributions have a significant effect on the total inertia, which depends on how much wire is paid out.

Hydraulic Transmission Lines. The hydraulic system of a crane includes piping, hoses, and hydraulic gate valves. All these components affect the eigenfrequency of the system. As reported by Nachtwey [23], "hydraulic capacitance should not be ignored in high-performance hydraulic systems using closed-loop control." In this model, the hydraulic capacitances where the pressures build-up has been adjusted such that the simulated dynamic response matches real-life measurements.

Volumetric Efficiency of the Hydraulic Units. The active winch system, responsible for winch position control, is highly influenced by the volumetric losses of the hydraulic pumps and motors. The terms involved are the external, internal, and compression losses. The external leakage path is set to twice as restrictive as that of the internal leakage path, assuming a dominant internal flow loss. The total volumetric loss is modeled as a variable hydraulic conductance. The pump leak conductance is assumed independent of pressure variations but dependent on pump displacement. The pump leak conductance is calculated based on test data from the manufacturer of the units A4VSG355, namely Bosch-Rexroth [24]. The efficiency variations between the different pump sizes are neglected. For the motors, the same pressure independence is assumed, and a simplified conductance model dependent on the motor's shaft speed is used (Eq. (5))

$$C_{leak} = C_1 + C_2 \cdot n_m \tag{5}$$

where C_{leak} is the total leak conductance. The parameters, C_1 and C_2, are adjusted to make the model represent the data provided by the sub-supplier [25]. A comparison between the adjusted model for an A6VM series 63 size 250 and the supplier data is depicted in Fig. 8.

Simplifications. In addition to the aforementioned simplifications and modeling techniques, the following features have been neglected or heavily simplified in the digital twin. The safety systems (e.g., overload protection systems) are not modeled in detail since the criteria for the use of the model is that the load scenario remains within the winch specifications. Temperature variations of the working fluid are neglected because active

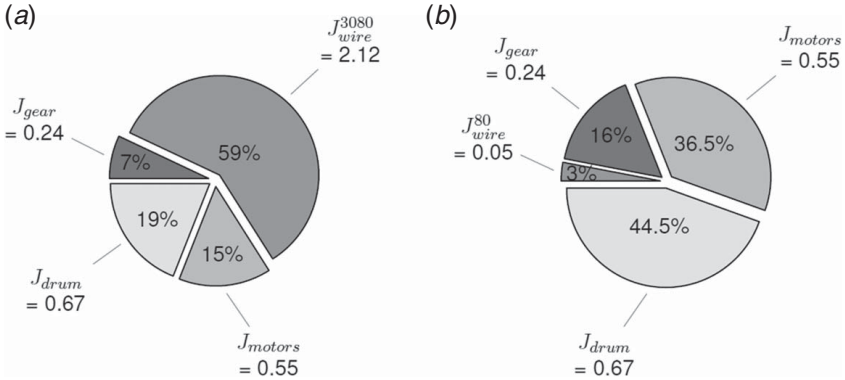

Fig. 7 Rotational inertia with respect to motor shaft: (*a*) total inertia of 3.58 kg/m^2 when the wire is fully retracted (3080 m of wire on drum) and (*b*) total inertia of 1.51 kg/m^2 when the wire is fully extended (80 m of wire on drum)

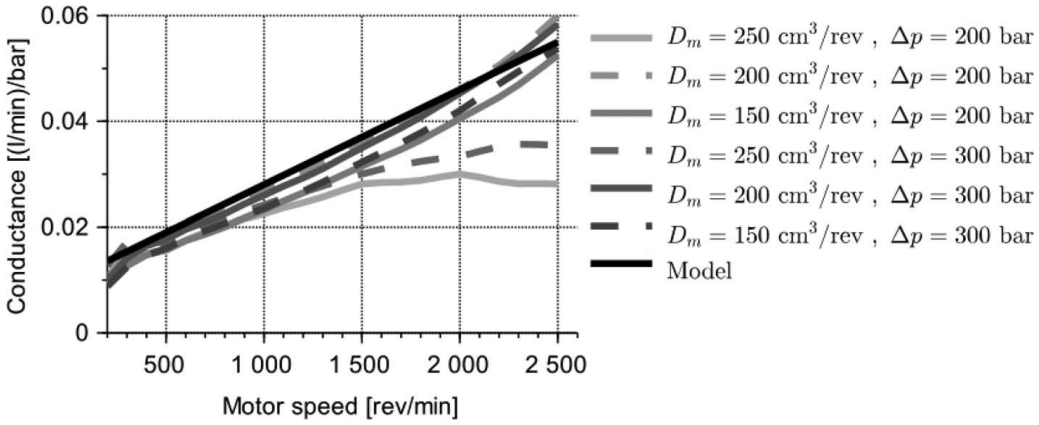

Fig. 8 Comparison of sub-supplier measurements and the leak conductance model for a A6VM s63 size 250

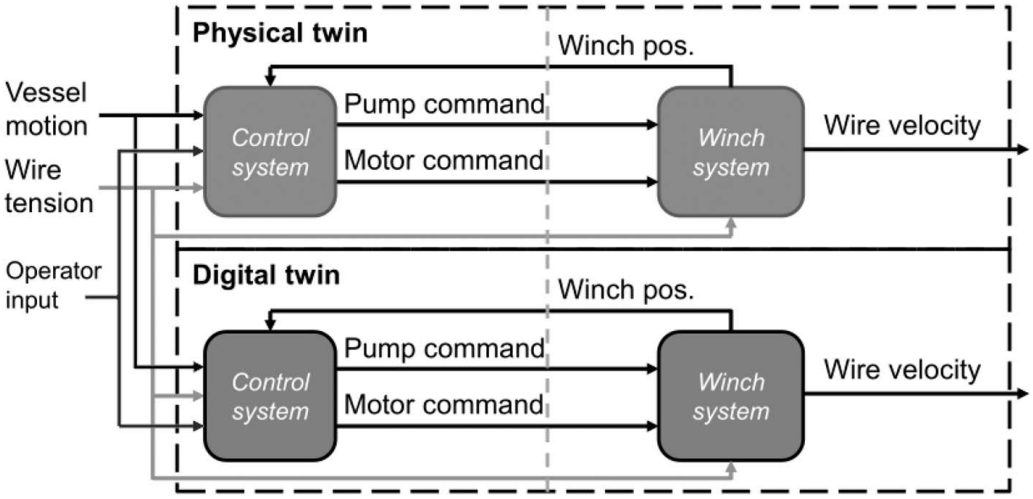

Fig. 9 Simplified sketch showing signal flow in a real versus simulated winch

temperature control is standard in these cranes. Finally, backlash and flexibility of the gear transmissions are also omitted.

Verification of the Digital Twin

Every offshore crane is subjected to a wide spectrum of load scenarios that affect the performance of the hydraulic system. Hook load, pump displacements, motor displacements, paid-out wire-length, and the crane's tip positions are those parameters that influence the crane's dynamics. Therefore, it is neither feasible nor necessary to test all the resulting scenarios with real experiments. With the right model and system knowledge, it is sufficient only to verify the following elements:

(1) System variables and parameters
(2) Simulated controllers
(3) Winch velocity limitations
(4) Winch dynamics
(5) Active heave compensation

(1) System variables and parameters

It is key to ensure that the model is using the correct sizes of pumps, motors, leakage terms, and controller parameters.

(2) Simulated controllers

Correct modeling of the control of the pumps' and motors' displacements are essential to achieve a good overall simulation performance. The controllers are first validated manually towards code structure and parameters, then the commanded signals are verified. The controller is verified separately from the rest of the model to remove potential sources of error. Controller inputs from measured data are used as inputs to the simulated controller. The results are verified by comparing the control system output from the digital model with control output from the controller commands measured on the real system. As seen in Fig. 9, the outputs to be compared are the motor displacement command and the pump displacement command.

Table 3 Scenarios considered for the experimental validation of the model

Load case	Winch load	Duration	Wire paid out
1	82 t	200 s	487 m
2	94 t	1500 s	487 m
3	164 t	200 s	2314 m
4	162 t	300 s	2281 m

(3) Winch velocity limitations

The winch limitations are checked during this stage of the verification (pump saturation is the typical scenario that may be seen as a result). A good correlation between simulated and real-life results indicates the correct use of pump and motor displacement, pump/motor efficiency, winch gear ratios, and wire-layer calculations. Although the fixed transmission ratio of the gears and the

relationship between the drum's angular velocity and wire's linear velocities are relatively simple to verify, the hydraulic transmission ratio is a bit more complex due to the effect of the pump and motor leakages. Additionally, there can be some small cumulative errors due to the slightly load-dependent speed of the electric motor, and uncertainties in actual pump and motor displacement. In any case, it will be challenging to achieve an exact match of the speed capacity. Thus, the adjustment is roughly tuned with the leakage models and pump end-stroke (maximum displacement). However, since the normal operation is prioritized, the adjustment should not be performed so that the general performance under normal operation scenarios is altered.

(4) Winch dynamics

To ensure realistic winch dynamics, the hydraulic capacitances are adjusted. This step is done such that the pressure gradients for both pressure lines A and B (see Fig. 3), as well as the dominant oscillation frequencies, are as close as possible to real-life measurements when accelerating the winch. For this specific test, it is chosen to consider a scenario where the hook load is zero, and the wire paid out is less than 20 m. In this way, the influence

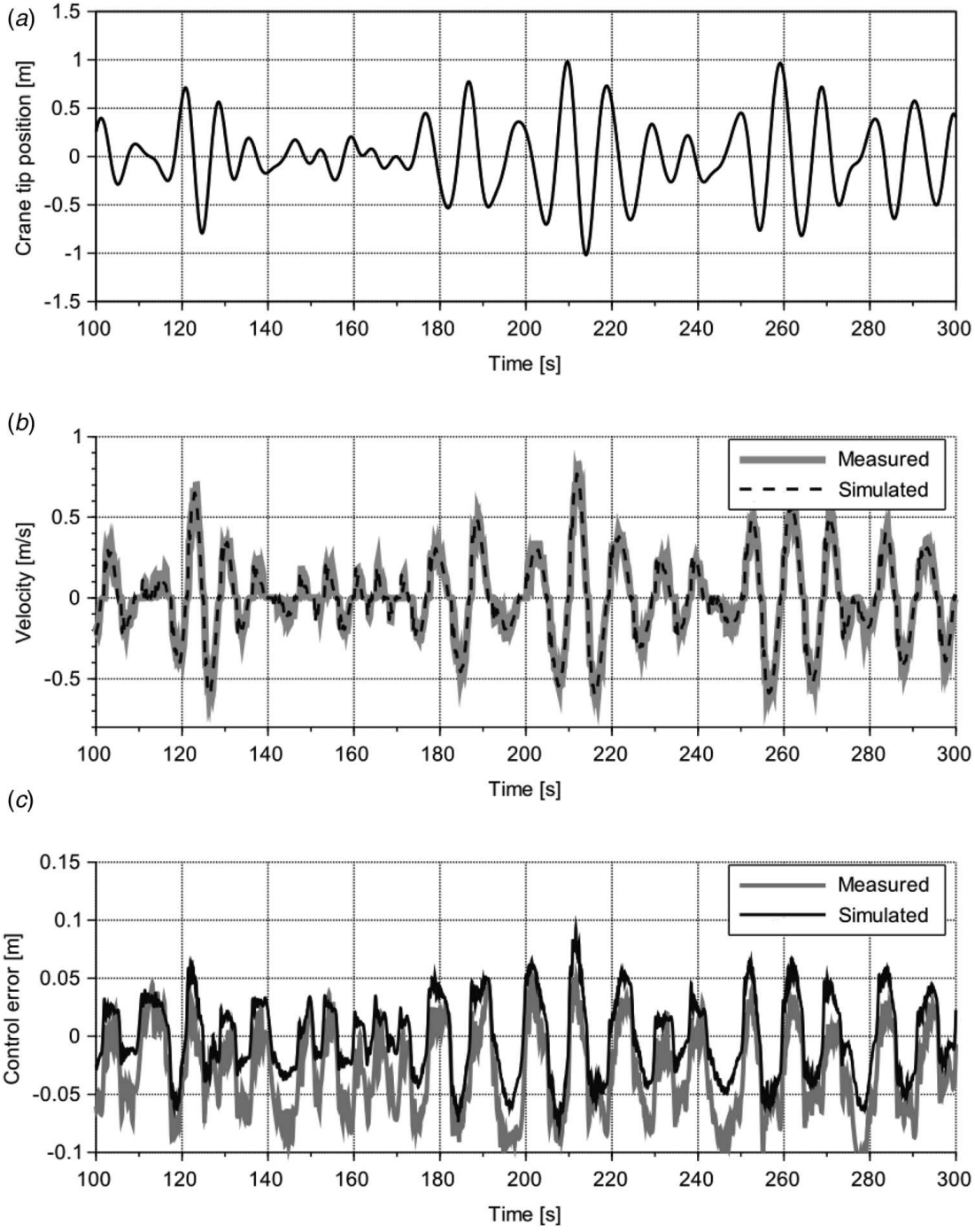

Fig. 10 Experimental validation of the digital twin: (*a*) measured crane's tip motion, (*b*) simulated and measured wire velocity, and (c) simulated and measured control error

of the wire and load dynamics on the hydraulic pressure is minimized. The oscillation's period between two significant pressure peaks is measured in three different places in the simulation.

(5) Active heave compensation

Lastly, the winch model, consisting of the hydro-mechanical system and the controller, is verified with real measurements. The test is performed for several scenarios that are listed in Table 3. All the scenarios are with the loads submerged in water. Typical subsea test loads made of steel are used. During the evaluated tests, the vessel has activated its dynamic positioning system, ensuring reduced horizontal movements of the vessel and crane-tip.

The vessel motion measurements from the tests are used in the simulation model to get a one-to-one comparison between the measurements and the simulation results. For this comparison, the crane-tip flexibility and wire dynamics were assumed to be negligible. The main focus of these verifications is to compare the position error. A comparison lasting 300 s is shown in Fig. 10 for the load case 4.

Discussion of the Validation Process. All these steps of verification have been performed to ensure a realistic performance of the digital twin's output (winch velocity) for any given input. To summarize what has been discussed: step 1 ensures a correct model with regards to fixed and variable parameters related to components and controller parameters. In step 2, the controllers are verified and implicitly validated. They ensure that any input parameter will give realistic pump and motor commands. Further, in steps 3 and 4, the hydro-mechanical portion of the winch system is verified so that any input command will lead to a realistic winch response and wire velocity. To crosscheck the steps form 1 to 4, a final test with a comparison of the whole model in an AHC scenario is tested and verified in step 5.

Statistical Analysis of the Results. A statistical analysis has been performed for a set of measurements based on a selection of tests completed according to both NOV's internal as well as official acceptance procedures for operating cranes. Therefore, the variations of the load scenarios are within those requirements that NOV, based on many years of experience, considers being sufficient to approve a crane. In the analysis, the peak-to-peak error in the last 30 s is calculated, and simulated results are compared with real-life measurements, see Fig. 11(*a*). The deviation between the measured and simulated results indicates how accurate the simulation model is.

The deviation between the simulated and measured peak-to-peak position error is calculated for all the chosen measurements. Then, a statistical approach is used where both the average and standard deviation are calculated for all the investigated scenarios. The standard deviation and average value are calculated based on Eqs. (6) and (7), respectively:

$$s = \sqrt{\frac{1}{N-1}\sum_{i=1}^{N}(x_i - \bar{x})^2} \tag{6}$$

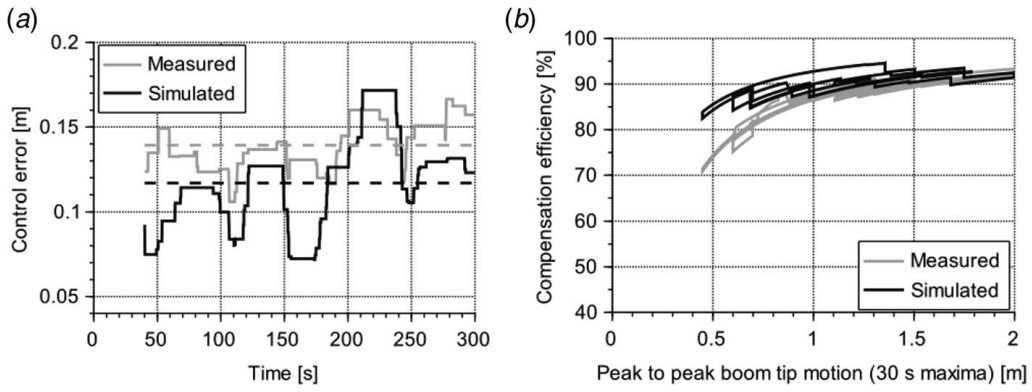

Fig. 11 Analysis of an offshore test conducted with a 162 t winch load: (*a*) control position error shown as the peak-to-peak maximum over 30 s (the dotted lines show the average value) and (*b*) compensation efficiency based on the peak-to-peak crane's tip motion and peak-to-peak position error

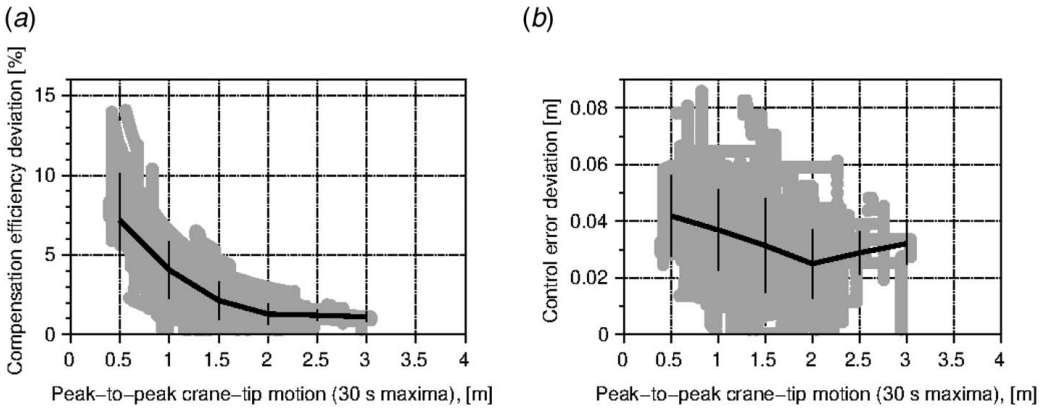

Fig. 12 Results from combined data (the black lines indicate the average): (*a*) deviation between measured and simulated compensation efficiency and (*b*) deviation between measured and simulated control position error

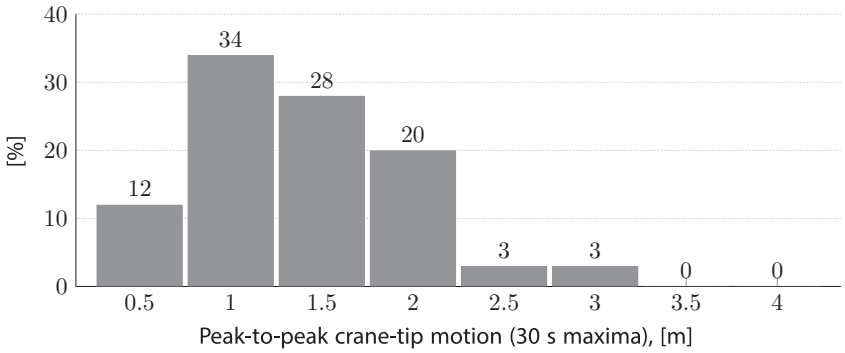

Fig. 13 Distribution of the different data-points used to analyze the four load cases in Table 3

$$\bar{x} = \frac{1}{N}\sum_{i=1}^{N} x_i \tag{7}$$

where N is the total number of samples, $\bar{x}$ is the deviation average, and x_i is the absolute deviation between the measured peak-to-peak position error and the simulated one. The results shown in Fig. 11 yield a standard deviation, s, equal to 1.5 cm and an average, $\bar{x}$, corresponding to 3.3 cm. Assuming a Gaussian distribution, this outcome means that the probability for a maximum deviation of 6 cm from the measurements is 96% and, similarly, for a maximum deviation of 5 cm it is 86%.

The results can also be analyzed for the compensation efficiency (Fig. 11(*b*)). The correlation between measured and computed values is acceptable. However, it is seen that the compensation efficiency deviation is higher at low crane-tip motions. While Fig. 11 displays the deviation between the digital twin and the in-field measurements of load case 4, then Fig. 12 displays the deviation between simulated and measured results for all four load cases. The average values are shown with the red line. The compensation efficiency deviation, in Fig. 12(*a*), confirms the findings from load case 4, where the relative deviation increased at low crane-tip motions. The absolute control error deviation in Fig. 12(*b*) shows that the average deviation between the digital twin and the in-field-measurements is less than 4 cm for crane-tip motions larger than 1 m.

To perform the analyses, the entire set of load cases from $1 \cdots 4$ are used. However, the peak-to-peak crane-tip motion is not evenly distributed in the real crane's tip motion. The normalized distribution of the different data-points being analyzed is shown in Fig. 13. It can be seen that the majority of the data-points are peak-to-peak motions between 1 m and 2 m. Therefore, it should be mentioned that the highest values of peak-to-peak motion have less data-points, introducing a higher uncertainty.

Conclusions

A digital twin of an active heave compensated winch with hydraulic drives is presented. The digital twin is, in this case, a simulation model that is developed specifically for lift planning purposes. To verify the model, general acceptance criteria are presented for the first time to describe and approve the accuracy of the simulated winch performance. For the 250 t crane used as an example for the field experiments, the verification shows that a position control accuracy in active heave compensation of less than 5 cm compared to the real system can be expected. Additionally, the deviation between the measured and the simulated control error is relatively constant, which means that an extended operational range can be explored with confidence.

Based on the aforementioned modeling criteria, the simulation model captures the behavior of the actual system to a sufficient degree of accuracy for lift analyses. With the achieved accuracy, the digital twin of the AHC system will significantly improve the accuracy of the predictions made during lift planning. Which, therefore, will reduce the use of conservatism and increase the operational weather window. Additionally, the digital twin forms a good starting point for further development to adaptable and embedded digital twin technology. The acceptance criteria and verification method can be used as a reference for optimization when adapting the digital twin to minimize the deviation between simulated and real-life performance.

Data Availability Statement

The datasets generated and supporting the findings of this article are obtainable from the corresponding author upon reasonable request.

Nomenclature

e_C = position/control error
e_{Cpp} = position/control peak-to-peak error
n_m = rotational motor shaft speed
s_{Tpp} = vertical crane-tip peak-to-peak motion
s_w = wire paid out
C_{leak} = total leak conductance
AHC = active heave compensation.
DT = digital twin
NOV = National Oilwell Varco
PHC = passive heave compensation
SWL = safe working load
η_C = AHC efficiency

References

[1] Matland, A. E., 2014, "Simulation of Marine Lifting Operations with Focus on Structural Response Control Arild Eriksen Matland," Master Thesis, Norwegian University of Science and Technology, Trondheim.
[2] You, D., Sun, L., Qu, Z., and Wang, T., 2013, "Roll Motion Analysis of Deepwater Pipelay Crane Vessel," J. Marine Sci. Appl., **12**(4), pp. 459–462.
[3] Moslått, G.-A., Padovani, D., and Hansen, M. R., 2019, "A Control Algorithm for Active/Passive Hydraulic Winches Used in Active Heave Compensation," ASME/BATH 2019 Symposium on Fluid Power and Motion Control, Sarasota, FL, American Society of Mechanical Engineers, p. 11.
[4] Moslått, G.-A., Hansen, M. R., and Padovani, D., 2020, "Performance Improvement of a Hydraulic Active/Passive Heave Compensation Winch Using Semi Secondary Motor Control: Experimental and Numerical Verification," Energies 2020, **13**(10), p. 2671.
[5] Zhang, C., Qian, Y., Dui, H., Wang, S., and Shi, J., 2020, "Component Failure Recognition and Maintenance Optimization for Offshore Heave Compensation Systems Based on Importance Measures," J. Loss Prev. Process Ind., **63**(October 2019), p. 103996.
[6] Committee, T. S., Board, T. P., and Board, T. P., 2015, DNVGL-ST-N001 Marine Operations and Marine Warranty.

[7] Nordås, S., Ebbesen, M. K., and Andersen, T. O., 2020, "Definition of Performance Requirements and Test Cases for Offshore/subsea Winch Drive Systems with Digital Hydraulic Motors," ASME/BATH 2019 Symposium on Fluid Power and Motion Control, FPMC 2019, Sarasota, FL.
[8] Vartdal, J. T., 2017, "An Investigation of Offshore Wind Installation Strategies Johanne Tomine Vartdal," Master Thesis, Norwegian University of Science and Technology, Trondheim..
[9] Eshkenazi, A., 2018, Real Benefits from Digital Twins.
[10] I-Scoop, 2017. Digital Twin Technology and Simulation: Benefits, Usage and Predictions 2018.
[11] Moi, T., Cibicik, A., and Rølvåg, T., 2020, "Digital Twin Based Condition Monitoring of a Knuckle Boom Crane: An Experimental Study," Eng. Failure Anal., **112**, p. 104517.
[12] Tao, F., Cheng, J., Qi, Q., Zhang, M., Zhang, H., and Sui, F., 2018, "Digital Twin-driven Product Design, Manufacturing and Service With Big Data," Int. J. Adv. Manuf. Technol., **94**(9–12), pp. 3563–3576.
[13] Madni, A., Madni, C., and Lucero, S., 2019, "Leveraging Digital Twin Technology in Model-Based Systems Engineering," Systems, **7**(1), p. 7.
[14] Stark, R., and Damerau, T., 2019, "Digital Twin," *CIRP Encyclopedia of Production Engineering*, S. Chatti and T. Tolio, eds., Springer Berlin/ Heidelberg, pp. 1–8.
[15] Jones, D., Snider, C., Nassehi, A., Yon, J., and Hicks, B., 2020, "Characterising the Digital Twin: A Systematic Literature Review," CIRP. J. Manuf. Sci. Technol., **1**(2019), pp. 36–52.
[16] Eriksson, K., Fjøsna, E., Ruså, R., and Myrseth, P., 2020, Digital Twins – Are They Valuable? Can you Trust Them?
[17] Chu, Y., Hatledal, L. I., Zhang, H., Æsøy, V., and Ehlers, S., 2018, "Virtual Prototyping for Maritime Crane Design and Operations," J. Marine Sci. Technology (Japan), **23**(4), pp. 754–766.
[18] Skjong, S., Kyllingstad, L. T., Reite, K. J., Haugen, J., Ladstein, J., and Aarsæther, K. G., 2019, "Generic on-board Decision Support System Framework for Marine Operations," Proceedings of the International Conference on Offshore Mechanics and Arctic Engineering, Glasgow, Scotland, June, ASME.
[19] Moslått, G.-A., and Hansen, M. R., 2018, "Modeling of Friction Losses in Offshore Knuckle Boom Crane Winch System," 2018 Global Fluid Power Society PhD Symposium, GFPS 2018, Samara, Russia, IEEE, pp. 1–7.
[20] Moslått, G.-A., Hansen, M. R., and Karlsen, N. S., 2018, "A Model for Torque Losses in Variable Displacement Axial Piston Motors," Model., Identif. Control, **39**(2), pp. 107–114.
[21] Wu, K., Zhang, Q., and Hansen, A., 2004, "Modelling and Identification of a Hydrostatic Transmission Hardware-in-the-loop Simulator," Int. J. Vehicle Design, **34**(1), pp. 52–64.
[22] Grabbel, J., and Ivantysynova, M., 2005, "An Investigation of Swash Plate Control Concepts for Displacement Controlled Actuators," Int. J. Fluid Power, **6**(2), pp. 19–36.
[23] Nachtwey, P., 2019, "Hydraulic Capacitance and Dead Time," Hydraulics & Pneaumatics, **6**(2), pp. 1–7.
[24] Hydromatik, B., and Bosch Rexroth, A. G., 2000, Testreport 1229 A4VSG355DS.
[25] Efficiency, T., Wirkungsgrad, V., and Wirkungsgrad, M.-h., 2003, Sales Information Variable Displacement Motor A6VM Series 63.